Performance of pulse-jet bag filter regarding particle removal for nano-waste incineration conditions

Rachid Boudhan

UNIVERSITE BRETAGNE LOIRE

جامعة محمد الخامس بالرباط
Université Mohammed V de Rabat

IMT Atlantique
Bretagne-Pays de la Loire
École Mines-Télécom

Thèse de Doctorat

Rachid BOUDHAN

Mémoire présenté en vue de l'obtention du
grade de Docteur de L'Ecole nationale supérieure Mines-Télécom Atlantique Bretagne-Pays de la Loire - IMT Atlantique
sous le sceau de l'Université Bretagne Loire
et du grade de Docteur de l'Université Mohammed V de Rabat

École doctorale : *SPIGA*

Discipline : *Génie des Procédés*
Spécialité : *Environnement*
Unité de recherche : *GEPEA UMR CNRS 6144*

Soutenue le *05/07/2017*
Thèse N° : *2017IMTA0022*

Performance of pulse-jet bag filter regarding particle removal for nano-waste incineration conditions

JURY

Rapporteurs :	**Dominique THOMAS,** Professeur, Université de Lorraine
	Gwenaëlle TROUVE, Professeur, Université de Haute Alsace
Examinateurs :	**Ahmed MZERD,** Professeur, Université Mohammed V, Rabat
	Benoit SAGOT, Enseignant-chercheur, ESTACA
	Esperanza PERDRIX, Maitre-assistante, IMT Lille Douai
Invité(s) :	**Danielle VENDITTI,** Docteur, TREDI R&D-Séché Global Solutions
Directeur de Thèse :	**Laurence LE COQ,** Professeur, IMT Atlantique
Co-directeur de Thèse :	**Kamal GUERAOUI,** Professeur, Université Mohammed V, Rabat
Co-encadrant :	**Aurélie JOUBERT,** Maître-assistante, IMT Atlantique

Acknowledgments

I would like to express my deepest gratitude to my advisor Pr. Laurence LE COQ for the immeasurable amount of support and guidance during my PhD studies. Pr. Laurence's insights into and patient endurance throughout this project have been a true blessing. She enabled me to develop and broaden my knowledge in this field. My sincere appreciation is extended to Dr. Aurélie JOUBERT for her invaluable support, encouragement and advice. She provided a scientific and technical guidance and inspiration during this research. My deepest thank for Pr. Kamal GUERAOUI for his advices and continued encouragement during this doctoral dissertation.

I would like to thank Pr. Dominique THOMAS, and Pr. Gwenaëlle TROUVE, for all their time and effort in serving on the committee as thesis referees of my manuscript. I am also indebted to Dr. Ahmed MZERD, Dr. Benoit SAGOT, and Dr. Esperanza PERDRIX, for having agreed to be inspector of my thesis.

Special recognition is given to Dr. Sylvain DURECU and Dr. Danielle VENDITTI, representative of TREDI company, for financial support and for help and valuable discussions on the research project. Thank's to Dr. Danielle VENDITTI, the invited member in my thesis defense.

I would like to acknowledge the program Partenariat Hubert Curien (PHC) « TOUBKAL» for the financial support of my thesis in France.

All the experimental work could not have been done without the invaluable help of the technical team. I am grateful to Yvan GOURIOU for the realization of the experimental devices described in the thesis (experimental setup, filter prototype, sampling probes, etc.) and for his technical advice. I would also like to thank Jérôme MARTIN and François-Xavier BLANCHET for the realization of the computer programs and the installation of electrical devices. I thank Eric CHEVREL, Katell CHAILLOU, and Patrick BRION for their valuable help during my laboratory experiments. I am grateful the all staff of Energy Systems and Environment Department (DSEE) of IMT Atlantique. My special thanks for Dominique BRIAND, DSEE administrative assistant, for her efficiency and help.

These 3 years of thesis were particularly pleasant thanks to the other PhD students and post-doctoral. So I thank Maxime, Thibault, Safaa, Mouna, Kevin, Elias, Nadine, Djihad, Agustina, Manal, Mexitli, Francis, Zhewei, Guillaume, Aurelian, Henrietta, and Jenny.

Special thanks to all my office colleagues during these 3 years of thesis: Auliaa, Jose, Ali, Nadia, Ivan, Stephano, Sylvester and Subodh.

Many thanks to my friends and especially Chantal, Mouheb, Victor and Zola, for making my stay very interesting and eventful.

Finally I am truly appreciative to my family for their moral support, without their encouragement, I would not have a chance to be at IMT Atlantique.

This Thesis is dedicated to my parents.

Résumé

Il n'existe à ce jour aucune réglementation française ou européenne sur la gestion des nanomatériaux manufacturés, que ce soit au niveau de la fabrication, de l'usage ou de la fin de vie. De tels produits ou nano-déchets peuvent se retrouver en unités d'incinération de déchets ménagers et assimilés. Des études (projet ADEME CORTEA NanoFlueGas No. 1181C0088 : Le Bihan et al. 2014 ; Ounoughene et al. 2015 ; Walser et al. 2012) ont montré la présence dans les fumées en sortie de chambre primaire, des nanoparticules originelles, seules, ou sous forme d'agrégats, lors de l'incinération de nano-déchets en conditions mimant les filières classiques d'incinération. Or, les nanoparticules sont responsables de problèmes sanitaires et environnementaux. En effet, des études toxicologiques démontrent clairement que leur très petite taille est un élément clé au niveau de la toxicité, en particulier les particules non ou peu solubles (Ostiguy et al. 2006). C'est pourquoi une attention particulière est portée sur le traitement des fumées d'incinération, en particulier sur l'efficacité des procédés dédiés à l'abattement des particules.

La technologie étudiée dans ce travail de thèse est la filtration par des filtres à manches, une technique simple et efficace pour la capture des particules et l'un des procédés de séparation les plus utilisés dans l'industrie (Le Coq, 2006).

Les travaux présentés dans ce rapport ont été réalisé dans le cadre d'une thèse en cotutelle entre IMT Atlantique et l'Université Mohammed V- Faculté des sciences, co-financée par le programme Hubert Curien TOUBKAL (campus France + CNRST) et TREDI – Groupe Séché.

L'objectif de ce projet est de quantifier les performances de filtration d'un filtre à manche à l'échelle du laboratoire lors de cycles de colmatage/décolmatage vis-à-vis d'un aérosol représentatif de celui émis par l'incinération de nano-déchets. Les applications visées sont les émissions de particules issues de l'incinération des déchets ménagers et/ou industriels et en particulier des déchets contenant des nanomatériaux. Le projet se propose d'étudier expérimentalement l'influence des paramètres opératoires tels que l'humidité et la température du gaz, la vitesse de filtration, et la nature des particules sur les performances de filtration d'un filtre à manche. Ainsi, des campagnes expérimentales sur une unité pilote de filtration sont complétées par des simulations numériques de transport des particules.

Afin de satisfaire aux conditions réalistes de fonctionnement rencontrées dans les lignes de traitement des fumées, le filtre à manche opère dans des gammes de température autour de 150°C, de teneur en eau de 10 -12%, et de vitesse de filtration autour de 1,9 $cm.s^{-1}$. Les

particules co-injectées sont des réactifs (charbon actif et bicarbonate de sodium) ainsi que des particules représentatives de celles issues de l'incinération de nano-déchets contenant des nanomatériaux (projet ADEME CORTEA NanoFlueGas No. 1181C0088 : Le Bihan et al. 2014). Les performances de filtration sont évaluées en termes d'évolutions de l'efficacité de collecte des particules et des pertes de charge du filtre à manche au cours des cycles colmatage/décolmatage.

Une étude bibliographique présentée dans le **chapitre I,** porte sur le traitement des fumées d'incinération, et présente notamment le procédé de traitement par filtre à manches. Ce chapitre présente également les caractéristiques structurales des médias fibreux, la distribution des tailles des aérosols ainsi que les forces agissant sur les particules dans un écoulement de gaz conduisant au dépôt et à la capture des particules dans un média fibreux.

Ce chapitre aborde également les performances des médias fibreux en fonction du temps en termes d'évolution de la perte de charge et de l'efficacité de filtration. La théorie de la filtration distingue deux étapes dans l'évolution des performances du filtre. Dans la première étape, la collecte des particules se produit à la surface des fibres constituant le média fibreux grâce aux mécanismes de filtration (principalement diffusion brownienne, interception et impaction) ; durant cette étape, l'évolution de la perte de charge est négligeable mais l'efficacité de filtration augmente. Dans la deuxième étape, un gâteau de particules se construit à la surface du média filtrant et devient le principal responsable de la collecte des particules et de l'augmentation de la perte de charge du filtre et de l'efficacité de collecte. Ainsi, le gâteau de particules joue un rôle essentiel dans la collecte des particules.

Ce chapitre présente également une revue bibliographique sur l'influence de l'humidité, la température, la vitesse de filtration, la taille et la nature des particules sur le dépôt des particules et par conséquent sur les performances de filtration par un média fibreux.

Les matériels et méthodes employés durant les campagnes expérimentales sont décrits dans le **chapitre II**. Deux configurations expérimentales ont été utilisées pour le colmatage de deux géométries de filtre différentes (filtre à manche et filtre plan). Quelle que soit la géométrie du filtre, il est constitué du même média filtrant issu de 2 manches industrielles respectivement lavée (en cours de vie) et neuve fournies par l'entreprise TREDI, composé de fibres de Téflon (polytétrafluoroéthylène PTFE). Il s'agit d'un média non tissé, aiguilleté et traité en surface. La manche filtrante testée est un filtre prototype de diamètre de 150 mm et de hauteur réduite à 440 mm pour une surface de filtration d'environ 0,225 m^2. La configuration est celle d'une manche verticale équipée d'un système de décolmatage à impulsion Jet-Puls. Au cours de

cette procédure de décolmatage en ligne, les particules déposées sur la surface du média filtrant sont retirées en utilisant l'injection d'air comprimé (à 6-7 bars) pendant 0,3 s dans la direction opposée au flux de gaz.

L'unité pilote de filtration, développée dans le projet NanoFlueGas (Le Bihan et al. 2014) pour l'étude du filtre à manche en conditions opératoires représentatives des lignes de traitement des fumées d'incinération, a été améliorée durant ces travaux de thèse. Le pilote de traitement a notamment été équipé d'un système de nettoyage par rétro-soufflage à air comprimé (jet d'impulsions), afin de pouvoir quantifier les performances de filtration du filtre à manche pendant plusieurs cycles de colmatage/décolmatage. Dans le pilote de filtration, quatre zones se distinguent : tout d'abord i) l'alimentation du pilote par de l'air filtré, puis ii) une zone de chauffage de l'air jusqu'à 70°C avec injection et mesure de l'humidité de l'air, la zone de test entièrement chauffée à 150°C et calorifugée comprenant l'injection des particules, iii) le module de filtre à manche et les points de prélèvement amont/aval du filtre pour la mesure de l'efficacité par le compteur SMPS, et enfin iv) le rejet après condensation des gaz et filtration des particules résiduelles. Le décolmatage de la manche filtrante est assuré par rétro-soufflage (6-7 bar). Un réservoir amovible chauffé à 150°C permet de récupérer les poussières en bas du module de filtration. L'ensemble du pilote est situé dans un laboratoire dédié à l'étude des nanoparticules.

Le second banc d'essais développé durant ces travaux de thèse a été utilisé pour tester le filtre en géométrie plane (sans système de décolmatage en ligne) à température ambiante (24°C) et humidité relative ambiante (environ 45%) pour 2 différentes vitesses de filtration (1,4 et 1,9 $cm.s^{-1}$).

La perte de charge maximale des filtres en géométrie manche et plane durant les colmatages en conditions ambiantes (24°C - 45% HR) a été fixée à 120 Pa, et à 150 Pa en conditions fumées d'incinération (150°C - 3% HR). Cette différence de valeur de perte de charge maximale du filtre a été fixée en raison de l'influence de la température et de l'humidité sur la viscosité de l'air.

Les premiers résultats de performances du filtre à manche ont été décrits dans le **chapitre III**. Les performances du filtre à manche sont évaluées lors de plusieurs cycles de colmatage/décolmatage en conditions de fumées d'incinération. Le débit d'air et le filtre à manche ont été chauffés à 150°C, la teneur en eau a été maintenue dans le flux d'air à 3% HR, tandis que la vitesse de filtration à travers le filtre à manche était de 1,9 $cm.s^{-1}$. Un mélange de particules en suspension de taille submicronique de charbon actif et de bicarbonate de sodium,

utilisées dans les conduites de traitement des gaz de combustion principalement pour l'élimination des dioxines/furanes et des gaz acides, a été généré simultanément avec l'aérosol de combustion en amont de la manche filtrante.

Les performances du filtre à manche ont été étudiées sur 11 cycles de colmatage/décolmatage. L'étude a caractérisé l'évaluation des performances de filtration au début de la durée de vie du filtre à manche avant la stabilisation de la perte de charge résiduelle résultant des cycles de filtration précédents. La perte de charge maximale a été fixée à 150 Pa pour tous les cycles de filtration. Une fois que la perte de charge a été atteinte, le filtre a été décolmaté. La filtration a été ensuite poursuivie jusqu'à la perte de charge maximale. Les performances du filtre à manche testé ont été étudiées en termes d'évolution de la perte de charge, et des efficacités fractionnelle et totale de capture des particules.

Les principales conclusions de cette étude expérimentale sont les suivantes :

(1) Pour chaque cycle de filtration, les essais au laboratoire montrent une efficacité totale du filtre à manche qui augmente avec le colmatage d'une valeur minimale de 98,5% jusqu'à 99,98%.

(2) L'efficacité fractionnelle varie en fonction de la taille des particules, avec un minimum d'efficacité de collecte (98,5%) mesuré pour des particules de taille 74 ± 15 nm (MPPS).

(3) La durée de colmatage diminue de 630 min pour le premier cycle de filtration à environ 70 min pour le dernier (cycle 11), en raison de la perte de charge résiduelle qui augmente avec les cycles de filtration.

(4) Les résultats ont montré une diminution de l'efficacité de collecte des nanoparticules en fin de cycles de colmatage/décolmatage et une augmentation de la résistance du gâteau de particules, expliquées dans ces travaux par l'augmentation de la vitesse interstitielle de filtration. Le gâteau résiduel et la distribution non uniforme du gâteau de filtre sont les principales raisons qui pourraient conduire à une répartition non uniforme de la vitesse de filtration sur la surface du filtre, ce qui contribuerait à augmenter la vitesse interstitielle dans les zones du filtre moins chargées de particules.

En général, ces résultats ont montré une efficacité élevée du filtre à manche pour la filtration de particules submicroniques et nanométriques dans des conditions réalistes rencontrées pour le traitement des fumées d'incinération des déchets.

Dans le **chapitre IV**, une étude expérimentale et théorique a été menée sur l'influence de différents paramètres sur les performances du filtre en géométrie manche et plane. Les paramètres opératoires étudiés étaient l'humidité (3% HR contre 0% HR à 150°C), la

température (150°C contre 24°C), la vitesse de filtration (1,9 $cm.s^{-1}$ contre 1,4 $cm.s^{-1}$) et la présence de réactifs.

Les résultats expérimentaux ont montré que l'humidité a une influence importante sur les performances du filtre à manche à 150°C. Pour un même nombre de particules collectées, l'efficacité de collecte augmente avec l'humidité pour les particules de plus de 110 nm de diamètre, alors qu'aucun effet significatif n'a été observé pour les nanoparticules (particules < 100 nm). En termes d'évolution de la perte de charge, l'humidité est un facteur clé qui provoque l'élévation rapide de la résistance du filtre à manche expliquée par la formation d'un gâteau de particules compacte lors du colmatage en raison de condensation capillaire entre les particules, et l'augmentation des forces d'adhésion entre les particules en présence d'humidité conduisant à un décolmatage du filtre moins efficace en présence d'humidité qu'en air sec. En bref, l'humidité augmente l'efficacité de collecte du filtre à manche mais accélère l'augmentation de la perte de charge et réduit l'efficacité de décolmatage et peut donc conduire à réduire la durée de vie du filtre à manche.

L'influence de la température sur les performances du filtre à manche a également été étudiée expérimentalement dans ce chapitre. En termes d'efficacité de filtration, la collecte des particules est plus élevée à 150°C qu'à 24°C. Cela s'explique par l'influence de la température sur le mécanisme de diffusion brownienne. La force brownienne traduit l'effet des chocs entre les particules et les molécules du fluide environnant. Cette agitation aléatoire est influencée par la température du fluide : plus que la température est élevée, plus la fréquence des chocs entre les molécules et les particules est importante, par conséquent le mouvement des fine particules devient important et leur probabilité de capture par les fibres augmente ce qui explique une haute efficacité à 150°C par rapport à 24°C. Avec le colmatage, l'évolution de l'efficacité est plus rapide à haute température et atteint une efficacité maximale de 99,99% à 150°C contre 99,8% à 24°C.

En termes de perte de charge du filtre, la température n'a pas une influence directe sur la résistance du gâteau de particules formé. Les écarts de valeurs de perte de charge entre 150°C et 24°C s'expliquent par la viscosité du fluide qui augmente avec la température de filtration. Indépendamment de la variation de la viscosité du gaz en fonction de la température, les résultats n'ont montré aucune influence de la température sur la structure du gâteau de particules formé.

Concernant l'influence de la présence de réactifs, les résultats ont révélé que l'efficacité de collecte augmente plus rapidement pour le filtre à manche colmaté uniquement par les

nanoparticules de combustion, mais que dans ce cas le décolmatage est moins efficace, conduisant à une augmentation significative de la perte de charge résiduelle du filtre au cours des cycles de colmatage/décolmatage. Par conséquent, la taille des particules pour les conditions de cette étude est un facteur clé qui affecte l'efficacité de décolmatage du gâteau de particules.

L'influence de la température et de l'humidité sur l'efficacité de filtration théorique (calculée à partir de modèles de la littérature) a été étudiée à 150°C et 24°C pour 1,9 $cm.s^{-1}$ de vitesse de filtration. Les résultats ont montré tout d'abord que les particules de moins de 90 nm de diamètre sont les plus influencées par la température à 150°C par rapport à 24°C. Ceci est conforme aux résultats expérimentaux obtenus en termes d'efficacité. Théoriquement, aucune influence de l'humidité sur l'efficacité de filtration n'a été observée à 150°C (3% HR par rapport à 0%). Cependant, les résultats expérimentaux ont montré que, à une humidité plus élevée, l'efficacité de collecte est significative. Cela peut confirmer l'hypothèse de l'influence de l'humidité sur la compacité du gâteau formé à la surface du filtre en raison de condensation capillaire, non prise en compte dans les modèles étudiés.

L'efficacité de filtration et la perte de charge de filtres plans ont été évaluées durant des colmatages avec l'aérosol de combustion afin d'étudier l'influence de la vitesse de filtration ainsi que du pré-colmatage du filtre (filtre neuf versus filtre lavé). Les principales conclusions obtenues expérimentalement sont:

(1) l'efficacité de filtration diminue avec l'augmentation de la vitesse de filtration, en particulier pour les diamètres de particules compris entre 50 et 140 nm,

(2) les filtres neufs sont nettement moins efficaces que les filtres lavés en début de colmatage,

(3) la taille de particules la plus pénétrante dans le filtre (MPPS) diminue avec le colmatage du filtre de 76 ± 15 à 39 ± 4 nm.

La simulation numérique de l'écoulement d'un mélange de fluide et de particules pour étudier la trajectoire des particules a été décrite par l'intégration Lagrangienne de l'équation de Langevin. Le fluide obéit à une loi de comportement newtonien, et les particules solides sont des sphères. Les résultats de la simulation numérique montrent l'effet notable des paramètres de fonctionnement du filtre sur la trajectoire des particules, en particulier la taille des particules et la température du fluide. En effet, la fluctuation verticale des particules autour de la fibre filtrante à 150°C est plus importante que pour une température de 24°C. Ce résultat indique que la probabilité de collecte des nanoparticules par la fibre augmente avec l'augmentation de la température. D'autre part, l'effet de la taille des particules sur leur

trajectoire est important. Les résultats indiquent clairement que les fluctuations de la trajectoire des particules augmentent avec la diminution du diamètre des particules. En revanche, les résultats ont révélé un effet peu significatif de la vitesse sur le comportement des nanoparticules dans la gamme étudiée expérimentalement (entre et 1,4 et 1,9 $cm.s^{-1}$), mais un effet de la vitesse plus important à partir de 10 $cm.s^{-1}$. La simulation numérique actuelle est un travail préliminaire pour calculer théoriquement l'efficacité du filtre dans des conditions opérationnelles similaires à celles de l'étude expérimentale. Cependant, un travail supplémentaire serait nécessaire pour étudier les mécanismes de capture des particules et pour calculer l'efficacité du filtre, en particulier la modélisation de la structure du filtre et le comportement du fluide à travers le média filtrant.

Mots clés : Incinération de déchets, performances de filtration, filtre à manche, cycle de colmatage/décolmatage, particules submicroniques et nanométriques

Abstract

Filtration performance of a pulse-jet bag filter was evaluated at the laboratory-scale regarding submicronic particles with a nanosized fraction during clogging/unclogging cycles. The particle size distribution was representative to those encountered at the outlet of a nano-waste incineration device at laboratory-scale. The bag filter was operated in conditions as similar as possible to those found in flue gas treatment of waste incineration plants, in terms of temperature, humidity, filtration velocity, injection of sorbent reagents and unclogging conditions. The air flow and the bag filter were heated to 150°C, the water content was maintained in the air flow in the range of 10-12% (3% of relative humidity RH), and filtration velocity throughout the bag filter was fixed at 1.9 $cm.s^{-1}$. A mixture of submicronic suspended particles of activated carbon and sodium bicarbonate, both used in flue gas treatment systems mainly for the removal of dioxins/furans and acid gases, was generated simultaneously with the aerosol representative of combustion emissions.

The study focused on the filtration performance at the beginning of the bag filter's lifetime filter for the 11 first clogging-unclogging cycles before stabilizing the residual pressure drop reached after pulse-jet unclogging. The maximum pressure drop was set at 150 Pa for all filtration cycles. Once the maximum pressure drop was reached, the filter was unclogged using the pulse-jet system. The performance of the bag filter was evaluated in terms of the evolution of pressure drop, fractional and total particle collection efficiencies, during the clogging/unclogging cycles.

Moreover, an experimental and theoretical study was carried out on the influence of different parameters on the filtration performance of bag filter and flat filter, such as influence of humidity (3% RH versus 0% RH at 150°C), temperature (150°C versus 24°C), filtration velocity (1.9 $cm.s^{-1}$ versus 1.4 $cm.s^{-1}$) and the influence of the injection of sorbent reagents.

The main results of this study are: (i) high collection efficiency of the bag filter in representative conditions of flue gas treatment of waste incineration: minimun particle collection efficiency of 98.5% for particle diameter of 74 ± 15 nm (electrical mobility diameter), (ii) influence of residual particle cake at the beginning of the filtration cycles on the bag filter performance, (iii) significant influence of humidity on the porosity of the particle cake due to the capillary condensation of water between the particles in presence of humidity (150°C - 3% RH i.e. almost 100 g of water per kg of dry air). Faster increase of bag filter pressure drop in presence of humidiy (150°C - 3% RH) as compared to the dry conditions (150°C - 0% RH).

Keywords: Waste incineration, filtration performance, bag filter, clogging/unclogging cycles, submicronic and nanosized particles

Contents

List of Figures

List of Tables

Nomenclature

A_{12}	Hamaker constant	[$kg.m^2.s^{-2}$]
A(t)	Random acceleration	[N]
C_D	Drag coefficient	[-]
C_d	Correction term for the diffusion slip flow effect	[-]
C_c	Cunningham coefficient	[-]
C_d'	Correction term for the diffusion slip flow effect	[-]
C_i	Number concentration of generated particles of diameter d_i	[#/cm^3]
C_r	Correction term for the interception slip flow effect	[-]
D	Coefficient of Brownian diffusion	[$m^2.s^{-1}$]
d_{filter}	Bag filter diameter	[m]
d_p	Particle diameter	[m]
d_{50}	Mass median diameter	[m]
d	Particle separation distance	[m]
d_f	Fiber diameter	[m]
d_{pores}	Fiber mean diameter of the pores media	[m]
$E_{d_p}(t_n)$	Fractional efficiency	[-]
E	Electric field	[$N.C^{-1}$]
E_t	Overall collection efficiency of a filter	[-]
e	Radius of fluid envelope	[m]
F_A	Archimedes force	[N]
F_B	Brownian force	[N]
F_{cap}	Capillary force	[N]
F_{el}	Electrostatic force	[N]
F_{ext}	External force	[N]
F_r	Random force	[N]
g	Gravitational acceleration	[$m.s^{-2}$]
G_i	Gaussian distribution of random numbers	[-]
H	Bag filter height	[m]

H_{Ku}	Hydrodynamic factor	[-]
k_B	Boltzmann constant	[$m^2.kg.s^{-2}.K^{-1}$]
h_k	Empirical constant of Kozeny and Carman	[-]
K	Air permeability	[m^2]
K_1	Media filter resistance	[m^{-1}]
K_c	Specific cake resistance	[$m.kg^{-1}$]
K_{th}	Thermophoric diffusion coefficient	[-]
L	Filter thickness	[m]
L'	Cake thickness	[m]
L_{cake}	Overall surface of residual cake	[m^2]
m_p	Particle mass	[kg]
$N_{upstream,dp}$	Particle number concentration upstream of filter	[$particles.cm^{-3}$]
$N_{downstream,dp}$	Particle number concentration downstream of filter	[$particles.cm^{-3}$]
n_0	Ionic concentration of solution	[mol]
n_1, n_2	Number of molecules per unit volume	[m^{-3}]
n_p	Number of charges/particle	[-]
Pe	Peclet number	[-]
Q	Gas flow rate	[l/min]
q_1	Electric charge of particles	[C]
q_2	Electric charge of fiber	[C]
U_f	Filtration velocity	[$m.s^{-1}$]
u_p	Particle velocity	[$m.s^{-1}$]
S_0	Given spectral density	[-]
S_f	Specific surface area of the fibers	[m^{-1}]
S	Filter total surface	[m^2]
Stk	Stokes number	[-]
T	Gas temperature	[K]
T′	Absolute temperature of the particle	[K]
R	Interception number	[-]
Re	Reynolds number	[-]
r_p	Particle radius	[m]

w	Collected particle mass per unit area	[$kg.m^{-2}$]
V_A	Potential interaction	[N]
V_f	Fluid velocity	[$m.s^{-1}$]
V_p	Particle volume	[m^3]
V_{pores}	Pore size volume	[m^3]
V_{total}	Total volume of the material	[m^3]
ν'_0	Gaussian random variable	[-]
Z_p	Particle electric mobility	[$m^2.s^{-1}.V^{-1}$]
z	Distributed random numbers	[-]

Greek letters

$\Delta C_{upstream}$	Experimental uncertainty	[-]
Δt	Time step	[s]
ΔE	Uncertainties related to the filter efficiency measurements	[-]
ΔP	Pressure drop across the filter	[Pa]
ΔP_{cake}	Pressure drop across the cake filter	[Pa]
ΔP_{res}	Residual pressure drop after unclogging	[Pa]
ΔP_0	Pressure drop across the filter media at the beginning of clogging	[Pa]
τ	relaxation time of particle	[s]
τ_b	time step between successive collisions of particle	[s]
τ_F	Time step leading to an appreciable change in particle displacement	[s]
μ	Dynamic fluid viscosity	[Pa.s]
ξ	Filter resistance	[m^{-1}]
γ	Superficial tension of the liquid film	[$N.m^{-1}$]
χ	Dynamic form factor of particle	[-]
μ	Location parameter	[-]
σ	Standard deviation of the particle size distribution	[-]
λ	Mean free path of gas molecules	[m]

η_d	Unit efficiency of fiber collection by Brownian diffusion mechanism	[-]
η_r	Unit efficiency of fiber collection by the interception mechanism	[-]
η_i	Unit efficiency of fiber collection by the inertial impaction mechanism	[-]
η_{dr}	Efficiency of fiber collection by combination of diffusion and interception mechanism	[-]
ρ_p	Particle density	[$kg.m^{-3}$]
ρ_f	Fluid density	[$kg.m^{-3}$]
ρ_{eff}	Effective density	[$kg.m^{-3}$]
ε_i	Filter media porosity	[-]
α	Packing density	[-]

Abbreviations

BC	Black Carbon
CPC	Condensation Particle Counter
DMA	Differential Mobility Analyser
MPPS	Most Penetrating Particle Size
NP	Nanoparticle
PSD	Particle Size Distribution
PTFE	Polytetrafluoroethylene
SMPS	Scanning Mobility Particle Sizer
SEM	Scanning Electron Microscope

Framework

There is no French or European regulation on the management of manufactured nanomaterials, regarding either the manufacturing, use or end of life. Such nano-containing products or nano-waste can end up in municipal solid waste or hazardous waste incineration plants. Studies (ADEME CORTEA NanoFlueGas Project No. 1181C0088: Le Bihan et al., 2014; Ounoughene et al., 2015; Walser et al., 2012) demonstrated the presence of the original nanoparticles, either alone or as aggregates, in the raw fumes leaving the primary chamber during the incineration of nanowaste in conventional incineration plants. But nanoparticles can be responsible for some health and environmental problems. Indeed, toxicological studies clearly demonstrated that their very small size is a key element in toxicity, particularly non-soluble particles (Ostiguy et al. 2006). This is why special attention is paid to the treatment of incineration fumes, in particular to the efficiency of processes dedicated to the removal of particles.

Incineration is the thermal treatment at high temperature of waste in order to convert the undesirable materials into char, flue gas containing particles, and heat. The process is conducted within a special furnace designed for burning these materials. During the incineration, the particles are generally formed from the inorganic components of the waste and can be accumulated in the incineration device or carried out by the flue gas.

The air pollution control techniques used must achieve compliance with standards to control the ambient air quality and reduce the exhausted hazardous air pollutants from the flue gas. A variety of physical processes can be used to remove coarse and fine particles from polluted airstreams, such as cyclones, bag filters, electrostatic precipitators and scrubbers.

Bag filter is one of the common particle collection device used in industries to remove suspended particles from flue gas treatment lines. It is generally housed in a casing commonly known as a baghouse, which is a gathering of several hundreds cylindrical bags. At the bottom of baghouse, a hopper is installed to remove continuously the dust collected from the bags during filtration.

There are many studies in the literature (Alkiviades et al. 1976; Billings 1966; Endo et al. 1998; Song et al. 2006; Leung & Hung 2008;..) which focus on the performance of fibrous filters, mostly in flat geometry and ambient air conditions. For example, the influence of particle size or filtration velocity on the change in filter pressure drop and particle collection efficiency was studied both experimentally and theoretically. Regarding bag filter configuration, few studies are available (Saleem et al. 2011; Park 2012; Förster et al. 2016; Cirqueira et al. 2017). However, the geometry of the filter, the special operating conditions

(often high temperature and humidity conditions) or the on-line unclogging system are parameters which can greatly affect the performance of the bag filter compared to the filtration theory.

The aim of this thesis is to study the filtration performance of a bag filter with a synthetic aerosol emitted from nanowaste incineration at laboratory scale but representative of the conditions encountered within incineration flue gas treatment, in terms of temperature, humidity, filtration velocity and clogging/unclogging cycles. Moreover, the influence of operating conditions on the filtration performance was studied, such as the gas humidity, temperature, filtration velocity or nature of clogging particles.

The studies described in this dissertation were conducted as part of a co-supervised thesis between IMT Atlantique and Université Mohammed V- Faculté des sciences, co-funded by the program Hubert Curien TOUBKAL (campus France + CNRST) and TREDI – Groupe Séché. According to the previously exposed research objectives, the manuscript is organized as follows:

Chapter I proposes a bibliographic review on the aerosol science and filtration theory of fibrous media, especially the mechanisms of particle collection by fibrous filters and the evolution of pressure drop and collection efficiency as a function of cake filter. The literature review about the influence of operating conditions on filtration performance is also provided in this chapter.

Chapter II presents the methodology for the experimental studies at the laboratory-scale. The two experimental setups and the methodology adopted to evaluate the performance of two filters geometries (flat filter and bag filter) are described.

Chapter III presents the results of the filtration performance of the bag filter for clogging/unclogging cycles regarding the filtration of submicronic and nanosized particles. This under operating conditions as close as possible to those found in waste incineration plants in terms of gas filtration velocity, concentration of particle reagents, gas temperature and humidity, pressure and duration of the cleaning pulse-jet.

Chapter IV presents the results regarding the influence of operating conditions on the filtration performance. The investigations were carried on the influence of humidity, temperature, and characteristics of the particles used for clogging on the bag filter performance, and the influence of filtration velocity and filter aging on the performance of filter in flat configuration. To complete the experimental results, numerical investigations were conducted on the influence of gas temperature, particle size and velocity.

Finally, the general conclusion summarizes the main conclusions achieved from the work presented in this manuscript.

Chapter I State of the Art

I Introduction

Over the past few decades, the industries exhibited a growing interest for the implementation of nanotechnology for producing nanomaterials with increased performance. In 2008, the global markets of nanotechnology-based products were estimated around $200 billion and the production has been increasing at a rate of 25% per year (Roco et al. 2011). To date, manufacturing nanomaterials is still in a growing economy (Charitidis et al. 2014) and is often seen as a new industrial revolution. In many areas of the world, nanoparticles have become an essential part in human daily life. They are present in different fields and application, such as textile, medicine, food and fertilizers. In fact, the main reason of developing nanomaterials is that they create unique properties compared with coarse particles of the same materials. The products made of nanomaterials can be stronger, lighter, more durable, more reactive, UV resistant, anti-stain, anti-shrinkage in the fabrics or better electrical conductors.

Nanotechnology is the production and design of the materials by their manipulation at molecular level and controlling their shape and size at nanometer scale in order to exploit the unique quantum and surface phenomena that such matter exhibits at the nanoscale, increase of the surface area, which makes the materials more chemically reactive and affect their strength or electrical properties (Aslan et al. 2005).

Many different existing manufactured nanomaterials are produced industrially (Figure 1), such as: TiO_2, ZnO, FeO_x, AlO_x, SiO_2, CeO_2, Ag, Carbon Nanotubes (CNTs), fullerenes (buckyballs**),** and Quantum Dots (QD).

According to the second annual declaration of the first of June 2014, the quantities and uses of substances at nanoscale produced, distributed or imported in France are as the following (R-Nano):

- 10,417 submitted declarations (compared with 3,409 in 2013)
- 1,713 active accounts corresponding to declarants in France and to European entities based outside France (83% increase compared to 2013)
- more than 1,500 reporting entities (compared to 732 in 2013)
- In France: 274 667 t produced and 122 464 t imported

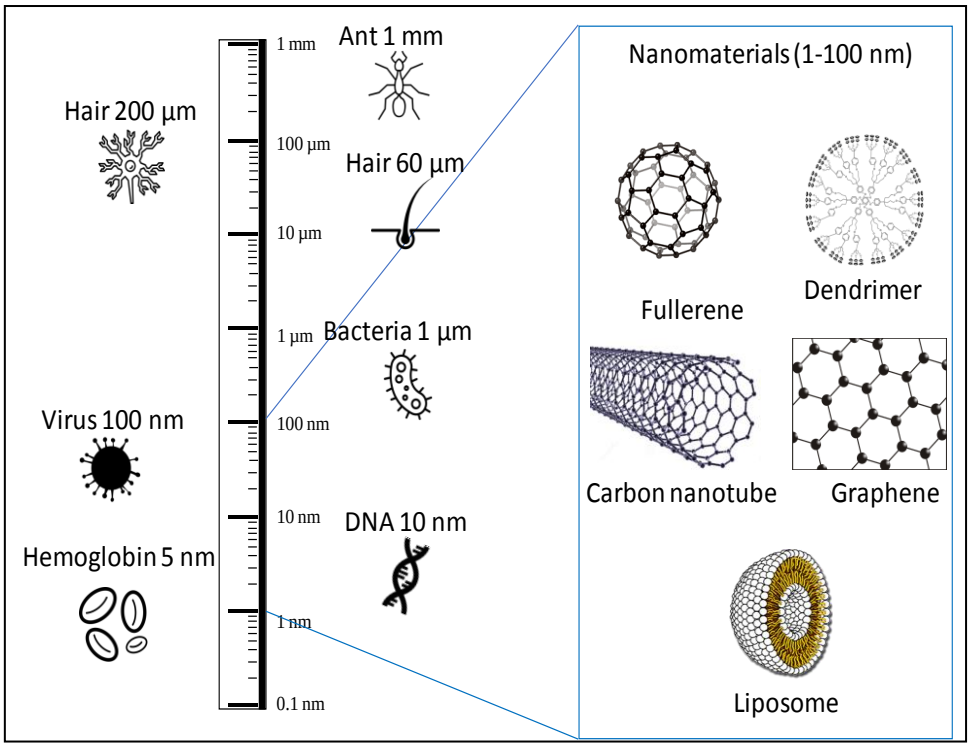

Figure 1: Different manufactured nanomaterials

As the demand of nanomaterials products increases, there is a growing challenge in assuring the treatment of their waste. Nano-waste management is considered as an essential condition to ensure the safety of their end-of-life.

Different types of wastes containing nanomaterials could be distinguished, such as wastes generated during manufacturing of nanomaterials, wastes generated during product use, (i.e. degradation, abrasion), and wastes generated from the disposition process such as incineration.

To date, there are no French or European regulations on the management of manufactured nanomaterials, whether at the level of manufacture, use, or end-of-life. No specific treatment for wastes containing nanomaterials was determined; they are considered as any other waste and undergo the Waste Framework Directive. Furthermore, no measure was designed specifically for management of possible risks associated to waste containing nonmaterial.

II Nanomaterials end-of-life

Nanomaterials contained in products are ultimately entering the waste stream and find their way into disposal method such as incineration or landfills. According to the Report of Design and Operating Criteria (1992), the waste containing nanomaterials is the main sources of anthropic nanoparticles released to the environment. Thereby, controlling the release of

nanoparticles from the disposal centers of waste containing nanomaterials is an important topic.

Currently, incineration is considered as an efficient high-temperature treatment of industrial waste. It reduces the volume of materials while producing heat and converts it into a flue gas, and ashes that can be safely disposed of (**Figure 2**). The nature of aerosol and gas produced from the incineration process depend on the nature of waste materials and incineration conditions and process mastery. During the waste incineration, H_2O and common but climate-relevant compounds are emitted, (CO_2 …), and occasionally some pollutants may be released beyond an acceptable value, like NO_x and acidic components (HCl, SO_x …).

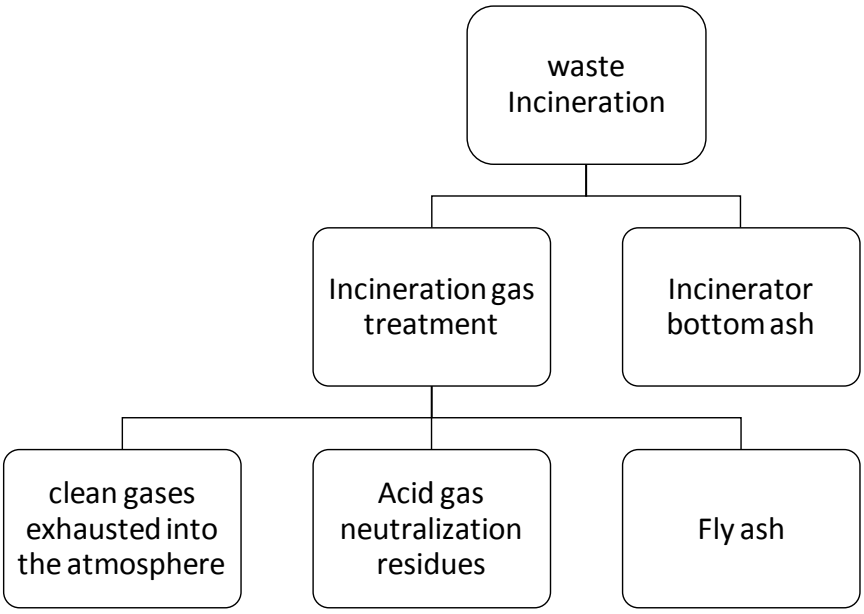

Figure 2: Exhaust of waste incinerators

II.1 Incineration of nano-wastes

In the literature, degradation of nanocomposites during incineration has attracted many authors in order to study their behavior (Fornes and Paul 2003; Marney et al. 2008; Lewin et al. 2006; and Bouillard et al. 2013). As a function of the waste natures and their initial states, ultrafine particles can be emitted from the incinerators in different ways. In certain conditions, during incineration, nanoparticles can become aerosolized or can form aggregates, this transformation in materials state may be the main reason to change the pathway of incinerated nanoparticles (Holder et al. 2013). For example, the incineration of nanoparticles suspended in solid or liquid waste is more likely to form aggregates. Depending on the combustion conditions, these aggregates may not entirely burn.

Recently Ounoughene et al. (2015), have investigated the behavior of PA6/HNTs nanocomposite (nylon-6 incorporating halloysite nanotubes) during the incineration at 850°C with high oxygen/fuel contact for at least 2 s residence time for the combustion gas.

The main purpose of this work was to study the hazardous compounds originating from the incineration of wastes containing nanomaterials from nanocomposites. The results showed the presence of the nano-objects in the raw combustion aerosol and in solid residues, which is likely to impact both flue gas and gas treatments.

II.2 Incineration technology

Operating conditions of waste incineration change as a function of the waste nature. The key drivers used to classify waste nature are especially: their chemical and physical composition (e.g. particle size composition), waste thermal characteristics, (e.g. calorific value), and humidity levels of the waste, etc.

In order to achieve efficient incineration and maximize the performance of incinerator, the following parameters must be continuously controlled: temperature, oxygen, carbon monoxide, hydrogen chloride (HCl) and possibly total hydrocarbon (Basel Convention Technical Guidelines on Incineration on land). Thus, the incinerators devices must be equipped with specific monitoring system for controlling and reporting functions continuously during the gas emissions. In the case of waste heat boiler installation, which is used to recover the energy from the exhaust energy, the monitors of CO and O_2 is placed downstream of the boiler to improve sampling and gas conditioning, where CO is considered as a key indicator of the combustion performance.

As a function of waste natures and their compositions, the incinerator system can be defined for an efficient disposition. Thus, the management option for certain types of waste requires extensive characterization to determine an appropriate system. Some kind of waste, such as municipal solid waste can be incinerated in several incinerators systems like: travelling grate, rotary kilns, and fluidized beds. However, their incineration by non basic furnace system, such as fluidized beds, requires some specific pretreatment and/or the selective collection of the waste in order to achieve the treatment in certain particle size range.

Incineration of sewage sludge requires some pretreatment in order to reduce the content of water and moisture level by drying or the addition of supplementary fuels to ensure stable and efficient incineration. Sewage sludge are usually incinerated in rotary kilns, multiple hearth,

or fluidized bed incinerators. While the incineration of hazardous and medical waste is commonly taking place in rotary kilns.

In the following section, some characteristics of the most used incinerators system are presented. Note that significant part of the following paragraph is based on BREF 2006, currently in course of modification.

Grate incinerators:

Approximately 90% of systems treating the municipal solid waste in Europe take place in Grate incinerators. According to the legislation Directive 2000/76/EC, the appropriate conditions for efficiency combustion of waste is fixed at minimum temperature of 850°C for 2 s of residence time with minimum oxygen content of 6% (modified by the most recent EC Directive). In the case of hazardous wastes with a content of 1% of halogenated organic substances (chlorine), the incineration temperature must be raised to 1100°C for 2 s of residence.

Rotary kilns:

Rotary kiln is incineration technology used almost for any kind of waste regardless their composition. In general, this technology is commonly applied high temperature range (note that gasification is not incineration…), up to 1450 °C (as a high temperature ash melting kiln). The operating temperature depends on the incinerated waste nature and their composition, for example incineration of hazardous wastes requires temperatures in the range of 900 – 1200°C.

Fluidized beds:

Fluidized beds are especially appropriate for the incineration of dried sewage sludge and Refuse derived fuel (RDF). The fluidized bed is an inclinator composed of double combustion chamber, at the bottom of the device, a bed of sand or ash on a grate is fluidized with air where some process of waste takes place such as drying, volatilization, ignition, and combustion.

The waste is fed continually into the fluidized bed from the top or side of combustion chamber. The temperature in the chamber combustion can be varied between 650 and 950°C. In the free space above the fluidized bed material, which is designed to allow retention of the gases in a combustion zone, the temperature is in the range of 850 and 950 °C, while the temperature of the bed is around 650°C.

Multiple hearth furnaces:

The multiple hearth is composed of a cylindrical lined steel jacket, and a rotating sleeve shaft with attached agitating arms. The waste is fed at the top of the incinerator and moves through the different hearths. The upper section of hearths provides waste drying, where the waste gives up moisture while the hot flue-gases are cooled. The incineration is operated at the central hearths with limited temperature of 980°C.

II.3 Examples of pollutants in waste incineration raw fumes

Incineration is a combustion process by which refuse and air are reacted to produce an acceptable gaseous effluent and an inert solid residue. Incineration of industrial waste generates different kind of compounds, typically H_2O and CO_2 (a harmless but climate-relevant gas) and can release some pollutants (acidic components, dust…), particularly in case of poor mastery of the whole process. All gases and aerosols in suspension at the outlet of the furnace (*i.e.* before the Air Pollution Control -APC- systems) are grouped together under the name of "raw fumes". These fumes are gaseous residues of combustion, which have been formed during thermos-chemical processes. The primary particles in raw fumes have almost the diffusion-equivalent diameters less than 0.5 µm, but the particles can be much larger because of agglomeration, especially at higher fume concentrations. The fumes are mainly composed of (Le Gléau 2012):

- Air component: N_2, O_2...
- Conventional combustion gases: CO_2, H_2O;
- Gaseous pollutants which may be a function of the composition of the fuel: CO, NO, NO_2, SO_2, HCl, HF, volatile metals, PAH...;
- Particles: soot, unburned fuel, fly ash, particulate matter condensation.

II.3.1 Nitrogen oxides

Nitrogen oxides (N_2O, NO, and NO_2) are formed by reaction chains from the nitrogen contained in the waste and the molecular nitrogen in the combustion air. The main oxides formed during combustion are nitrogen monoxide (NO) and nitrogen dioxide (NO_2). The name NO_x is relative to the mixture of these two constituents, but remains rich in NO: about 95% NO and 5% NO_2 during the household waste incineration.

Concentrations of NO_x from the incineration center for household and similar wastes are between 150 and 450 $mg.Nm^{-3}$ before treatment and 1000 to 1500 $mg.Nm^{-3}$ for hazardous waste incineration units.

Two types of NO_x can be distinguished:

- NO_x from the conversion of the nitrogen contained in the waste: combustible NO_x
- NO_x from the conversion of the nitrogen contained in the combustion air: thermal NO_x

Considering the combustion temperatures (T <1600°C), 70 to 80% of the NO_x formed are derived from combustible nitrogen, i.e. solid and liquid waste.

II.3.2 Sulfur dioxide

If the treated waste contains sulfur in organic form or as sulfates, it is mainly SO_2 that will be created according to the following reaction: $S + O_2 \rightarrow SO_2$.

Sulphur dioxide (SO_2) is cleaned from flue-gases by the injection of chemical or physical sorption agents.

The formation mechanism of sulfur oxides occurs in certain temperature ranges. From 250°C, sulfur is oxidized by oxygen to sulfur dioxide or sulfur dioxide (SO_2). Between 300°C and 500°C, sulfuric anhydride (SO_3) is formed by oxidation of SO_2 by the reaction:

$SO_2 + 1/2\ O_2 \rightarrow SO_3$

In household waste incineration, the proportion of SO_3 can reach 5% at the inlet of the smoke treatment line.

II.3.3 Carbon monoxide and carbon dioxide

The presence of carbon monoxide in incineration flue gas is mainly produced during the incomplete combustion of materials containing carbon. CO is produced when there is no enough oxygen locally and/or an insufficiently high combustion temperature (T<800°C). While in case of sufficient air and temperatures (T≈1000°C), the CO is completely converted into CO_2 during incineration process. For example, for 1 ton of municipal waste combustion, about 0.7 to 1.7 tons of CO_2 is generated. Carbon dioxide is not considered a pollutant, but excessive quantities of this gas within the atmosphere might produce a greenhouse effect.

The values of CO released into the atmosphere during the incineration of municipal waste and hazardous wastes are respectively in the range of 5-50 $mg.Nm^{-3}$ and <30 $mg.Nm^{-3}$. While for CO_2 the corresponding values are respectively 5-10 % and 5-8 %.

II.3.4 Dust

The produced dust from the industrial waste incinerators consists of fine solid particles that come from various sources and become part of the air or other gases. The dust formed during the combustion can be distinguished in two types, mainly fly ash and soot. These pollutants are different in composition and in morphology and particle size distribution. Dust can be also the carrier of certain pollutants such as heavy metals trapped in dust due to the vapor

pressures of their compounds, as contained in the flue-gas (mainly oxides and chlorides). Thereby, the separation of these pollutants from the flue-gas depends mainly on an effective collection of dust.

II.3.4.1 Fly ash

Fly ash is a powdery particle generated from waste incineration, usually grey in color, abrasive, mostly alkaline, and often refractory in nature. The incomplete combustion of particles is the main reason of fly ash formation (Chang et al. 2000) in flue gas, whose the size is generally between few micrometers and 100 μm, and mostly it consists of predominant spherical particles of solid or hollow shape (Ahmaruzzaman 2010), with specific area ranging from 170 to 1000 $m^2.kg^{-1}$ (Roy et al. 1981).

Fly ash is considered as a contaminated powder because of the content in toxic elements condensed from the flue gas (Ahmaruzzaman 2010). Inside the incineration system, an important quantity of fly ash is precipitated in the furnace and the boiler (bottom ash) while the remaining particles may leave the furnace chimney as coarse fly ash. The fly ash may contain an important quantity of heavy metals and harmful substances such as cadmium, lead, and dioxins (Hinozaki et al. 1998). However, the characteristics of fly ash especially physical and chemical characteristics are widely depending on the operating conditions, the type of incinerator and the Air Pollution Control system design. The common chemical compositions found in fly ash from for example municipal solid waste are: Si, Al, Fe, Mg, Ca, K, Na and Cl, while the common oxides are: SiO_2, Al_2O_3, CaO, Fe_2O_3, Na_2O, and K_2O.

II.3.4.2 Soot

Soot is one of the common types of aerosol particle that can be generated during the incineration of waste, which contains carbon substances, at certain conditions, mainly at high temperature of incineration and low oxygen concentration (Niessen 2010). Its main characteristic is a dark substance with high-optical density flue gas emission. Soot formation is considered as critical dysfunction of incineration process. Current TOC emission limit is typically below 10 mg/Nm³ (daily average, dry flue gas at 11% O_2) (BREF 2006).

III Aerosol classification

The size distribution, nature and geometry of particles are important characteristics that can influence their behavior. The particles in industrial gas-solid flows are usually non-spherical and polydispersed. Under certain conditions, the kinetic theory of gases can be applied to express their movements of particles and their deposition. For the sake of simplicity of mathematical models, the application of aerosol physics theories requires considering a spherical shape for the studied particles. Nevertheless, the form of particles in reality has irregular geometry (Züttel et al. 2008).

III.1 Equivalent diameter

For particles of irregular shape, several equivalent diameters can be defined either in terms of geometry parameters or flow dynamic characteristics. Thereby, for an irregular particle we can define more than one particle diameter.

III.1.1 Aerodynamic and stokes diameter

The aerodynamic diameter d_a is the parameter more used in filtration to characterize the dimension of particles. It is the diameter of a spherical particle whose density is 1 g.cm^{-3} and have the same velocity of fall in the gas as the studied particle.

The stokes diameter is the diameter of a spherical particle having the same drop velocity and the same density as the considered particle (**Figure 3**, Renoux & Boulaud 1998).

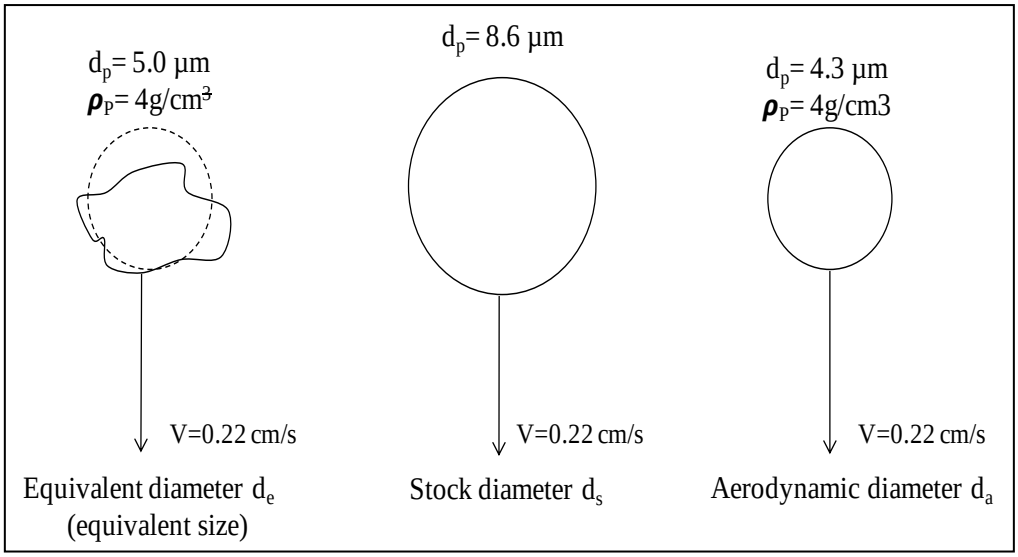

Figure 3: Different types of diameter

III.1.2 Electrical mobility diameter

Electric mobility corresponds to the velocity acquired by a particle of the charge $n_p.e$ in an electric field E. The electric mobility (Z_p) can be defined by the equation (2):

$$Z_p = \frac{V_{te}}{E} = \frac{n_p e C_c}{3\pi\eta \mathrm{d_e}} \quad (2)$$

V_{te}= terminal electrostatic velocity of the particle

C_c= Cunningham slip factor (dependent on particle diameter)

η = viscosity of surrounding gas

d_e= electrical mobility diameter of the particle

The electrical mobility diameter d_e is then defined as the diameter of a spherical particle having the same electric mobility Z_p as the particle in question according to the following equation (3):

$$d_e = \frac{neC_c}{3\pi\eta Z_p} \quad (3)$$

III.2 Particle size distribution

The particle number distribution (**Figure 4**) represents the particle number concentration as a function of particle diameter; particle distribution can also be represented as a function of particle mass concentration. The particle distribution can be gathered in class widths Δdp_i, the number of particles ΔN_i included in each class Δdp_i is counted. Two models of distribution can be distinguished for particles: normal and log-normal distribution (**Figure 4**).

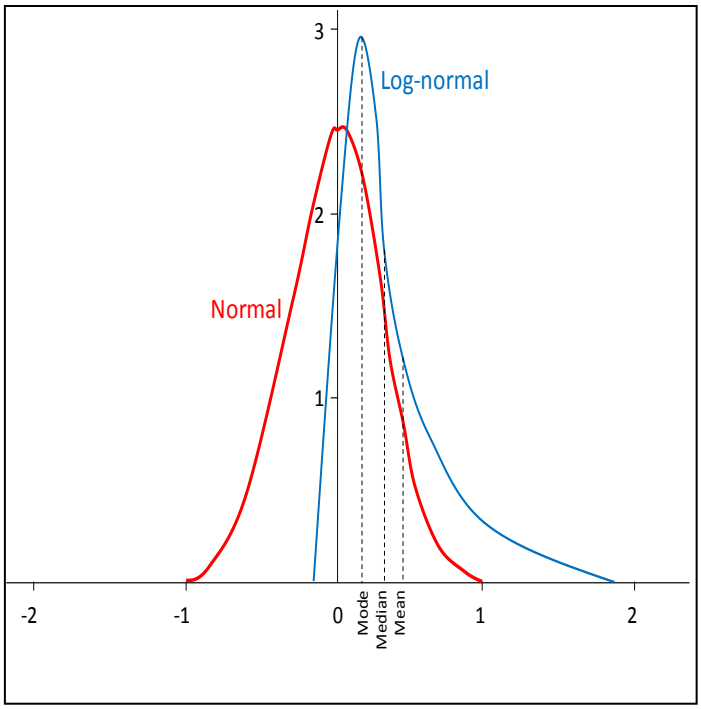

Figure 4: Normal and log-normal distribution

The normal distribution is a symmetrical curve where 68.3% of particles have a dimension between $\bar{d}_p - \sigma$ and $\bar{d}_p + \sigma$. While for lognormal distribution, 68.2% of particles are within the size of $\bar{d}_g/\sigma_g$ and σ_g.

III.2.1 Normal distribution

Normal or Gaussian distribution is the more used probabilistic model to describe the random variation for many scientific disciplines (Limpert et al. 2001). The main characteristic of the normal distribution is the central limit theorem. The general formula for the probability density function of the normal distribution is given by the equation (4):

$$f(x) = \frac{e^{-\left((d_p - \bar{d}_p) - \mu\right)^2 / (2\sigma^2)}}{\sigma\sqrt{2\pi}} \qquad (4)$$

Where d_p is the particle diameter, μ is the location parameter and σ is the standard deviation. The case where $\mu = 0$ and $\sigma = 1$ is called the standard normal distribution.

III.2.2 Log-normal distribution

A Log-normal distribution is a continuous probability distribution of a random variable X whose logarithm $Y = \ln(X)$ is normally distributed, with "ln" denoting the natural logarithm. The general formula for the probability density function of the lognormal distribution is writing as (5):

$$f(x) = \frac{1}{x\sigma\sqrt{2\pi}} e^{\left(-\frac{1}{2\sigma^2}(log(x)-\mu)^2\right)} \quad (5)$$

III.3 Simulation of particle motion and deposition

The following section describes the trajectory of a system of particles by the Lagrangian approach applied on the movement equation. The study requires a detailed description of different forces applied on particles carried by gases and treated individually with assumption of spherical solid form.

III.3.1 Method of Monte Carlo

The Monte Carlo Simulation is a technique used to calculate a numerical value by random processes. In other words, it is a probabilistic technique, commonly used in particle physics. It is applied by (Ermak & Buckholz 1980), to calculate the motion of the particles from the Langevin equation by Lagrangian integration and takes into account different forces such as drag forces, Van der Waals forces and electric Coulomb forces.

The Brownian particle trajectory is thus described by the following Langevin equation (6) (Ermak & Buckholz 1980):

$$m_p \frac{dv(t)}{dt} = F_d(t.X(t)) + \sum F_{ext}\big(t.x(t)\big) + m_p A(t) \quad (6)$$

With $A(t)$ the stochastic acceleration which depends only on time and represents the Brownian motion. $X(t)$ the particle trajectory is given by the formula (7):

$$\frac{d(X(t))}{dt} = v(t) \quad (7)$$

And the drag force F_d is proportional to the difference between the fluid velocity u_f and that of the particle u_p, given by the equation (8)

$$\text{with} \quad F_d = -\mathrm{C_D}\frac{\pi \mathrm{d_p^2}}{8}.\rho_\mathrm{f}.\left\|\mathrm{u_p} - \mathrm{u_f}\right\|(\mathrm{u_p} - \mathrm{u_f}) \quad (8)$$

C_D is the drag coefficient, a dimensionless number whose expression varies according to the flow regime which can be distinguished as a function of the particle Reynolds according to the following equation (9):

$$C_D = \frac{d_p \rho_f \|u_p - u_f\|}{u_f} \quad (9)$$

The next step is to arrange the first two equations in a system of ordinary equations; the purpose is to integrate the term of time to determine the velocity and position of each particle (Lantermann & Hänel 2007):

$$\begin{pmatrix} \frac{dv(t)}{dt} \\ \frac{dx(t)}{dt} \end{pmatrix} = \begin{pmatrix} -\beta I & 0 \\ I & 0 \end{pmatrix} \begin{pmatrix} v(t) \\ x(t) \end{pmatrix} + \begin{pmatrix} \beta u(t) + F_{ext}(t)/m_p \\ 0 \end{pmatrix} + \begin{pmatrix} A(t) \\ 0 \end{pmatrix} \quad (10)$$

The fluid velocity and the forces must be constant during the time unit $\Delta t = t - t_0$. With an identical matrix. So the complete solution of the (10) equation is written as (11):

$$\begin{pmatrix} v^{n+1} \\ x^{n+1} \end{pmatrix} = B^n \begin{pmatrix} v^n \\ u^n + \frac{1}{m_p \beta} F_{ext}^n \end{pmatrix} + \begin{pmatrix} 0 \\ x^n \end{pmatrix} + \begin{pmatrix} z_1 \sigma_v \\ z_1 \frac{\sigma_{vx}}{\sigma_{vx}} + z_2 \sqrt{\sigma_x^2 - \frac{\sigma_{vx}^2}{\sigma_v^2}} \end{pmatrix} \quad (11)$$

With B^n is given by the matrix (12):

$$B^n = \begin{pmatrix} e^{-\beta \Delta t} I & \left(1 - e^{-\beta \Delta t}\right) I \\ \frac{1}{\beta}\left(1 - e^{\beta \Delta t}\right) I & \left[\Delta t - \frac{1}{\beta}(1 - e^{\beta \Delta t})\right] I \end{pmatrix} \quad (12)$$

The proof of this equation is well detailed by (Lantermann & Hänel 2007).

F_{ext} represents the external forces exerted on the particles such as drag forces electrical force, etc.

III.4 Forces acting on particles

Important part of the following paragraph, based on Guiraud (2004), illustrates the main exerted forces on a solid particle:

III.4.1 Weight and Archimedes principle

The weight is the commune force that is applied almost on particles of different size and shape, is defined according to the relation (13):

$$P = m_p . g \quad (11)$$

Where m_{p} is the particle mass. The Archimedes force (F_A), opposed to the fluid volume weight can be defined by the relation (14)

$$F_A = -V_p \rho_f g \quad (12)$$

With V_p the particle volume and ρ_f is the fluid density.

III.4.2 Drag force

One of the major forces applied on the fluid particles is the drag force (F_D), the force which opposes the relative movement between the particle and the fluid surrounds it (fluid friction force).

For spherical particles, the general expression of drag force is given by (15):

$$F_D = \frac{F_{D,Stokes}}{C_c} = \frac{3\,\pi\,\mu_g\,u_p\,d_p}{C_c} \quad (15)$$

With u_p is the particle velocity, and C_c is the Cunningham coefficient. The balance between this thermophoric force and the drag force leads to the expression of the thermophoric diffusion coefficient and the thermophoresis rate according to the following equation (16):

$$\frac{3\pi\,\mu_g\,v_{th}\,d_p}{C_c} = K_{th}\,\frac{3\pi d_p}{C_c}\,\frac{\mu_g^2}{\rho_g}\,\frac{\nabla T}{T_g} \quad (16)$$

And $v_{th} = K_{th}\,\frac{\mu_g}{\rho_g}\,\frac{\nabla T}{T_g}$

with K_{th} the dimensionless thermophoric diffusion coefficient, depends mainly on the number of Knudsen and the ratio of the thermal conductivities gas / particle described as temperature gradient inside the particle.

III.4.3 Added mass force

Another force exerted on an isolated particle is the added mass force. This force represents the inertia of the fluid attached to the particle. The latter seems more difficult to accelerate, as if its mass was more important.

This force has little influence on solid particles which can be considered mostly neglected. On the other hand, it is one of the predominant phenomena in the case of bubble flow.

III.4.4 History force

The force of history translates the setting up of the viscous effects around the particle. The viscous stress needs a certain period for establishment at the interface. To consider the force of history is to take account of this delay, the history of the particle.

The force of history is mostly neglected, the other phenomena generally acting more quickly on the dynamics of the particle.

III.4.5 Brownian force

The Brownian force (F_B) translates the effect of the shocks between the particle and the molecules of surrounding fluid during the motion of random agitation. The Brownian force, defined by the equation (16) has an increasing influence as the particle diameter decreases.

$$\mathrm{F_B} = m_p G_i \sqrt{\frac{\pi S_0}{\Delta t}} \tag{16}$$

With G_i is the Gaussian distribution of random numbers whose variance is 1 and the mean is zero, Δt is the step time. and S_0 is the given spectral density.

The influence of the Brownian force is almost localized in the viscous sublayer of the fluid flow. The force is important with depositing submicron aerosols on the wall, and especially with decreasing of particle size.

III.4.6 Electrostatic force

Particle carrying a charge q submits, in presence of electric field E, an electrostatic force given by the following formula (17):

$$F_{el} = q.E \tag{17}$$

When subjected to this electric field, the particle acquires a velocity V_{te} such that $V_{te} = Z.E$ with Z is the electric mobility of the particle [$m^2.s^{-1}.V^{-1}$].

This greatness has for expression (18):

$$Z = \frac{q}{3\pi d_p \mu_f} \tag{18}$$

The velocity acquired by the particle is such that the drag force balances the electric force. It should be noted that electrical fields can be created by electric charges appearing on the surface of insulating walls after friction of the air flow (triboelectric effect, generally for walls made of polymers: PVC, neoprene, etc.). The deposition of charged particles can thus be modified.

III.4.7 Lift force

The lift force reflects the effects of speed gradients on a particle. In fact, a particle placed in a sheared flow is not subjected to the same fluid velocities and their extremities. This induces a migration of the particles towards the high velocity zones.

III.4.8 Thermophoresis effect

In the presence of a temperature gradient, the particles migrate from the areas of high temperature to the areas of lower temperature, particularly at the approximation of the wall: this is called the phenomenon of thermophoresis, where the force can be written as (19):

$$F_{th} = \frac{-3\pi\mu_f^2 d_p H}{2\rho_f T} . \frac{dT'}{dy} \quad (19)$$

With dT'/dy is the temperature gradient in the y-direction, T' is the absolute temperature of the particle, and H is the factor taking into account the temperature gradient inside the particle. Different models exist in the literature to evaluate the effect of thermophoresis for particles. For instance, according to Sagot (2013), the model of Beresnev and Chernyak (1995) is the most relevant to evaluate the effect of thermophoresis for spherical particles.

III.4.9 Turbophoresis

Turbophoresis is the movement of inertial particles from the area of high turbulence to the area of lower level of turbulence. The particles are migrating towards solid boundaries in turbulent flows similarly to thermophoresis phenomena. Turbophoresis is one of the mechanisms of particle deposition in turbulent boundary layers and requires the presence of inhomogeneities in the flow.

III.4.10 Other forces

Other phenomena can still be taken into account such as the Coriolis force due to the rotation of the Earth, the photophores is force due to the incidence of a light ray on the particle, the phoresis diffusion force due to concentration gradients constituents of the mixture, for example in the case of condensation of vapor in the wall.

III.5 Adhesion and entrainment force

The deposition of the submicron particles depends on the intermolecular forces. Currently, few studies take these forces into consideration. Given the computational complexity, a large majority of authors consider that all particles that touch the solid obstacle (fiber or another deposited particle) are immediately captured.

III.5.1 Capillary forces

The capillary force is due to the formation of a film by capillary condensation of a vapor between the particle or a surface and particles. According to Hinds (1982), for a perfect

contact between a sphere and a flat surface and a relative humidity greater than 90%, the capillary force F_{cap} is written as (20):

$$F_{cap} = 2\pi\gamma d_p \tag{20}$$

Where γ is the liquid-air surface tension (force/unit length).

The capillary force between two particles, as illustrated in the **Figure 5** is given by the relation (21):

$$F_{cap} = 4\pi\gamma \frac{cos(\theta_1 + \beta_1) + cos\theta_2}{2} . \frac{R_1 . R_2}{R_1 + R_2} \tag{21}$$

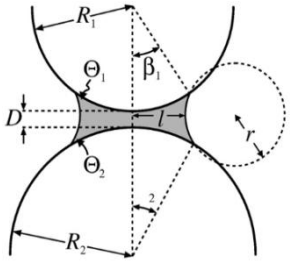

Figure 5: Capillary condensation between two spherical surface particles (Butt & Kappl 2009)

The presence of humidity increases the adhesion forces between the particles. Joubert (2009) explained that according to Butt & Kappl (2009) even for conditions well above dew point, liquid water is formed by capillary condensation at the outer roughness or pores of the particles. According to Feng & Yu (1998), this presence of water on the surface of the particles leads to the formation of liquid bridges between them and therefore to a capillary force which limits the relative movement between the particles.

III.5.2 Potential interaction

The potential interaction V_A between two spheres of radius $r_1$and r_2 having a separation distance d between their surfaces is given by the form (22):

$$V_A(D) = \mathrm{e}\frac{A_{12}}{6d}\frac{r_{p.1} r_{p.2}}{r_{p.1} + r_{p.2}} \tag{22}$$

With A_{12} is the Hamaker constant, used for measuring the dispersion interaction power between the colloidal particles. The theoretical expression of this quantity is:

$$A_{12} = \pi^2 n_1 n_2 C_{12}$$

With n_1 and n_2 are the number of molecules per unit volume, and C_{12} is a constant dependent on the polar characteristics of particles.

For the case of a particle and a plane, the expression of V_A is given by (23):

$$V_A(d) = \mathrm{s}\frac{A_{12}r_p}{6d} \tag{23}$$

While the potential due to the electrostatic attractions V_R is written as (24):

$$V_R = \frac{64n_0K_BT}{{K_D}^{-1}}\gamma^2\exp\left(-DK_D\right) \tag{24}$$

With n_0 the ionic concentration of the solution and γ the constant whose calculation depends on the potential at the surface of the particle. Hence, the force of interaction between two spheres is given by (25):

$$F_1(D) = -\frac{-64n_0K_BT}{{K_D}^{-2}}\gamma^2\exp(-DK_D) + \frac{A_{12}}{6D^2}\frac{r_{p.1}r_{p.2}}{r_{p.1}+r_{p.2}} \tag{25}$$

On the other hand, the force of interaction between particle and plane is given by (26):

$$F_2(D) = -\frac{-64n_0K_BT}{{K_D}^{-2}}\gamma^2\exp(-DK_D) + \frac{A_{12}r_p}{6D^2} \tag{26}$$

IV **Bag filter technology**

Dust and other pollutants can be efficiently removed from the raw flue gases by using in particular:

1. dry electrostatic precipitator (dry ESP)
2. wet electrostatic precipitator (wet ESP)
3. baghouse filter (BF)

To increase the efficiency of these cleaning systems, the industries can use the following principal processes, of which many can be combined to advantage, for example electrostatic precipitators and bag filters (BREF 2006):

- 54 % of the installations are equipped with a dry ESP
- 70 % of the installations are equipped with a bag-house filter
- 25 % of the installations combine these two techniques
- One installation is equipped with two bag-house filters installed

Bag filters (**Figure 6)** are frequently used within industries for flue gas treatment because of their high efficiency and their ability to collect fine particles. They are designed to handle high dust concentration and high temperature resistance. To date, they are among the most effective (meaning they give the expected results) and efficient (meaning they work in an organized way) gas/particle separation processes.

IV.1 Principle of operation

The principle of filtration is simple; the dust-laden air enters through a tangential inlet of cyclonic type into the filtration chamber. The air passes through the sleeves and exits through the top of the bag filter. The filter media which retains the dust particles is usually cleaned most often via an efficient system of unclogging by compressed air while the dust is eliminated by the lower outlet as illustrated in the Figure 6 (inspired from Simon (2005)).

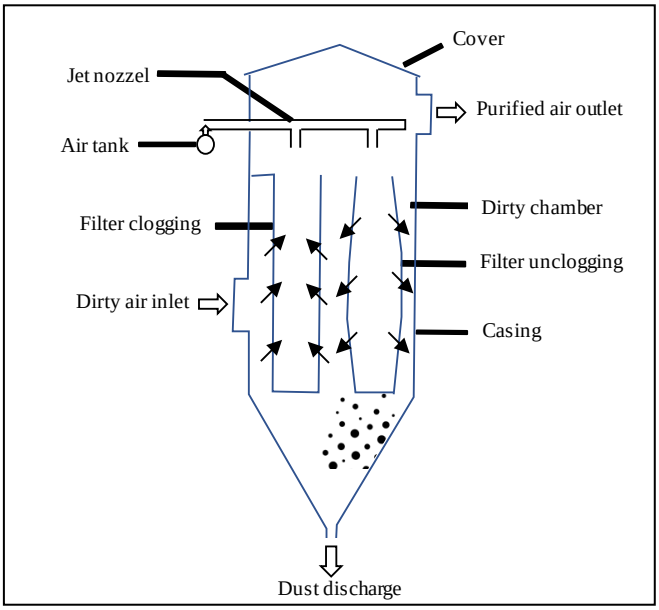

Figure 6: Air flow in a bag filter

Bag filters can be characterized according to two main factors:

Position of bags

Basically, the bags could be installed inside baghouse hanging either vertically or horizontally. The bags could also be installed at any angle in between, but the vertical module is the most common position of the industrial bag filter. They apply the same filtration rules as horizontal filters.

Cleaning of bag filter

Filter cleaning is often carried out by injecting compressed air in the opposite direction of the flow (countercurrent). However, it can also be performed by shaking or at low pressure by a fan assigned for this purpose, in particular for media with low mechanical resistance.

IV.2 Bag filter types

As a function of cleaning method of bag filter, three kinds of baghouse can be distinguished (**Figure 7**) (Ivell 2012):

- Pulse-jet
- Reverse Air
- Mechanical shakers

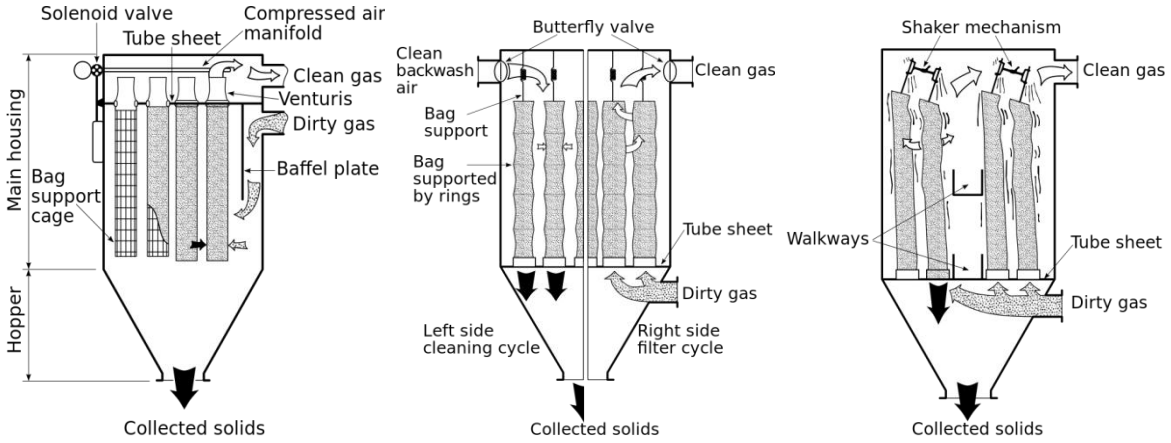

Reverse Jet Reverse Air Mechanical Shaker

Figure 7: The three types of bag filter (Ivell 2012)

IV.2.1 Mechanical Shaker

Bag filters are attached to the bottom plate of the filter casing. The particle-laden gas rises in a tube and passes through the filter media from the inside to the outside. Therefore, the deposition of particles is carried out on the filter inner surface.

The bag filters, in this case, are suspended from horizontal bars and a shaker mechanism of this latter makes it possible to clean them in an efficient manner.

IV.2.2 Reverse Air

The structure of the filtration casein is compartmentalized to allow continuous operation of clogging/unclogging of bag filters. Before cleaning operation, the filtration is stopped to clean bag filters. The cleaning is ensured by a countercurrent flow of compressed air, while, the particle deposition is carried out on the inner surface of the handle. After cleaning, the compartment is returned to the main stream to restart the bag filter clogging.

IV.2.3 Pulse-jet (Reverse Jet)

Dirty gas enters from the bottom of the baghouse and flows from outside to inside the bags. Thereby a collected dust is formed on the outer of bag filter surface. Each bag filter is supported by a filter cage which is fastened at the top of the baghouse.

Cleaning of bag filters by a short pulse of compressed air is ensured thanks to a series of the head at the top of the filters. A short burst of air creates a wave of shock that crosses the entire bag. The injection of the compressed air into the filter is normally controlled by two timers, the first for the frequency of the injection and the second for the duration of the injection. Generally, the pulse time is very short, it is estimated to be 0.1 sec per cleaning. The frequency of the injection is regulated by a filter pressure drop controller which systematically triggers the cleaning operation once it detects a maximum pressure drop in the system.

Many operating parameters can influence the performance of pulse-jet cleaning including pulse duration, dust properties, and nozzle diameter.

IV.3 Operating conditions

The corrosive nature of industrial gases and the sensitivity of filter media to high temperature are the main reasons of limited utilization of bag filters for certain applications. Thus, the pre-treatment of gases and loaded aerosols must be done before starting filtration in order to eliminate or reduce the negative effect of these compounds on the filtration performance. In some applications, decorating and cooling chambers or even recovery boilers should be used to condition the aerosols in order to treat the particles and to recover the thermal energy from off-gases before dedusting.

Furthermore, filtration velocity, defined as the velocity of the gas flowing through a fabric surface unit, is an important parameter that must be taken into account for filtration efficiency. Depending on the application, the type of filter and the type of fabric, the filtration velocity in industrial gas treatment is generally between 1 and 4 $cm.s^{-1}$.

Moreover, to choose the suitable fabric type of bag filter, an accurate beforehand study must be carried out to determine a set of parameters, such as the composition of the gas, nature and particle size of the dust, the cleaning method, and the required efficiency. Gas temperature is also taken into account as well as the method of cooling the gas if necessary.

The main characteristics of the fabric filter are the chemical resistance, permeability, fabric finishing, fiber shape, resistance to abrasion and flexion, its robustness, its collection efficiency.

IV.4 Fiber properties used for bag filter

Physical and chemical properties of filter media play an important role in the filtration performance. For instance, the porous structure is an important parameter to evaluate the

mechanisms responsible for the collection of fine particles and to determine their interactions and behaviors with the filtering media.

Regarding the structure of bag filter media, three basic types can be distinguished: woven, nonwoven/Felt, and needle (Siret 1994). Generally, nonwoven (Felt) are usually used for pulse-jet devices, while bag filter whose a woven media is usually used for cleaning systems utilize shaking and reverse flow (Hesketh 1979).

The classic fabric is the most used in the sixties after it was replaced by needle-punched felts. In this category, we find several types of weaving, symmetrical and asymmetrical.

Needle felt are fibers obtained by inserting a mass of elementary fibers into a grid of mechanically compressed fibers without the use of a binder product. Woven fabrics tend to be preferred with cleaning by shaking or reverse air flow. For the cleaning by forced air, the needle is almost exclusively used.

Membrane media, obtained by plating a porous membrane with gas, are experiencing a marked rise despite their high price. They generally allow higher filtration velocity with less opportunity to be clogged.

The selection of suitable fibers media is based on technical and economic criteria. In fact, natural fibers such as wool, cotton and linen are not used mainly in industries because of their low resistance to oxidizing agents (oxygen in the air and oxides of nitrogen). The temperature resistance is also a primary criterion for selecting an appropriate fiber, it is necessary to distinguish the temperature in normal operation and the one that can be reached during rush period.

V Filtration theory of fibrous media

The behavior of fibrous filter as a function of time can be divided in two stages. At the first stage, called the stationary filtration, the modification of filter structure due to the deposited particles does not have an influence on its performance. On the other hand, at the second stage, the deposited particles are the main factor modifying the filtration process and increasing its performances over time, this stage is called the non-stationary filtration (Renoux & Boulaud 1998).

The stationary filtration is founded on two basic assumptions: 1) all particles touching the filter media are considered collected and trapped by the fibers, 2) the collected particles have

no influence on the filtration process. In this case, the filter performance, i.e. collection efficiency E and pressure drop ΔP are almost invariant and independent over time.

At the stage of non-stationary filtration, the change in E and ΔP over time is called "secondary processes" (particles deposition attaching one over another, loss of electric charge, etc) which distinguished the "primary processes" relative to the stationary filtration and which is represented by a collection of mechanisms (diffusion, inertia, and impaction) (Matteson & Orr 1986).

V.1 Stationary Filtration

V.1.1 Mechanisms of particle collection

Dealing with fibrous media, four main mechanisms can be distinguished as the responsible for particle collection. As a function of particle size range, some mechanisms can intervene in the absence of the other, while several mechanisms can work simultaneously during the particle collection, such as Brownian diffusion, interception, and inertial impaction.

V.1.1.1 Brownian diffusion

Brownian diffusion is the main mechanism responsible for collecting the fine particles such as nanoparticles. Under the effect of gas molecules stirring and the resulting shocks, the fine particles immersed in the fluid are widely affected by random motion that called Brownian movement which is the main reason of random movements for carried nanoparticles. Thereby, the fine particles do not precisely follow the flow current lines and are collected by the fibers during their random movement (**Figure 8**).

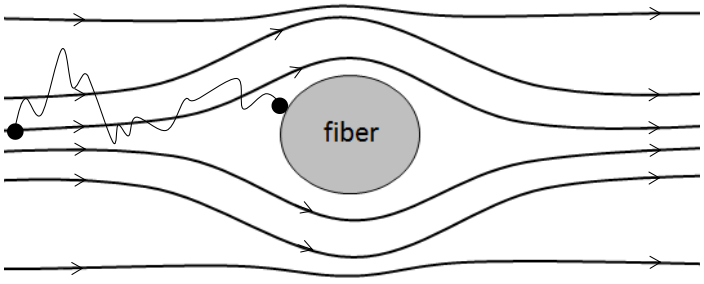

Figure 8: Particle collection by diffusion mechanism

In general, particle collection is governed by the relative importance of the diffusion movement with respect to the fluid convective motion, which is called the Peclet number (P_e) and can be expressed by the equation (27):

$$P_e = \frac{U_f . d_f}{D} \qquad (27)$$

Where U_f is the gas filtration velocity, d_f is the fiber diameter, and D is the coefficient of Brownian diffusion, in which the movement of the particles is quantified (28). According to the equation of stokes-Einstein, D can be written as:

$$D = \frac{k_B . T . C_u}{3\pi\mu d_p} \quad (28)$$

Where k_B is the Boltzmann constant ($k_B = 1.37.10^{-23} J.K^{-1}$) and T is the temperature of the gas. C_u is the Cunningham coefficient, a correction factor that takes into account the discontinuities of the media and it is defined by the equation (29) (Rader 1990):

$$C_u = 1 + Kn\left(A + B\ exp(-C/Kn)\right) \quad (29)$$

Numerous studies were subsequently carried out to improve the determination of the Cunningham-Millikan-Davies C_u correction factor. The following table presents the published values of the coefficients A. B and C for the calculation of the correction factor C_u of the Stokes law.

Table 1: Coefficients A, B and C for the calculation of the Cunningham-Millikan-Davies correction factor

Author	A	B	C
Knudsen et Weber (1911)	1.034	0.536	1.219
Millikan (1923)	1.209	0.406	0.893
Davies (1945)	1.257	0.400	1.100
Allen et Raabe (1982)	1.155	0.471	0.596
Allen et Raabe (1985)	1.142	0.558	0.999

Where λ is the mean free path of gas molecules and d_p is the particle diameter.

The Brownian motion becomes important when the size of the suspended particles decreases, the decrease of fluid viscosity, and the increase of the temperature.

V.1.1.2 Interception

This capture mechanism is only applied for particles of small diameter. In fact, the particles immersed in a fluid often go after the flow lines (**Figure 9**), because of their low inertia, and the more these current lines approach the fibers, the more they are attracted to these collectors. Consequently, the particles will be collected by a fiber if they follow a current line at a distance less than $d_p/2$.

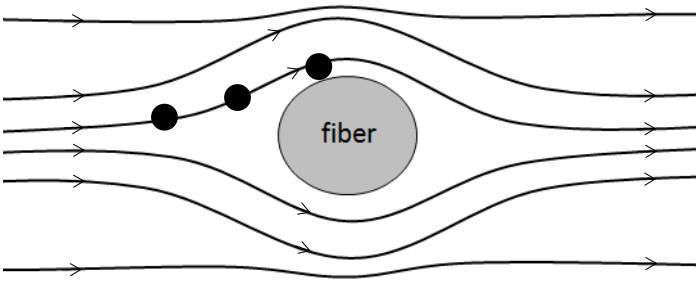

Figure 9: Particle collection by interception mechanism

In order to characterize the particle capture by interception, the interception number (R), which represents the ratio between the particle diameter and the fiber diameter, is determined as a dimensionless quantity (30):

$$R = \frac{d_p}{d_f} \tag{30}$$

V.1.1.3 Inertial impaction

This type of collection mechanism is particularly significant for large particles which can not follow the curvature of the current line due to their inertia. Indeed, because of their high inertia, the particles cannot be carried by the current line bypassing the fiber, which make them impact against the fiber (**Figure 10**). To characterize the particle captured by this mechanism, we use the Stokes number (31), which describes the ratio between the stopping distance of the particle and the characteristic length of the obstacle d_f:

$$St = \frac{Cu\rho_p d_p^2 \mathrm{U}_0}{18\mu d_f} \tag{31}$$

Where ρ_p is the particle density and U_0 is the gas velocity m.s^{-1}.

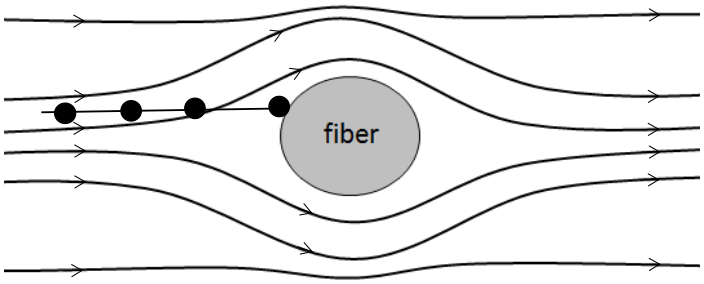

Figure 10: Particle collection by impaction mechanism

V.1.1.4 Electrostatic force

The electrostatic force (F_e) is the mechanism responsible for the collection of particles that have an electric charge opposite to that of the filter media. The charged particles which are not collected by the mechanisms mentioned above, will be exposed to this collecting force,

which significantly increases the filtration efficiency of the particles (**Figure 11**). Nevertheless, the effectiveness of this collecting mechanism decreases rapidly with the filter clogging; this is one of the disadvantages of electrostatic force (Le Coq 2006). The form of electrical force between particles and fiber is given by the equation (32):

$$F_e = \frac{q_1 . q_2}{4\pi\varepsilon d^2} \tag{32}$$

Where q_1 and q_2 are electric charge of particles and fiber respectively, and d is the distance between the particle and the fiber.

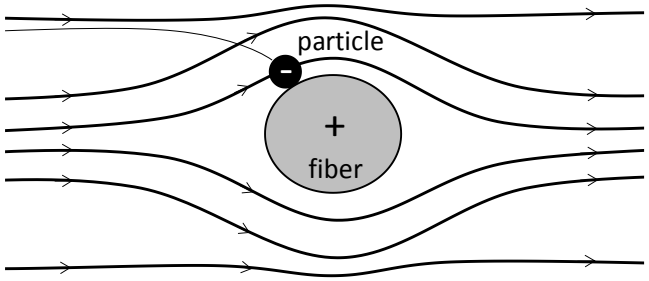

Figure 11: Particle collection by electrostatic force

V.1.1.5 Sieving

The principle of this collection mechanism is simple, it is enough that the distance between two fibers is less than the diameter of the targeted particles. This effect applies mainly to particles of large diameters. For higher porosity of the employed filter media, this collection mechanism is neglected at the beginning of clogging, but it can become significant in the presence of the particle cake.

V.1.2 Most Penetrating Particle Size (MPPS)

The MPPS is defined as the most difficult particle size to be stopped by the filter media. The main reason of this particle penetration is due to the non-predominant collection mechanism for this particle size, the fact that leads to less collection efficiency in this area. As the **Figure 12** illustrates, the increase of particle diameter relative to the MPPS leads to an increase on the efficiency of the filter due to two collection mechanisms: interception and impaction.

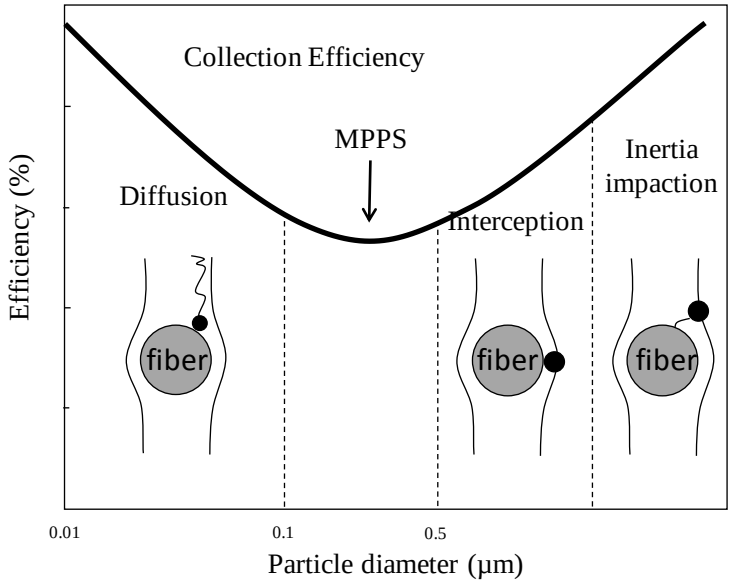

Figure 12: Filtration mechanisms as a function of particle diameter

V.1.3 Particle collection efficiency

V.1.3.1 Single fiber efficiency

The collection efficiency of a single fiber is called unit efficiency (η). It can be determined from the unit efficiencies of each capture mechanism, which are derived from theoretical or semi empirical models. In general, it is assumed that a particle colliding with a fiber is retained by special forces such as Vander Waals forces, electrostatic or intermolecular phenomena (Le Coq 2006).

There are two approaches used to calculate the unit efficiency of a single fiber. The first is to adjust the results of previous experiments by adapting the new filtration conditions. The second approach is to study numerically the trajectory of the particles during their flow around the fibers of the filter.

The first approach mentioned is the most common to calculate the unit efficiency of fiber collection, it is namely the adaptation of the calculation modules of collection efficiency.

In the literature, several expressions are found to calculate the overall and unit efficiency per each collection mechanism, especially Brownian diffusion, interception and impaction, and some of them are presented in the following section.

Lee and Liu (1982), combined the effect of two mechanisms: Brownian diffusion η_d and interception η_r in order to calculate the efficiency using a boundary layer theory associated to the Kuwabara flow filed, taking account the influence of neighboring fibers.

$$\text{where} \qquad \eta_d = 2.6\left(\frac{(1-\alpha)}{H_{Ku}}\right)^{1/3} Pe^{-2/3} \qquad \text{and} \qquad \eta_r = \left(\frac{(1-\alpha)}{H_{Ku}}\right)^{1/3} \frac{R^2}{(1+R)} \tag{32}$$

H_{Ku} is the hydrodynamic factor according to Kuwabara (1959).

The two individual efficiencies of diffusion and interception were added to obtain a combined efficiency, assuming that the impaction mechanism is not important:

$$\eta = \eta_d + \eta_r \tag{33}$$

η is the theoretical equation the single fiber efficiency where the flow is transverse to it.

Then, Lee and Liu 1982, adapted the previous equations to match with experimental results, using data based on filtration of particle size diameter ranging from 0.05 to 1.3 µm by Dacron filter. The individual efficiencies are given by:

$$\eta_d = 1.6\left(\frac{(1-\alpha)}{H_{Ku}}\right)^{1/3} Pe^{-2/3} \qquad \text{and} \qquad \eta_r = 0.6\left(\frac{(1-\alpha)}{H_{Ku}}\right)\frac{R^2}{(1+R)} \tag{34}$$

The latter study was followed by Liu and Rubow (1990) who corrected two terms, taking into account the slip flow effect (Spurny, 1998):

$$\eta_d = 1.6\left(\frac{(1-\alpha)}{H_{Ku}}\right)^{1/3} Pe^{-2/3} C_d \qquad \text{and} \qquad \eta_r = 0.6\left(\frac{(1-\alpha)}{H_{Ku}}\right)\frac{R^2}{(1+R)} C_r \tag{35}$$

Where C_d is the correction term for the diffusion slip flow effect, given by:

$$C_d = 1 + 0.388 Kn_f \left(\frac{(1-\alpha)Pe}{H_{Ku}}\right)^{1/3} \tag{36}$$

And C_r is the correction term for the interception slip flow effect, given by:

$$C_r = 1 + \frac{1.996\, Kn_f}{R} \tag{37}$$

Following the work of Liu and Rubow (1990), Payet (1991) adjusted the last equation according to his experimental data, by introducing a new term related with the mechanism of diffusion, therefore, the new diffusion equation took the following form (38):

$$\eta_d = 1.6\left(\frac{(1-\alpha)}{H_{Ku}}\right)^{1/3} Pe^{-2/3} C_d C_d' \qquad \text{and} \qquad \eta_r = 0.6\left(\frac{(1-\alpha)}{H_{Ku}}\right)\frac{R^2}{(1+R)} C_r \tag{38}$$

where C_d' is the correction term for the diffusion slip flow effect (Payet et al. 1992), given by the equation (39):

$$C_d' = \frac{1}{1+\eta_d} \tag{39}$$

From the work of Stechkina & Fuchs (1966), Miecret & Gustavson (1989) suggested the following expression (40) for the total fractional efficiency:

$$\eta = \eta_d + \eta_r + \eta_i + \eta_{dr} \tag{40}$$

η_d efficiency by diffusion, η_r efficiency by interception, η_i efficiency by impaction, η_{dr} efficiency by combination of diffusion and interception.

The total efficiency of fibrous filter is the combination of all filtration mechanisms. The simple way to predict the total efficiency, if all individual mechanisms are small compared with unity, is to add all predicted values by using the following equation (41):

$$\eta = \eta_d + \eta_r + \eta_i + \eta_{dr} \tag{41}$$

While if the different mechanisms acting in independent way of each other, the adequate equation is:

$$\eta = 1 - (1-\eta_d)(1-\eta_r)(1-\eta_i)(1-\eta_{el})(1-\eta_g) \tag{42}$$

From the other side, Gutfing & Tardos (1979) valid this equation for the case of diffusion, interception, and impaction:

$$\eta = 1 - (1-\eta_d)(1-\eta_r)(1-\eta_i) \tag{43}$$

The **Table 2** summarizes some of the overall of fractional efficiency and collection mechanism models.

Table 2: Overall of fractional efficiency and collection mechanism models

Authors	Expression of η	η_d	η_r	η_i	η_{dr}
Kasper	$1-(1-\eta_d)(1-\eta_r)(1-\eta_i)$	Davies	Kuwabara	Langmuir	
Miecret, Gustavsson (1989)	$\eta_d + \eta_r + \eta_i + \eta_{dr}$	Davies	Kuwabara modifié par Cai	Suneja, Lee	Stechkina, Fuchs
Lee, Liu (1982)	$\eta_d + \eta_r$	Lee, Liu	Lee, Liu		
Liu, Rubow (1990)	$\eta_d + \eta_r$	Liu, Rubow	Liu, Rubow		
Payet (1992)	$\eta_d + \eta_r$	Payet	Liu, Rubow		
Gougeon (1994)	$\eta_d + \eta_r + \eta_i$	Payet	Liu, Rubow	Gougeon	
Stechkina et al. (1969)	$\eta_d + \eta_r + \eta_i + \eta_{dr}$ $\eta_{dr} = 1{,}24 H_{Ku}^{-\frac{1}{2}} I^{\frac{2}{3}} Pe^{-\frac{2}{3}}$	Stechkina	Yeh et al.	Stechkina	Stechkina
Kirsch et al. (1978)	$\eta_d + \eta_r + \eta_i + \eta_{dr}$ $\eta_{dr} = 1{,}24 H_{Fan}^{-\frac{1}{2}} I^{\frac{2}{3}} Pe^{-\frac{2}{3}}$	Kirsch	Kirsch		Fuchs

V.1.3.2 Overall filter efficiency

The overall efficiency (44) of a filter is calculated from the total unit efficiency. Thus, in the case of deep filtration on fibrous media (filter paper and nonwoven fabric), the initial filtration efficiency can be determined as follows (Brown 1993):

$$E_t = 1 - \exp\left(-4\eta \frac{\alpha_f}{(1-\alpha_f)} \frac{\mathrm{L}}{\pi \mathrm{d_f}}\right) \tag{44}$$

The overall efficiency can be also calculated experimentally from the relation between the particles concentration of the filter upstream $N_{\mathbf{upstream,dp}}$ and the concentration of particles of the filter downstream $N_{\mathbf{downstream},dp}$ according to the following relationship (45):

$$E_t = 1 - \frac{N_{\mathbf{downstream},dp}}{N_{\mathbf{upstream,dp}}} \times 100 \tag{45}$$

An efficient filter is the filter that ensures maximum particle collection efficiency and minimal pressure drop during the clogging and after the cleaning operation.

V.2 Non-stationary filtration

The next section examines the various parameters that can influence the filter performance. Before discussing the filter performance, it is relevant to understand the mechanisms of different steps of deposition and collection of particles by fibrous media.

V.2.1 Dendrites and particle collection

In fibrous media, the captured particles lead to formation of particle dendrites or agglomerates (chains of deposited particles) on the surface of fibers. The geometry of the deposited particles differs according to their size: for submicron particles, the deposit is dendritic, whereas for micronic particles the deposit takes a form of agglomerates. For several decades, the assessment of deposited particles on the fibrous media has attracted many authors for its importance to understand cake structure and filter performance evolution. The significance of pattern particle deposition lies on its dependence to filtration conditions and filter permeability. Better understanding of dendrite and agglomerates structure may lead to better prediction of pressure drop through the filter. Billings (1966) was the first author who studied experimentally the behavior of deposited dendrites (Payatakes & Gradoń 1980). Later, Alkiviades et al. (1976) studied dendrite structure of dust cake in the fibrous filtration media. The study consists to assume an ideal tree structure as similar as the tree actual structure in order to predict the dendrite deposits behavior as a function of time and position on the fibers. The dominant filtration mechanism is a crucial factor affecting the dendrites formation upon a fibrous filter. That is, the dendrite is formed on the entire surface of fiber in the case of diffusion deposition. In the case of interception, dendrites will be mainly deposited on the sides of fiber surface. While for impaction mechanism, the dendrites are formed on the front of fiber surface perpendicular to flow direction. As illustrated in the **Figure 13** (inspired from *(Kanaoka et al. 1986)*, a dendrite formation was described as a function of Stokes number (Stk), Peclet number (Pe) and interception number (R).

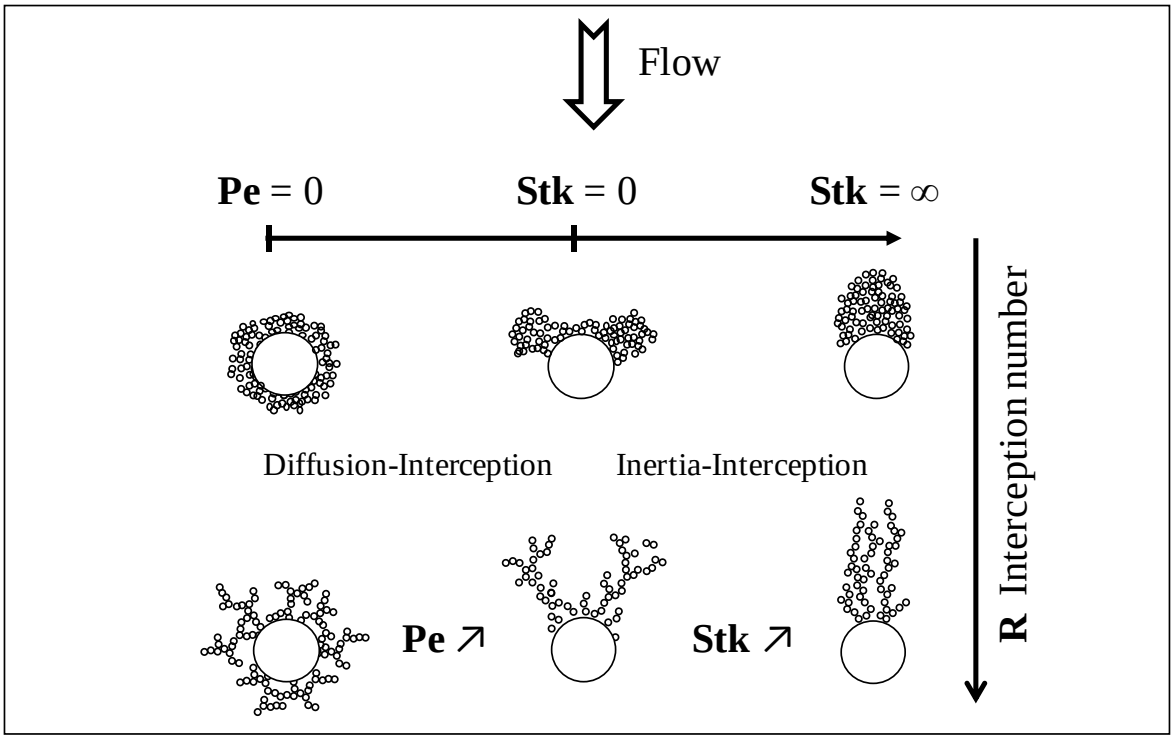

Figure 13: Dendrite formation as a function of Stk, Pe and R

From the other side, Thomas (2001) had clearly explained the different forms of deposit particle geometry. As a function of particle size, the deposit can be formed in two different geometries. For submicron particles, the deposit is dendrite as shown in the **Figure 14-a** and the **Figure 14-b**, whereas for micronic particles, the deposit takes a form of agglomerates.

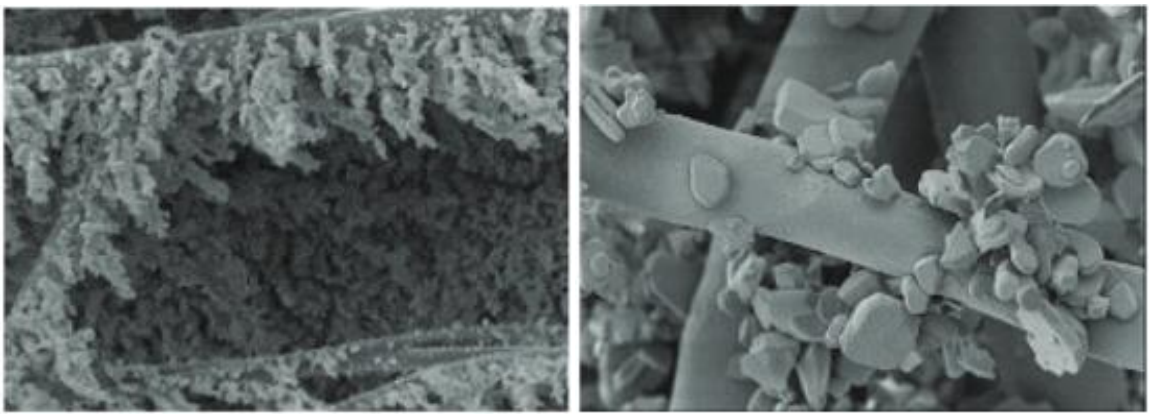

a) Clogging of fiber with submicronic particles

b) Clogging of fiber with micro-sized particles

Figure 14: Deposit particles on fibers (Thomas 2001)

Thomas (2001) explains that for particle having a small diameter, the specific surface area is important, which leads to a greater pressure drop of the filter and dendrite formation. While for the coarse particles, the deposit has a greater compactness, but the specific surface area is

lower than for the submicron particles, this leads to a lower pressure drop for the same mass of deposited particles.

V.2.2 Filter pressure drop

V.2.2.1 Air permeability

Each filter has a specific air permeability value (K), which differs according to its properties and characteristics. The permeability is a widespread quantity used to control the performance of the filter (Seville 1997). According to the Darcy's equation, the expression of the air permeability (K) can be determined by the following formula (46):

$$K = \mu \frac{V_f . L}{\Delta P} \tag{46}$$

Where, ΔP is the pressure drop across the filter, L is the filter thickness, V_f is the filtration velocity, and μ is the air viscosity.

V.2.2.2 Pressure drop of clean and clogged flat filter

Experimentally, the pressure drop is defined as the difference of the pressure between upstream P_{upstream} and downstream $P_{\text{downstream}}$ of the filter media, according to the following equation (47):

$$\Delta P = P_{upstream} - P_{downstream} \tag{47}$$

As previously explained, the filter clogging occurs in two main phases, stationary and non-stationary. In the literature, the pressure drop expression of a clean filter is different from that of a filter in a non-stationary phase. To evaluate the total pressure drop of a clogged filter, it is essential to take into account the pressure drop of the clean filter and that of the filter cake, as indicated by the equation (48) (Novick et al. 1992):

$$\Delta P = \Delta P_m + \Delta P_c \tag{48}$$

ΔP_c is the pressure drop of the fluid through the dust cake that can be expressed by Kozeny formula (for spherical particles):

$$\Delta P_c = \mu . h_k \frac{\alpha_c}{(1-\alpha_c)^3} \frac{36}{d_p^2 \rho_p . C_u} V_f . W_p \tag{49}$$

With α_c the cake compacity and h_k the empirical constant of Kozeny and Carman, ρ_p is the particle density, and W_p is the surface mass of collected particles.

Davies (1973) has also developed the formula (50) for pressure drop of clean filter whose compacity is between 0.005 and 0.4 (the range of compacity commonly used for industrial filter media):

$$\Delta P_m = 64.\mu.V_f.L\frac{\alpha_f^{\frac{3}{2}}(1+56.\alpha_f^3)}{d_f^2} \quad (50)$$

With α_f is the volume density of the fibers.

The pressure drop of the clogged filter media can be also written according to the equation (51):

$$\Delta P = 64.\mu.V_f.L\frac{\alpha_f^{\frac{3}{2}}(1+56.\alpha_f^3)}{d_f^2} + \mu.h_k\frac{\alpha_c}{(1-\alpha_c)^3}\frac{36}{d_p^2\rho_p.C_u}V_f.W_p \quad (51)$$

In the literature, several empirical formulas of pressure drop may be used according to state and filter characteristics. For instance, Davies' empirical formula of pressure drop ΔP (52) can be used for clean non-woven fibrous filter (Hung & Leung 2011):

$$\frac{\Delta P d_f^2}{4\mu U_0 L} = 16\alpha_f^{1.5}\left(1+56\alpha_f^3\right) \quad (52)$$

The formula is obtained through testing of fibrous filter with fiber diameter (d_f) ranging from 1.6 to 80 µm and compacity (α) smaller than 0.3, which include the current range used in industrial dust.

V.2.2.3 Cake and filter resistance

Since the face velocity is low at Reynolds number $Re < 1$, Darcy's law can be applied to calculate ΔP_m and ΔP_c from the following expression (53):

$$\Delta P = K_1\mu V_f + K_2\mu W_p V_f \quad (53)$$

Where µ is the gas viscosity, $V_f$is the filtration velocity. K_1 and K_2 are respectively the media filter resistance [m^{-1}] (fabric resistance, or "drag"), and the specific resistance of the dust cake [$m.kg^{-1}$] can be defined by the equations (54).

$$K_1 = \frac{\Delta P}{V_f\mu} \quad and \quad K_2 = \frac{\frac{\Delta(\Delta P)}{\Delta(t)}}{W_p.V_f\mu} \quad (54)$$

Where $W_p = \frac{\Delta m}{A}$ is the collected particle mass (cake area load) on the filter surface.

K_2 can be experimentally determined based on experimental data of collecting particles on a filter. From the slope of the line describing the increase in the pressure drop as a function of the collected mass per unit area we can calculate the constant of the cake resistance K_2.

V.2.3 Filter clogging

During clogging of clean filter, three stages can be distinguished (**Figure 15**): (1) depth filtration (2) transition filtration (3) cake filtration. In the first stage of filtration, the carried particles by the gas stream are collected in filter depth only by filter fibers of the filter media. The interaction between collected particles increases as the quantity of captured particles becomes important. During this stage, the evolution of pressure drop is slow. Later, the captured particles might play the role of filter fibers by collecting the future particles, contributing to the performance rise of filtration efficiency but the rise of pressure drop still slow across the filter. As a deep filter is loaded, dendrites formed on the filter media surface begin to bridge together to form the so called cake filter, the flow resistance through the filter and pressure drop rise become markedly linear. This change in mechanical structure within fibrous filter was clearly observed by several studies.

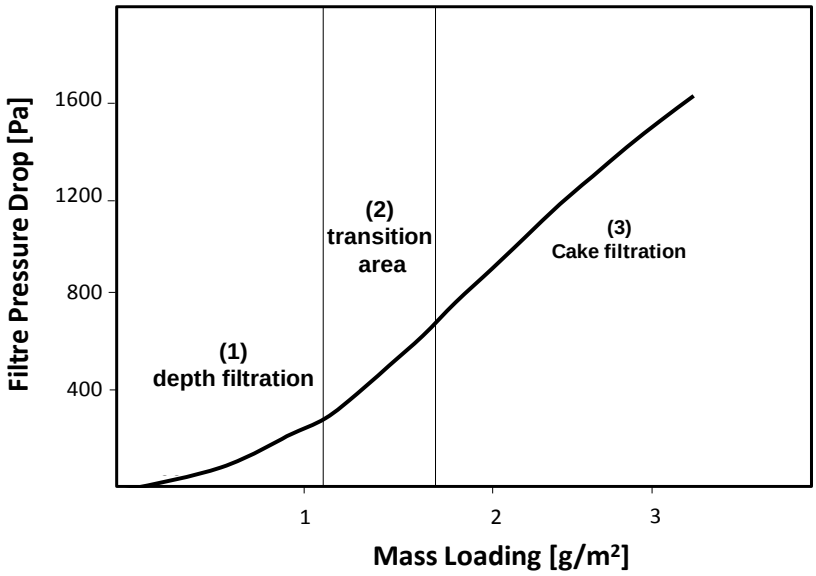

Figure 15: Illustrated graph of ΔP evolution vs loaded mass

The study of filter cake structure is important to understand its effects on filter efficiency and the evolution of pressure drop across filter media.

As explained by Förster et al. (2016), in industrial applications, clean bag filters are never used immediately for aerosol filtration. In fact, their conditionnement is a necessary process that must be applied for new filters by pre-coating their media with thin layer of reagent (such as lime or sodium bicarbonate). The process of precoating is applied not only to increase filtration efficiency, but also to increase the chemical attack resistance and dust cake release.

V.2.4 Filter cleaning

The collected particles on the filter media are responsible for the pressure drop evolution. For this reason, the particle cake must be detached to a predefined value of the pressure drop or within a time interval. The formation and detachment of the cake (**Figure 16**, inspired from Park (2012)) are among the main causes that can influence the filter performance. Thus, investigating these processes is very important to understand the filter performance.

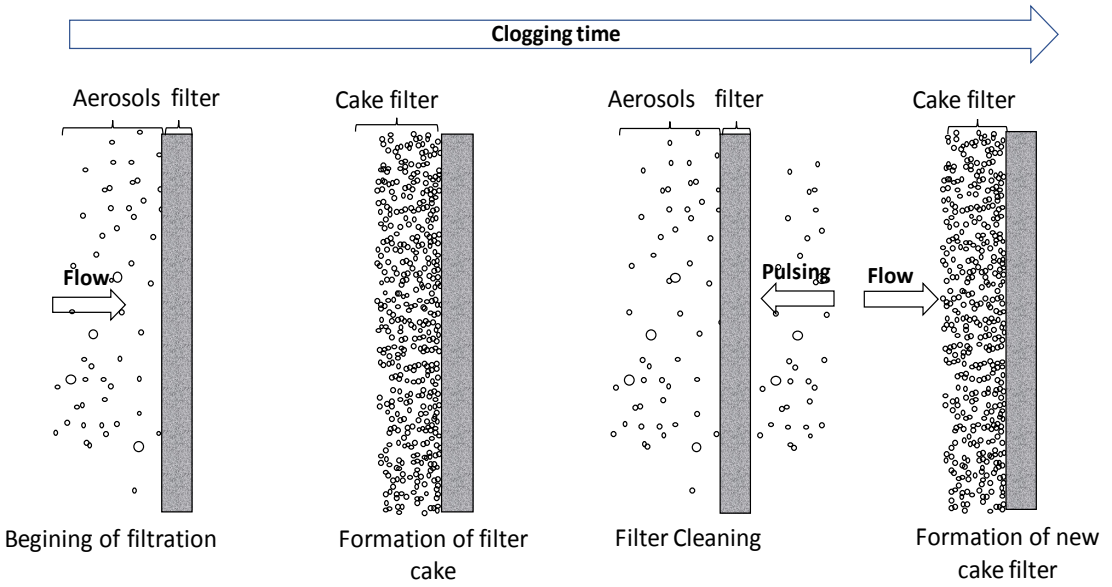

Figure 16: Influence of dust cake on filtration efficiency

In fact, the pressure drop of the filter depends on the aeraulic resistance of the filter media and also on the dust cake formed on the filter surface. These two quantities are conditioned by several factors such as the cake porosity, its specific resistance, the distribution of the charge of the cake zones, the distribution of the filtration speed and the media itself.

During the regeneration of a dust cake, the collected particles can not be totally removed from filter media, which may remain the residual pressure drop not stable and increase during clogging/ unclogging cycles. The fact that increase the flow resistance across the filter media. Thus, the residual particles can have benefits or disadvantages for filter performance. In fact, collected particles plays a major role with regard to the collection efficiency of future particles. Neverthless, the huge increase in residual pressure drop may be the mean reason leads to change the filter. Thereby, the liftime of the filter is highly dependent on unclogging efficiency.

An incomplet detachement of cake filter (the patchy cleaning) occurs where some area of the filter media are completely unclogged while others still holding the dust cake (Dittler et al.

1998). The patchy cleaning is the major cause of inefficiency filter cleaning (Mukhopadhyay 2010).

Patchy cleaning is attributed to several factors, for instance, the non-uniform filtration velocity pass through the filter media due to the non-homogeneity of pore of the media structure. The fact that leads to form a non-uniform cake thikness and variation of cake porosity which can be responsible of uneven cake removal.

Saleem et al. (2011) have investigated the formation and detachment of cake dust from pulse-jet bag filter. The experiments were carried out on clogging needle felts media with limestone particles. The rise of pressure drop was faster at the beginning of filtration and takes a concave rise, while after certain moment of filter clogging the evoltion of ΔP becomes slower. This was explained by the fact that after engagement the unclogging system, some areas of bag filter are completely get rid of cake while others still holding residual cake. By resuming the clogging in next filtration cycle, the gas flow becomes higher through area holding no cake as compared to the area holding thick cake at the same overall pressure drop. At constant dust concentration, the cake high will increase faster at cleaned area than the residual cake laden area. Therefore, the pressure drop increases rapidly until the cleaned area get layer of cake and the entire cake surface become homogeneous. At this point, the flow resistance becomes balanced across the media filter and a linear rise seems to be observed.

VI Influence of operating conditions on filtration performance

Before discusing the influence of operating conditions on filtration performance of bag filters when results are available in the literature, it is important to recognize their influence on filtration mechanisms especially diffusion, interception and impaction. The **Table 3** gathers main factors that affect the efficiency of filtration mechanisms mainly filter characteristics, particle characteristics, and filtration velocity. These results were observed in litterature from cloggings with fibrous filters in flat geometry.

Table 3: Influence of operating conditions on filtration mechanisms (Thomas 2001)

Filtration mechanisms	Aerosol		Operating conditions	Filter characteristics		
	ρ_P↗	d_P↗	V_f↗	d_f↗	α↗	L↗
Diffusion	↘	↘	↘	↘	↗	↗
Interception	--	↗	--	↘	↗	↗

Impaction	↗	↗	↗	↘	↗	↗

↗ : increase ↘ : decrease

VI.1 Filtration velocity

VI.1.1 Particle collection efficiency

Förster et al. (2016) investigated the influence of filtration velocity on nanoparticle filtration (5-40 nm in diameter). The filter was from one side a clean bag filter without dust cake, and from the other side, bag filter contained dust cake with a pressure drop of 250 Pa, which was built up at a filtration velocity of 3.3 $cm.s^{-1}$. The filtration velocity during nanoparticles filtration was varying between 1.5 and 5 $cm.s^{-1}$. The results showed that, for both filters, the filtration velocity has a significant impact, so that, the efficiency increases with decreasing of filtration velocity. This result is consistent with the influence of filtration velocity on Brownian diffusion, the main mechanism explaining the collection of nanoparticles by fibrous filters.

VI.1.2 Dust cake resistance

According to Dennis & Dirgo (1981), the filtration velocity affects the specific resistance of the dust cake (K_2). Numerous studies have shown the following relationship (55) between K_2 and V_f (Cheng & Tsai 1998):

$$K_2 = fV_f^n \quad (55)$$

With f and n are positive constants. The value of n depends on the particle type used during filtration, for instance $n = 0.19$ for nanosized Arizona particles (Rudnick & First 1978), $n = 0.5$ for coal fly ash (Dennis et al. 1979). The findings showed that K_2 increases with V_f.

VI.2 Air humidity

VI.2.1 Particle collection efficiency

The influence of humidity on filtration performance must be taken into consideration during clogging of filter media. Kim et al. (2006) tested the filtration of NaCl nanoparticles with diameters ranged between 3 and 70 nm at a velocity of 2.5 $cm.s^{-1}$ by a fiberglass filter. By changing the values of the filtration humidity during clogging of the filter media, the results showed that the humidity has no influence on the filtration efficiency. The efficiency remains constant for the three humidity values of 10.6, 305, and 23000 ppm, corresponding to 0.04, 1.22 and 92% of relative humidity.

VI.2.2 Filter pressure drop

Joubert et al. (2010) conducted experiment study to investigate the influence of humidity on pressure drop. Flat filters were clogged with sodium chloride and aluminum oxide. The results of clogging with hygroscopic sodium chloride aerosols showed that the specific cake resistance decreases with the increase in relative humidity. Regarding the non-hygroscopic aluminium oxide, no significant influence of humidity during clogging was observed on the change in filter pressure drop.

Most of the studies which investigated the influence of humidity on filtration performance were carried out on filters in flat or pleat geometries. To the best of our knowledge, no study was carried out to investigate the influence of humidity on bag filter performance.

VI.3 Air temperature

VI.3.1 Filter pressure drop

In order to investigate the effect of temperature on filter performance, Kim et al. (2008) studied the evolution of the pressure drop across dust cake of ash aerosol deposited on ceramic filter clogged at different values of temperature (room temperature - 673 K). The study showed that the pressure drop of the filter increases with filtration temperature. The main reason was traced back to the change of fluid viscosity which increases with filtration temperature. The equation which relates temperature to fluid viscosity can be obtained using the Sutherland formula (56) (Allen & Raabe 1982):

$$\mu_T = \mu_{23} \left(\frac{T}{T_0}\right)^{1.5} \left(\frac{T_0 + 110.4}{T + 110.4}\right) \quad (56)$$

VI.3.2 Particle collection efficiency

Förster et al. (2016) conducted experiments study in order to investigate the influence of temperature on nanoparticles filtration. In this regard, flat filter was clogged with particles of 5-40 nm in diameter at constant filtration velocity of 3.3 cm.s^{-1} for three different value of temperature: 20, 150 and 200°C. The results showed a high collection efficiency of nanoparticles at higher investigated temperature (200°C) which was measured between 95 and 100%, while for ambient temperature (20°C), the efficiency was between 93 and 100%. This result is consistent with the increase of Brownian agitation with the increase of temperature which promotes the collection of nanoparticles by Brownian diffusion mechanism.

VI.3.3 Cleaning efficiency of pulse-jet system

According to Kim et al. (2008), the cleaning efficiency of ceramic filter decreases with increasing of filtration temperature, as a result of increasing of pressure drop which in turn increases the compaction effect of dust cake.

Low unclogging efficiency by pulse-jet method can be also explained by the fact that, the more temperature increases the more filtered air density pulsed in bag filter become low which makes the unclogging operation less efficient (Mukhopadhyay 2010).

VI.4 Particle loading

VI.4.1 Particle collection efficiency

Leung & Hung (2008) conducted experimental studies in order to investigate the influence of particle loading on filtration efficiency. Clean micro-fibrous and nano-fibrous filters were loaded with NaCl particles of size ranging from 41 to 514 nm in electrical mobility diameter. The results showed that, at the first filtration step, the MPPS was 203 and 103 nm for respectively micro-fibrous and nano-fibrous filter. As a function of particle loading, the MPPS of micro-fibrous filter shifted to 128 nm after 70h of clogging. While for the nano-fiber filter the MPPS decreased from 103 nm to 90 nm after 6h of aerosol loading.

VI.5 Particle concentration

VI.5.1 Filter pressure drop

Several studies were carried out by many authors to investigate the effect of aerosol concentration on pressure drop of fiber filters. For instance, Song et al. (2006) have clogged several fibrous filters of the same type by PSL particles at different inlet concentration ranging from 1.44 and 2.23 $mg.m^{-3}$. The results showed that at the high loading level, from the masse loading particles of $1g.m^{-2}$, the pressure drop of filter increases as the particle concentration increases. The authors explained the results by the effect of concentration on particle deposition, subsequently on the cake structure. In fact, with higher inlet concentration, the packed patterns of deposited particles become important which may be the main reason of higher pressure drop.

For the same purpose Thomas (2001) investigated the influence of particle concentration on HEPA glass fiber filter. The study revealed no significant influence of aerosol concentration (5 and 21 $mg.m^{-3}$) on the evolution of filter pressure drop.

VI.6 Particle shape

VI.6.1 Particle collection efficiency

An experimental study carried out by Boskovic et al. (2005) showed the influence of particle shape on filtration efficiency. According to the results of this study published on filtration of spherical particles of iron oxide and cubic particles of magnesium oxide by fibrous filters at 2 $cm.s^{-1}$ of face velocity, the filtration efficiency for spherical particles is greater than cube particles for particle size in the range of 50 to 300 nm. The difference in efficiency increased with particle size. Boskovic et al. (2005) explained this difference by the fact that the way which particles move on the fiber surface is different. In fact, the movement of cubic particles is rolling on the fibers before the capture. In this case, the contact area of fiber/cubic particle is lower than fiber/spherical particle, which means that the probability of particle detachment from the fiber is higher for cubic particles than spherical particles.

Nanoparticle agglomerations are a collection of particles made up of clusters or chains of primary particles. The shape of nanoparticles agglomeration has interested authors to study the influence of particle shape on filtration efficiency. In this regard Kim et al. (2006) conducted experiments of filtration with silver NP agglomerates with which diameter ranging from 30 to 500 nm. Loading of fiberglass filter media which diameter is 1.9 µm were carried out with the face velocity of 5.3 $cm.s^{-1}$. The results showed that for the same mobility diameters, the collection efficiency of NP agglomerates due to their larger interception length is higher than spherical particles.

VI.6.2 Dust cake porosity and filter pressure drop

Porosity is a physical quantity determines the flow and retention capacities of a substrate. It is also a numerical value defined as the ratio between the void volume and the total volume of a porous media (57):

$$\Phi = \frac{V_{pores}}{V_{total}} \quad (57)$$

With ϕ is the filter media porosity, V_{pores} is the pore size, and V_{total} is the total volume of the material (the sum of the solid and pores volume).

Cheng & Tsai (1998) have experimentally determined the relationship between the filtration rate and the porosity of the dust cake. During this study, three different types of dust have been studied: fly ash (MMDA = 6.28 µm), limestone (MMDA = 2.53 µm), and fine dust SAN (MMDA = 3.88 µm).

The results showed that the porosity of dust cake decreases with increasing of filtration velocity for the three types of tested dust. This result has been explained by the fact that for higher filtration velocity, the particles of large size are more compressed into the bottom of the cake, and especially when the driving force of the fluid is greater than that of particles adhesion.

By comparing the cake of the three types of dust, it is found that the limestone and SAE particles have larger cake porosity than that of fly ash whose a spherical shape. This is due to a random arrangement of the limestone particles and SAE relative to the spherical particles of fly ash. Based on this result, it can be said that the porosity of the cake is strongly related to the shape of the particles which in turns affects the evolution of filter pressure drop.

Endo et al. (1998) have studied the effect of particle types on filter pressure drop and filter cake structure. Under the constant filtration velocity (9.87 $cm.s^{-1}$), the air filter was clogged with three types of particle, mainly alumina, Talc, and Arizona particles. The results showed the highest pressure drop for filter clogged with alumina and the lowest resistance to air flow with Talc particles.

VI.7 Filtration cycles

VI.7.1 Particle collection efficiency

The fractional collection efficiency of a bag filter is one of the most important parameters in filtration. Park (2012) analyzed the distribution of particles upstream and downstream of a bag filter during several cycles of clogging/unclogging. The results showed that during 6 filtration cycles, the unclogging filter by countercurrent system, affects the penetration of fine particles, and the particle penetration decreases with filtration cycles.

VI.7.2 Filter pressure drop

VI.7.2.1 Bag filter conditioning

After conditioning of bag filter, the collection of particles takes place on the surface of filter media. To mimic the status of the filter in the industrial application and to create approximately the same conditions of filtration, the filter must be tested during the stage of surface filtration. In other word, the bag filter must be conditioned by building up the dust cake after several cycles of clogging/ unclogging until reaching a constant residual pressure drop of bag filter (**Figure 17**) and ensure no dust inclusions in depth filter media.

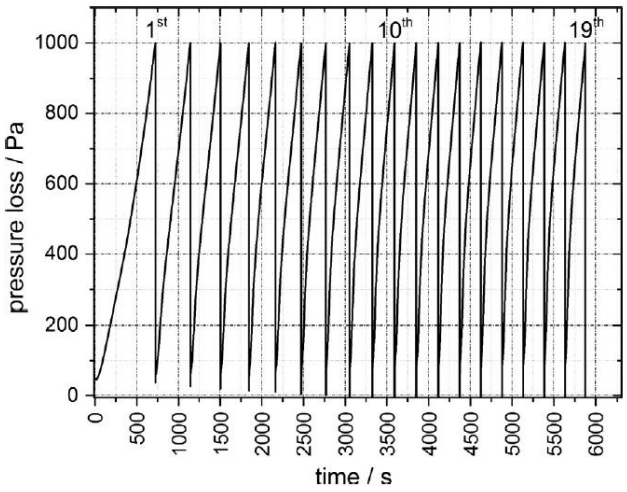

Figure 17: Pressure drop curve for a new filter media with 19-fold filter cake build-up (Förster et al. 2016)

VI.7.2.2 Gradual increase in residual pressure drop

The residual cake on the surface and the trapped particles inside filter media are the main reasons of increasing in residual pressure drop (ΔP_{res}) which becomes aggravated with cycle numbers of clogging/ unclogging. Depth filtration can affect seriously the performance and lifetime of bag filter (Mukhopadhyay 2010). Simon (2005) has clearly explained the reason of (ΔP_{res}) increasing over filtration cycles.

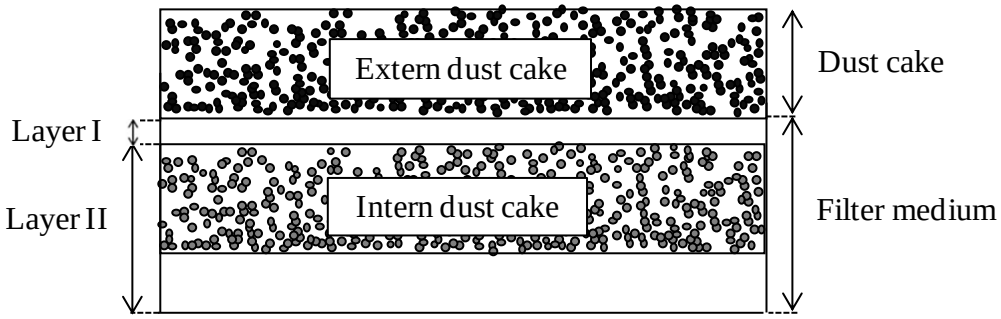

Figure 18: Illustration scheme of the filter layer

As illustrated in the (**Figure 18**, inspired from *Stöcklmayer & Höflinger (1989)*) the filter media can be devised into two layers. The layer I represents the area of the media for which the trapped particles can be detached by pulse-jet system. The layer II represents the area in which the particles can no longer be detached and are definitely trapped within the internal fibrous structure of the media. It is these latter particles which would be responsible for the increase in the residual pressure drop. Immediately after unclogging, the layer I is empty and new particles can penetrate in the layer II, where they are captured in the upper part of this zone and form an intern dust cake. The residual pressure drop is mainly dependent on the compression of this layer of internal dust cake. Thus, if the internal cake is close to

incompressibility, the particles trapped in the layer I will not be able to evolve and the residual pressure drop increases gradually.

VI.8 Influence of upper pressure drop on filter resistance

Effect of upper pressure drop limit on filter media and dust cake resistance parameters was studied by Saleem et al. (2012). The tested media was needle felts made of two polymers; polyimide (PI) and polyphenylensulfide (PPS). In bag filter geometry, the media was clogged at two different filtration velocity 2.7 and 5.5 $cm.s^{-1}$; the filters were loaded with the same and constant cake area load. The results showed that the residual resistance of the media is independent of upper pressure drop in condition that the bag filters are properly cleaned. While the cake resistance decreases with upper pressure drop limit. Furthermore, the effect of maximum pressure drop on resistance of filter cake is important at high filtration velocity as compared to low filtration velocity.

VI.9 Bag filter damage

The damage of bag filter is a serious issue that could be happen because of corrosion in the case of abrasive materials contained in treated gases or because of fire risk. To avoid such problems, it is essential to establish filter performance monitoring systems by monitoring the pressure drop indicators in order to check and to ensure that there is no leakage of particles through damaged filter.

For example, pulse-jet cleaning can cause a serious damage because of the high applied pressure during injecting of the compressed air. In fact, the air flow can damage the filters and the spray tube, which leads to uncontrolled leakage of the particles, by consequence this leads to a reduction in filtration performance.

The most significant influential parameters are: the angle of the nozzle on the filter surface and the distance of exposure of the filter by the flux. Increasing the filter efficiency is essential to optimize the cleaning operation of the system (Leparoux & Siegmann 2003).

Triboelectric or optical devices can be used to measure the evolution of emitted dust from the bag filter to detect possible damage and can be also used to detect dust peaks during unclogging cycle. When these measures are integrated into a zoning system, the area containing damaged filters (**Figure 19**) can be identified and thereby repairs can be carried out locally (BREF 2006).

Figure 19: Damaged bag filter (Zhou et al. 2012)

VII Conclusions of the chapter

Over decades, a diverse group of Air Pollution Control devices have been developed to remove particulates and/or gases from industrial exhaust streams. Thanks to these modern technologies of flue gas treatment system, the emissions of hazardous substances to the environment have been drastically reduced. Bag filter is one of the most efficient Air Pollution Control device for gas-particles separation with large area of woven or needled fabric which the flue gas must flow through.

In the present chapter, a brief overview was provided on the conditions of industrial flue gas treatment and the filtration mechanisms of aerosols by fiber filters was detailed. Moreover, the structural characteristics of fiber media, size distribution of aerosols, and their physical and chemical characteristics were also discussed in this chapter.

The chapter discussed also the performance of fibrous filter as a function of time in terms of pressure drop and filtration efficiency. The filtration theory of fibrous media distinguished two stages of filter performance evolution. In the first stage, the collection of particles during filtration occurs on the surface of filter fibers thanks to the filtration mechanisms. In second stage, the constructed dust cake on the surface of filter media is the main responsible for particle collection and the increase of filter pressure drop and collection efficiency. Thus, the dust cake plays an essential role to increase the collection efficiency for fibers filter.

To understand the effect of different filtration conditions on fibrous filters, a background of the influence of operating parameters on filtration mechanisms and on the structure of constructed dust cake was provided in this chapter.

Chapter II Materials and methods

I Introduction

The present chapter describes the materials and methods used in this work. Two experimental setups were used for clogging of two different filter geometries (bag filter and flat filter). All filters are made from the same filter media (Polytetrafluoroethylene, PTFE). Bag filter experimental setup was developed in order to be representative of the bag filter unit in waste incineration flue gas treatment in terms of temperature, humidity, filtration velocity, unclogging, and aerosol load. The second experimental setup dedicated for flat filter was a simple filtration conduct with the absence of on-line unclogging device. The particulate pollutants used in the study are also described in terms of particle size distribution as well as concentration in different filtration conditions namely: (150°C, 3% RH - 100 g water/kg air) and (24°C, 45% RH - 10 g water/kg air). Finally, the general experimental methodology followed during the thesis is described.

II Description of experimental setups

II.1 Bag filter setup

The experimental setup (**Figure 20**) was developed in order to be representative to the bag filter unit in waste incineration flue gas treatment in terms of temperature, humidity, filtration velocity, unclogging and aerosol load. This setup is dedicated to filtration/on-line regeneration tests at incineration conditions (150°C, 3% RH) and at ambient conditions (24°C, 45% RH). As can be seen from the figure, the experimental setup can be divided into 4 areas.

In area 1, a centrifugal fan (SC10C 0.75 kW) flows filtered air (F9 filter according to European standard EN779:2012) into the setup. The airflow is measured with a flow meter located upstream of the fan.

In area 2, the air is heated up to 70°C (heating collar 500 W) and moistened by steam countercurrent injection (steam generator semiautomatic NEMO 1.6 kW). The relative humidity (RH) is measured using a capacitive hygrometer downstream of the steam injection. Area 3 corresponds to the test zone. It is composed of a heating zone at 150°C (for the tests at incineration conditions) and comprises two particle injections. The reagent particles, i.e. a mixture of activated carbon and sodium bicarbonate, were injected by the powder dispersed generator SAG 420, TOPAS, while carbon agglomerates, i.e. condensation aerosol, were emitted from graphite monoliths (generator DNP 2000, Palas). A straight length (internal

diameter 48.6 mm) for gas flow stabilization and the filtration module containing the bag filter (150 mm in diameter and 440 mm in length). Particle counting (with SMPS, Grimm) was performed upstream and downstream of the bag filter thanks to sampling probes. The whole area, namely the pipes, the filtration module and the injection or sampling probes are heated to 150°C and thermally insulated to prevent condensation on the walls. Unclogging of the bag filter is provided by pulse-jet method. During this on-line procedure, the cake is removed from the filter using the injection of compressed air (at 6-7 bar) for 0.3 s in the opposite direction of the gas flow. A removable tank allows the dust to be recovered at the bottom of the filtration module.

Finally, in the area 4, gas condensation is ensured by means of a multi-tube heat exchanger followed by a lost water condenser. Before discharging to an extraction device at the room temperature, the gas is filtered with a H14 filter (European standard EN1822:2009). The entire pilot is installed in an under-pressure laboratory dedicated to the study of nanoparticles with entrance hall, and both areas 3 and 4 are under a ventilated hood.

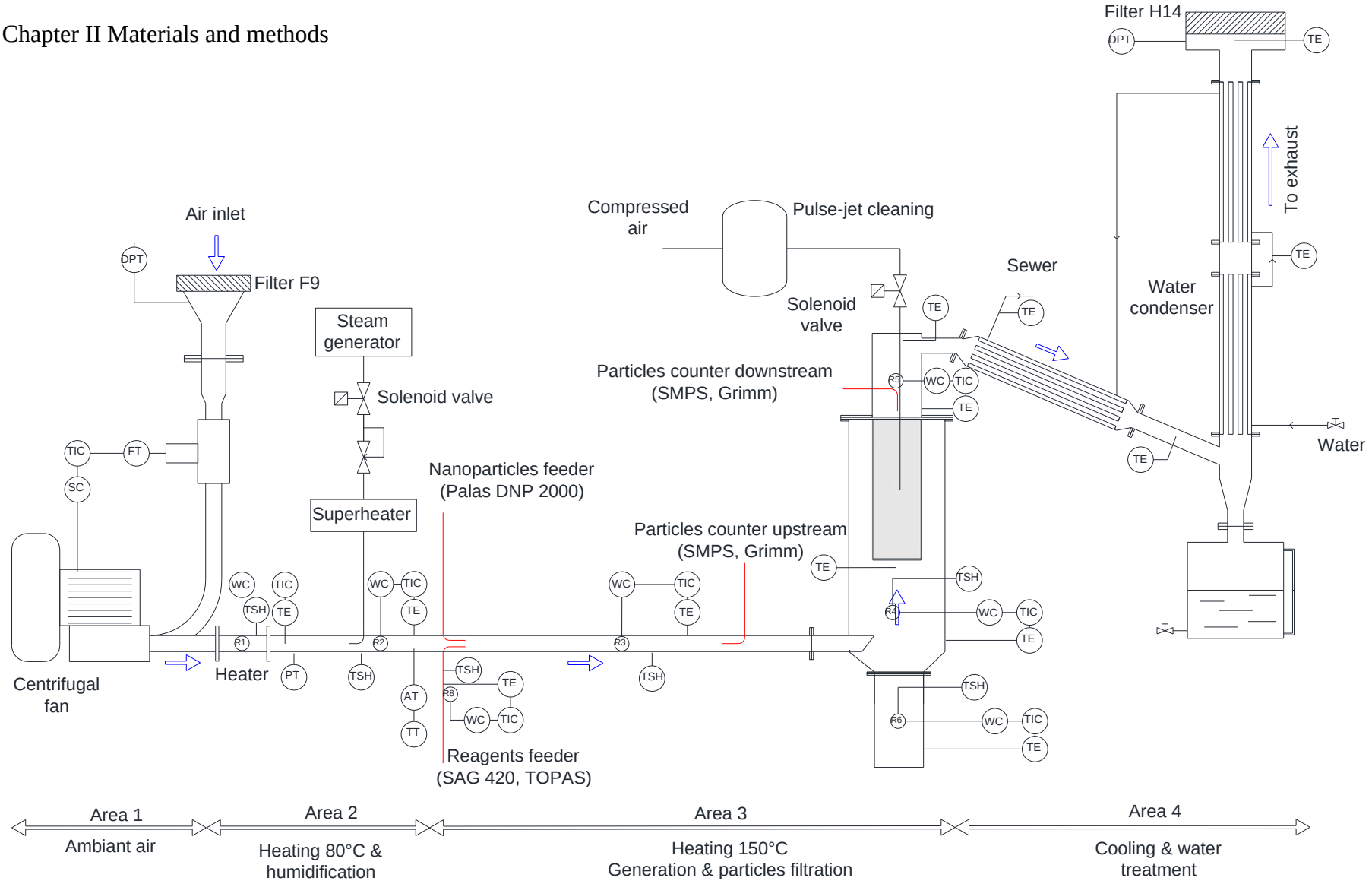

Figure 20: Experimental setup for bag filter clogging tests

The **Figure** 21 shows the real picture of the bag filter experimental setup in laboratory.

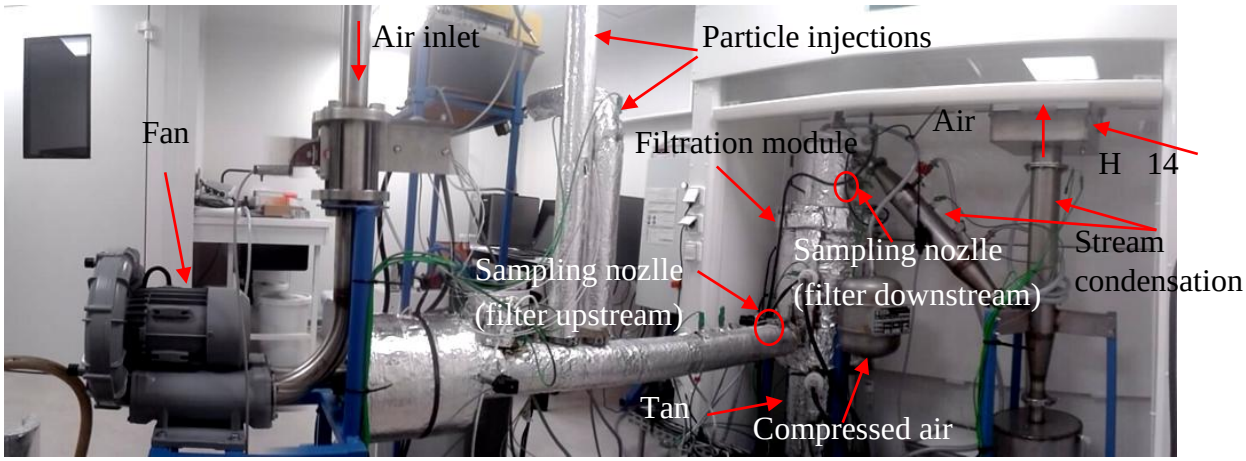

Figure 21: Photograph of experimental setup for bag filter clogging tests

Tests were carried out at constant air flow of 10 $Nm^3.h^{-1}$, corresponding to a filtration velocity of 1.9 $cm.s^{-1}$, and the bag filter pressure drop was measured continuously during the clogging until 150 Pa as the maximum value (for the tests at incineration conditions). The measurement of temperature and pressure were performed at various points in the setup in order to accurately calculate the actual flow rates and relative humidity.

Bag filter regeneration is carried out by pneumatic filter cleaning. The compressed air injection nozzle whose orifice of 15 mm in diameter, is centrally placed inside of the filter at 0.15 m from top. For good mechanical strength of the bag filter, three support rings were fastened on their overall height in order to ensure their rigidity that prevents the crush during filtration. The compressed air reservoir volume is 44 L and a safety valve is set at 7 bars. The pressure of the compressed air tank can be varied between 6 and 7 bars.

II.2 Flat filter setup

Flat filter set-up is dedicated to single filtration tests (without on-line filter regeneration) at ambient temperature close to 24°C and relative humidity of 45% for different filtration velocities (1.4 to 1.9 $cm.s^{-1}$), and for flat geometry of the filter.

An overall view of the filter unit and the filter mounting is given in the **Figure 22**. The experimental setup used for flat filters is a simple straight filtration conduct with the same equipment as the previous setup (particle injection, sampling upstream and downstream of the filter).

A distance of 1.5 m was established between the filter tested and the particle injection in order to establish a stabilized flow path and homogeneous dispersion of generated particles. The

flow is maintained constant during filter clogging due to the pressure drop control generated by air flow through diaphragm by acting on the centrifugal fan frequency.

The setup is fed by the laboratory air after preliminary filtration (G4 and H14 filters) to ensure that no particles other than the generated are present. The maximum pressure drop of flat filters testing at ambient conditions (24°C - 45% RH) was fixed at 120 Pa. The gas viscosity is influenced by the change in operating parameters and increases with temperature. Thus, the filter pressure drop of 150 Pa at 150°C and 3% RH which was fixed for bag filter conditions, corresponds to 120 Pa of pressure drop at ambient conditions (24°C - 45% RH) for a similar filter permeability.

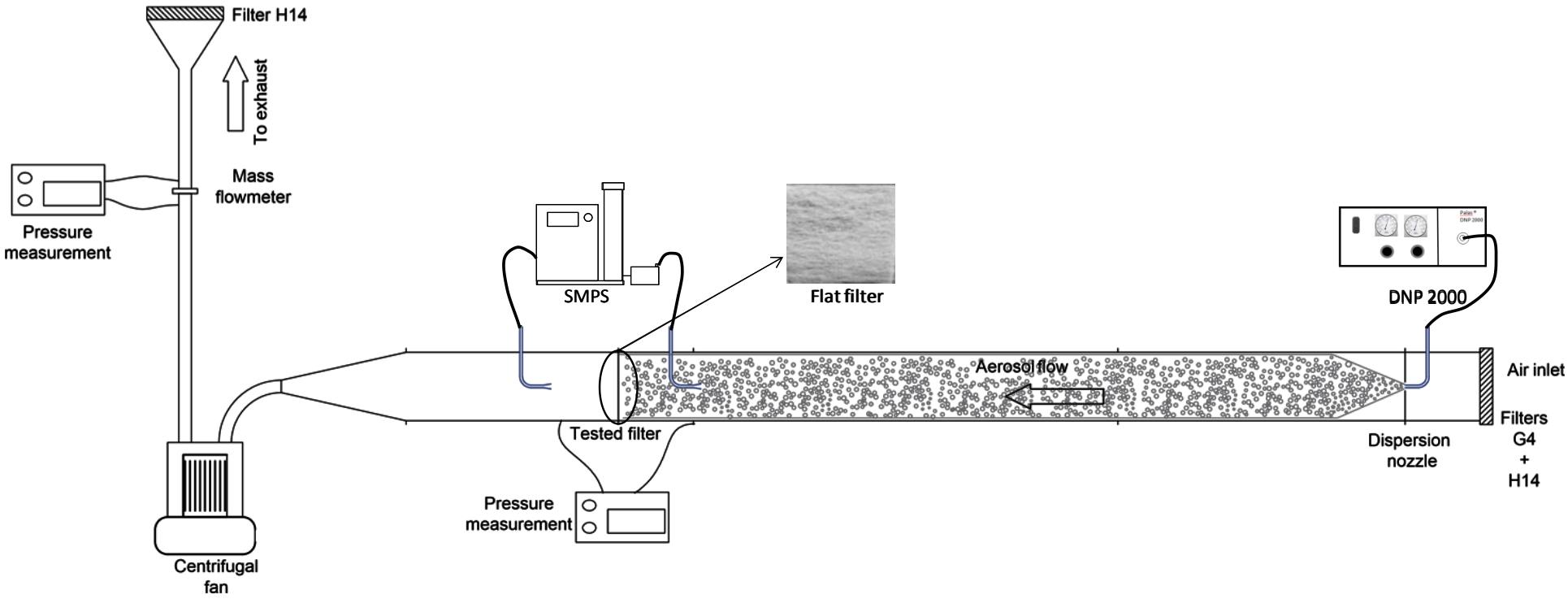

Figure 22: Experimental setup for flat filter clogging tests

II.3 Aerosol sampling

According to Hinds (1999), the isokinetic sampling of aerosols depends on their properties especially size and particle density. For nanometric and submicronic particle sampling, the isokinetic sample error is not significant (Baron & Willeke 2001; Arouca et al. 2010).

Arouca et al. (2010) showed that the isokinetic sampling conditions for nanometric aerosol within the size range of 12-130 nm does not depend on the sampling velocity, nor on the flowing duct flow rate nor on the diameter of the sampling nozzle.

However, as the tested aerosols are not only made up of nanoparticles, we decided, as a safety precaution, to follow the isokinetic sampling conditions for all aerosol and filtration conditions because obtaining a representative aerosol sampling is the crucial condition that must be achieved during particle measurement. The objective of this process is to capture the quantity of particles as similar as possible to that existing in a volume of flow inside the setup without disturbing their path. Absence of divergence of flow lines around the sampler inlet is the main condition that must prevail in isokinetic sampling. Thus, velocities of the sampled and sampling streams must be equal. In fact, the air flow inside the sampling probe nozzle must be equal to the flow at the point of the sampling area. To avoid or minimize the divergence of sampled stream, the inlet sampling nozzle must face the flow lines as illustrated in **Figure 23-a**. When the sampling velocity is too low inside of sampling probes, compared with inlet flow, the particle concentration entering the sampling probes is higher than the particle concentration in the main stream due to their greater inertia, while the gas is diverted around the tube as illustrated in **Figure 23-c**. If the velocity in the sampling tube is higher than the mainstream, the concentration inside sampling probes becomes lower than the mainstream and particles follow the streamlines (**Figure 23-d**). The geometry of the sampling nozzle also influences the quality of the sampling (**Figure 23-b**).

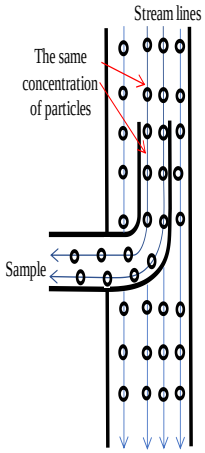

a: illustration of isokinetic sampling

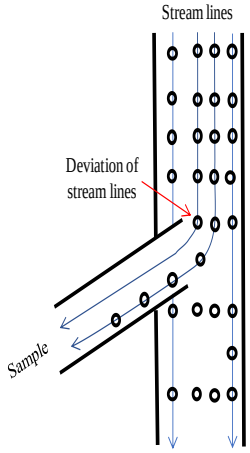

b: Too few large particles collected

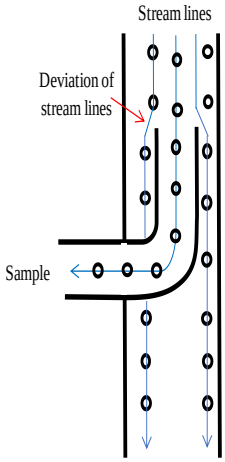

c: Too many large particles collected

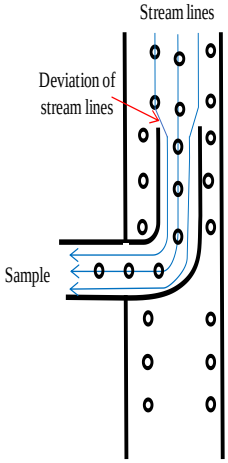

d: Too few large particles collected

Figure 23: Schematic illustration of air sampling (inspired from James & Lodge 1988)

The particle sampling is realized by nozzles introduced into the flow, upstream and downstream of the filter at the center of the straight length.

Flat filter setup

The location of the sampling nozzle from the upstream and the downstream of the filter are 25 cm and 30 cm respectively. The sampling is carried out respecting isokinetic conditions. Thus, the nozzles are changed with filtration velocity. Indeed, the sampling nozzle diameters at 1.4 and 1.9 $cm.s^{-1}$ of filtration velocity are respectively 21 and 18 mm (**Figure 24-a**).

Bag filter setup

The nozzles from the bag filter are 10 cm and 15 cm upstream and downstream of the filter respectively. The diameter of the sampling changes with the gas velocity, which in turns

varies as a function of the pipe diameter of the setup at a constant flow rate (167 $l.min^{-1}$). Nozzle diameters upstream and downstream of the filter are 1.7 and 7 mm respectively (Figure 24).

a) Nozzle for flat filter at V_f=1.9 $cm.s^{-1}$ (d=17 mm)

b) Nozzle for flat filter at V_f=1.4 $cm.s^{-1}$ (d=21 mm)

c) Nozzle for upstream bag filter (d=1.7 mm)

d) Nozzle for downstream bag filter (d=7 mm)

Figure 24: Sampling nozzle for flat and bag filter setups

III Tested aerosols

In order to be representative of the particle size distribution (PSD) emitted from waste incineration containing nanomaterials, carbon agglomerates were generated, i.e. condensation aerosol emitted from graphite monoliths (generator DNP 2000, Palas). Moreover, a mixture of reagents (activated carbon and sodium bicarbonate) was generated to be representative of dry treatment process of incineration fumes where those components are injected in the fumes upstream of the bag filters.

III.1 Aerosol description

III.1.1 Carbon particles

Soot or black carbon nanoparticles are the unwanted byproduct from the combustion of carbon-based materials for disposal of waste containing nanomaterials. Black soot nanoparticles (**Figure 25**) are the major investigated particles in the present study. The properties and the particle soot formation depend on several parameters such as the precursor, temperature, pressure, and concentration (Haynes & Wagner 1982; Glassman 1989; Kennedy 1997; Richter & Howard 2000; Frenklach & Wang 1994; D'Ann et al. 2001; Wang et al.

2013; Eremin 2012). At high temperature (between 1000 and 2500°C) (Wagner 1978) and low oxygen concentration, the burning of wastes containing carbon compounds can lead to the formation of soot (Niessen 2010). A great deal of the research that has been carried out on particle soot has focused on the use of carbon black as a substance of elemental carbon of particles soot generated from combustion (Bockhorn et al. 2009).

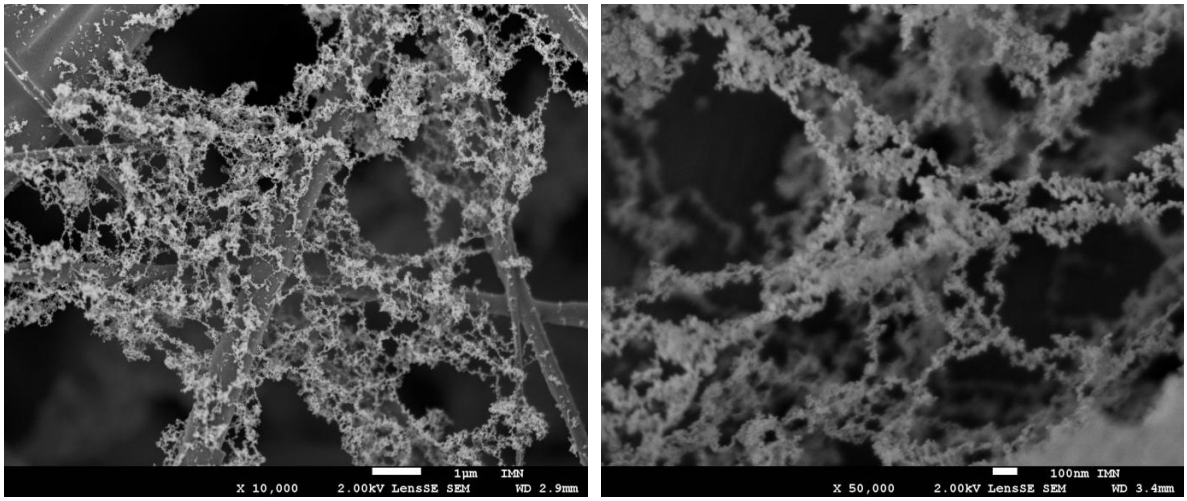

Figure 25: SEM observation of agglomerates generated by the DNP 2000 generator (Palas)

III.1.2 Reagents: activated carbon and sodium bicarbonate

The treatment of acid gases generated by waste combustion such as SO_2 and HCl is done by reaction with a basic compounds. The reagent particles used in this study (**Figure 26**) in a dry treatment, are a mixture of activated carbon and sodium bicarbonate powders, generated (generator SAG 420, TOPAS) simultaneously with the carbon particles during some clogging tests, because the reagents are commonly introduced upstream of the bag filter in flue gas treatment line for dioxin/furan and acid gas removal. The efficiency of dioxin/furan removal during the flue gas treatment depends on several factors, such as the quality of the adsorbent injection, efficiency of the adsorbent-flue gas mixing, the mass flow rate of the reagents.

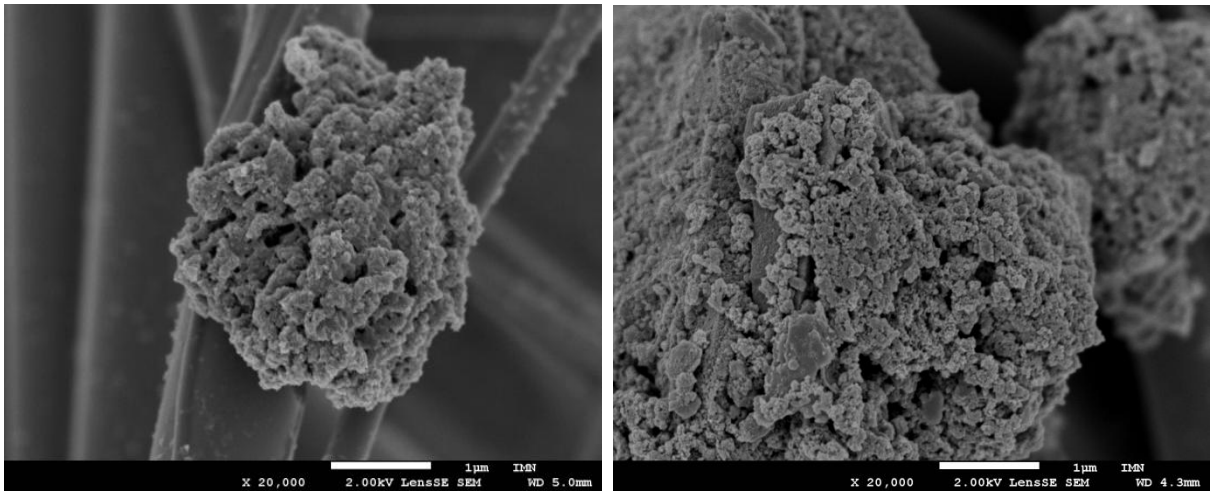

Figure 26: SEM observation of reagent particles (sodium bicarbonate + activated carbon)

III.1.2.1 Sodium bicarbonate

Sodium bicarbonate is a chemical compound described with the formula $NaHCO_3$. One of its major applications in industrial field is waste gas treatment. In powder form, sodium bicarbonate can be used for industrial gases treatment as anti-pollution agents, mainly for flue gas desulfurization, it can be also added to regulate and stabilize pH and alkalinity level in gases. The reaction between acid gases and sodium bicarbonate is a surface reaction. The solid is therefore generally ground in order to increase its specific surface area when decomposing into sodium carbonate, the release of gas (CO_2, H_2O) further increases the specific surface area by increasing the porosity (Bockhorn et al. 2009).

Powdered sodium bicarbonate is generally injected directly into the flue gases at the outlet of the boiler, where it decomposes from the temperature of 100°C (Heda et al. 1995). The sorbent is then retained by a filter media and becomes part of the formed cake filter. The decomposition of sodium bicarbonate ($NaHCO_3$) generates the sodium carbonate (Na_2CO_3) which in turn reacts with sulphur dioxide according to the following reactions (Bicocchi et al. 2009):

$2NaHCO_3(s) \rightarrow Na_2CO_3(s) + CO_2(g) + H_2O(g)$

$Na_2CO_3(s) + SO_2(g) \rightarrow Na_2SO_3(s) + CO_2(g)$

Na_2CO_3 also allows the treatment of HCl present in the hot gases (Duo et al. 1996) as follows:

$½Na_2CO_3(s) + HCl(g) \rightarrow NaCl(s) + ½CO_2(g) + ½H_2O(g)$

III.1.2.2 Activated carbon

Activated carbon is the substance usually used to remove undesirable components such as dioxins/furans from industrial gases during the utilization of a bag filter (BREF 2006). One of

its major properties is the huge specific surface due to their meso and micro-pores volume. The activated carbon powders are injected into the flue gas during their treatment. Similarly as sodium bicarbonate, the formed cake filter on the bag filter surface due to the filtration and the retaining particles of activated carbon, will be the mean surface of their contact to dioxins and other semi-volatiles (such as polycyclic aromatic hydrocarbons), the adsorption of this undesirable gases from the flue gas occurs until the bags are cleaned (Lu et al. 2013).

III.2 Particle generator and measurement equipment

III.2.1 DNP 2000 spark generator (Palas)

DNP 2000 (Palas) is a generator of nano-scale tests aerosols produced from graphite electrodes under high voltages that can be used for several hours non-stop. The applied discharge between carbon graphite electrodes leads to generate a high temperature that cause the evaporation of small fraction of the carbon which produce high number concentration of nano-sized particles (> 10^7 particles.cm^{-3}). In fact, the large number of elementary particles (3-10 nm) can coagulate to produce agglomerates which size (10-35 nm) can be adjusted by adding compressed air. In addition to the later, nitrogen is required as the carrier gas (Helsper et al. 1993; Horvath and Gangl 2003). The energy converted in each spark remains constant due to the constant spark over voltage, which allows the device to produce a constant particles concentration over time (Figure 27).

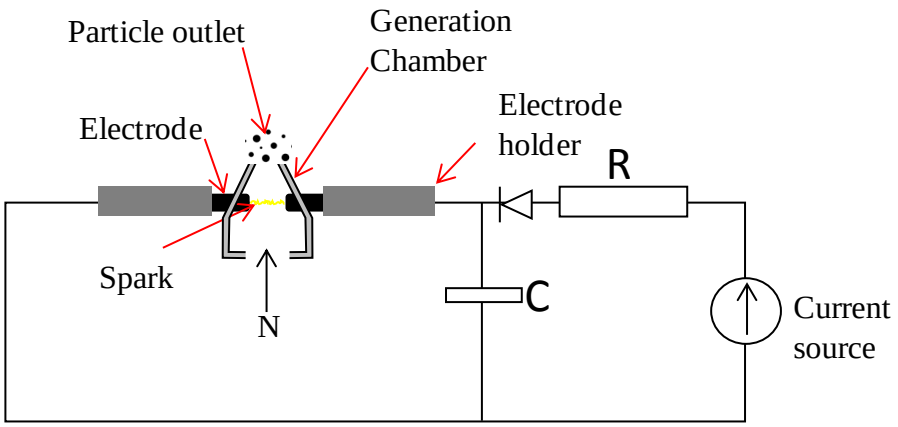

Figure 27: Principle of the spark generator

In order to ensure a good machine performance, a process of maintenance was periodically applied during operation tests. In fact, the flow channel should be cleaned after 4 to 100 operating hours. During the experimental tests, we decided to perform the maintenance after

each 15 operating hours. The aerosol outlet of the electrode unit was also cleaned within cotton buds dipped in a liquid ethanol or propanol.

The size distribution of the generated carbon aerosols depends on the spark frequency (2-999 Hz) and on the dilution air flow rate, which can be varied by tweaking the dilution air source. The size of the agglomerates increases with increasing spark frequency.

The particle size distribution as a function of spark frequencies is presented in **Figure 28** at constant air flow of 10 l.min^{-1}. In agreement with Helsper et al. (1993), the results showed the increase of particle size number as a function of spark frequencies. Moreover, the mean particle size was influenced by the spark frequency and increased from 42 nm at a frequency of 100 s^{-1} to 50 nm at 999 s^{-1}. While, during the increase of the air flow rates (from 10 to 30 l.min^{-1}) at constant spark frequency (f=999 s^{-1}) the measured mean particle size was shifted from 50 to 41 nm, leading to an increase in the particle number distribution (**Figure 29**). By consequence, the increase in the particles mass flow rate is only partially achieved by increasing the particle number concentration due to a strong coagulation phenomenon (Helsper et al. 1993).

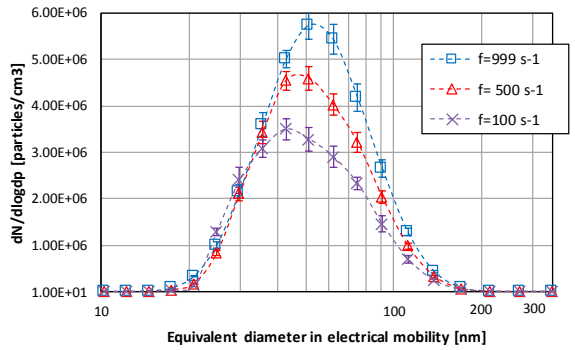

Figure 28: Particle number distribution of the carbon aerosol for different spark frequencies

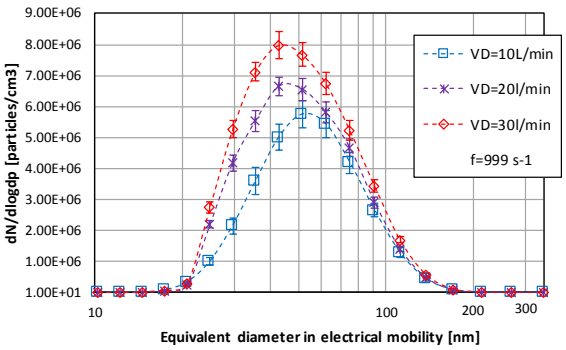

Figure 29: Particle number distribution of the carbon aerosol for different dilution air flow rates

III.2.2 SAG 420 dust disperser (TOPAS)

SAG 420 (TOPAS) is a dust disperser which generates solid aerosols by dispersion in air of a powdered solid feed at a constant flow rate to the disperser. The device conveys a constant mass flow rate of powder from a holding vessel (**Figure 30**) to a dispersion nozzle by means of a series of operations transport of powder on a driving belt at a given belt velocity and for a given thickness of powder on the belt, refining of powder passing through a scrapper screw, and dispersion of powder in compressed air passing through a dispersion nozzle.

SAG 420 (TOPAS), combines the dosing of particles and their dispersion quite reproductively and ensures relatively constant aerosol concentrations over prolonged periods.

The dosing of the reagents (activated carbon + sodium bicarbonate) is ensured by transporting of a defined amount from the holding vessel to the feeding screw. The stable quantity of dosed particles is ensured by the speed of dosing belt which is kept constant and can be adjusted in a wide range.

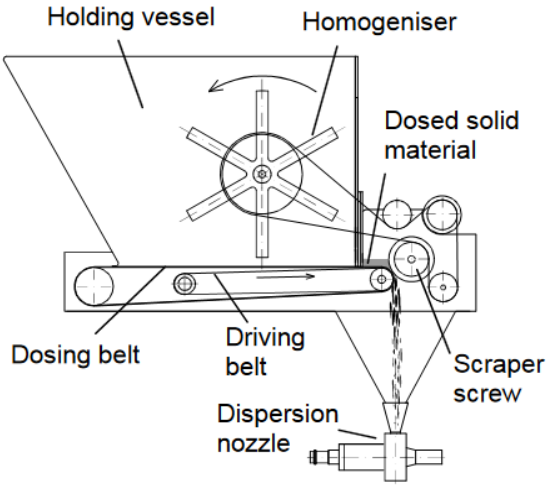

Figure 30: Schematic of the SAG 420 (TOPAS) dust disperser, side views

The concentration of the injected reagents was fixed from the TREDI incineration plant specifications: 2.5 $g.m^{-3}$ and 0.2 $g.m^{-3}$ respectively for sodium bicarbonate and activated carbon. Corresponding concentration of mixture (2.7 $g.m^{-3}$), the set mass flow rate of SAG 420 (TOPAS) was fixed at 4.5 $g.min^{-1}$ for the total flow of 167 $l.min^{-1}$ in the bag filter experimental setup.

III.2.3 Particle counter and mobility particle sizer SMPS, Grimm

SMPS (Grimm) (Scanning Mobility Particle Sizer) is the device used to measure particle size distributions and corresponding concentration based on electrical mobility. The measure consists first of all of imposing a charge law on the aerosol before selecting a precise electric mobility band using a classifier and counting the corresponding particles using an optical counter. It allows measuring particle distribution in the size range of 10-1000 nm, for single channel particle concentration in a range of $0\text{-}10^{7}$ $particles.cm^{-3}$ and sample flow of 0.3 $l.min^{-1}$. The device is well known for highest resolution information and lowest diffusion losses even for small particle because of the large number of used channels for particle classifications (23, 43 or 85 channels). As shown in Figure *31*, the device is composed of 2 important parts:

- Differential Mobility Analyser (DMA) + Impactor + particle pre-charger
- Condensation Particle Counter (CPC)

The input impact SMPS stops the largest particles which can carry several loads and prevents their presence in the column (DMA).

Differential Mobility Analyser DMA is an electrostatic classifier to sort particles based on their electrical mobility. CPC is an optical counter of particle artificially enlarged by butanol condensation; particle counting is performed for each class of particles classified by DMA.

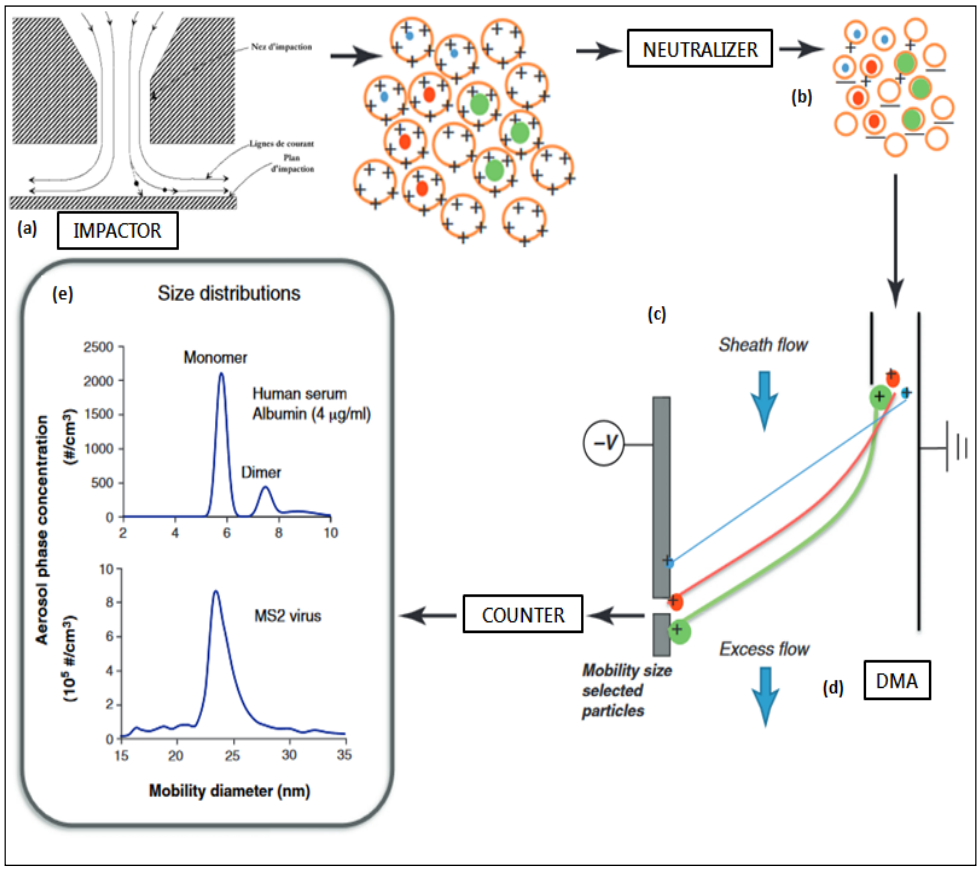

Figure 31 : Illustration scheme of different component of SMPS (Guha et al. 2012)

III.3 Particle size distribution and concentration

A monitoring of the particle concentration generated during filtration tests was realized. For each operating condition, the particle size distribution (PSD) and the concentration of generated aerosol were measured upstream of the filter. **Figure 32** represents the average PSD measured over 6 different sampling time periods of the generation, with the standard deviation as associated uncertainty.

As a function of filtration conditions and experimental setup, we can see different measured PSD. In the bag filter experimental setup, the particle size distribution at ambient conditions was found to be log-normal with a mode at 70 nm at the concentration of $1.69.10^{7}$ particles.cm^{-3} for overall diameter ranging from 0.01 to 0.315 µm. While at temperature conditions, of 150°C - 3% RH and 150°C - 0% RH, the concentration reduced because of the effect of thermophoresis phenomena on submicron particle movement inside the experimental setup despite a careful heating of the device walls. The concentrations of NPs were respectively 5.09×10^{6} and 5.79×10^{6} particles.cm^{-3} with a particle mode around 50 and 45 nm. For the mixed aerosols (nanoparticles + reagents) the concentration was 5.45×10^{6} particles.cm^{-3} for overall diameter ranging from 0.01 to 0.8 µm at incineration conditions (150°C - 3% RH).

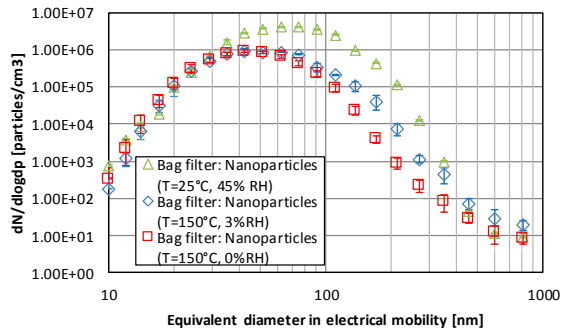

a) Upstream of bag filter, influence of T and RH conditions

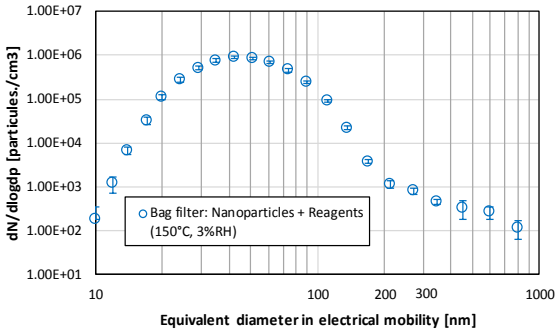

b) Upstream of bag filter T=150°C, RH=3%

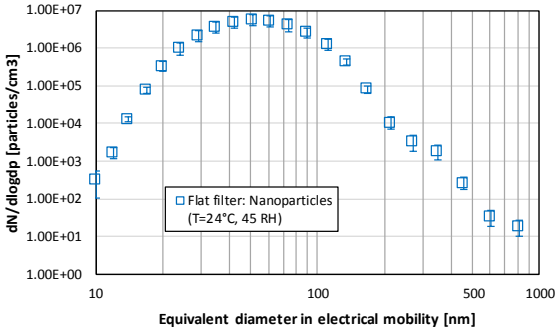

c) Upstream of flat filter T=24°C, RH=45%

Figure 32: Particle size distribution of bag filter (a, b) and flat filter (c) at different filtration conditions (T, RH)

Table 4: Evolution of geometric standard deviation and median diameter for different filtration conditions

	Electrical mobility median diameter d_{50} [nm]	Geometric standard deviation σ_g [-]
Bag filter BC NPs (150°C - 3% RH)	51	1.6
BC NPs (150°C - 0% RH)	45	1.5
BC NPS (24°C - 45% RH)	62	1.3
BC NPs + Reagents (150°C - 3% RH)	45	1.3
Flat filter NPs (24°C - 45%RH)	51	1.4

III.4 Stabilization of the generated aerosol

In order to stabilize the mass flow rate of generated particles and ensure their homogeneous dispersion in the flow, the particles generator DNP 2000 (Palas) was started-up outside of the experimental setup for a period of 90 min before starting the particle generation inside the filter device. **Figure 33** shows the evolution of generated particle concentration and the electrical mobility median diameter over the time. The results indicate that the BC generation is stabilized over the time in terms of concentration from 50 min of generation

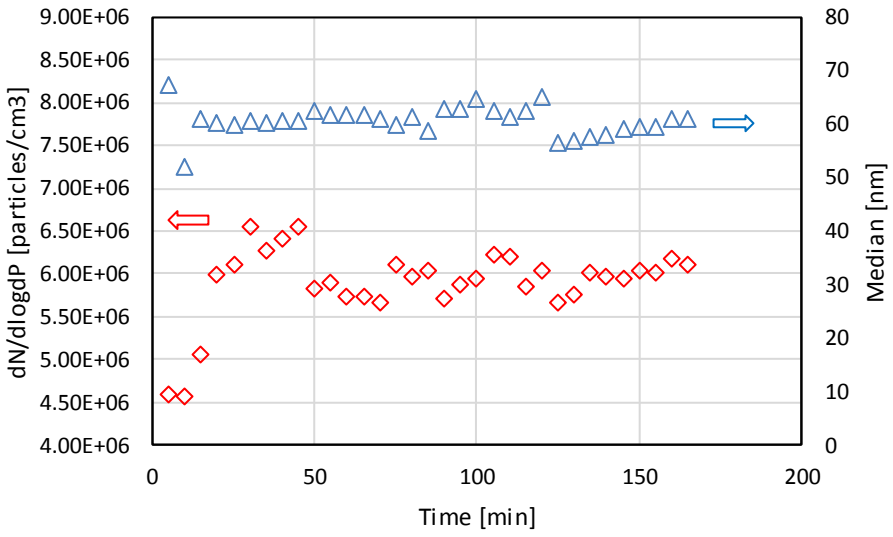

Figure 33: Evolution of nanoparticle concentration and electrical mobility median diameter as a function of time

IV Tested filters

IV.1 Filter geometries

Two filter geometries of the same filter media were tested in this study. The bag filter implemented is a down-sized filter of industrial bag filter with reduced length. As shown in the **Figure 34**, the bag filter is a cylindrical geometry total surface $S = 0.225\ m^2$ of the height $H = 0.44\ m$ and the diameter $d_{filter} = 0.15\ m$ $\left(\frac{d_{filter}}{H} \simeq \frac{1}{3}\right)$. The filter was developed in the Laboratory from a commercial filter ($d_{filter} = 0.15\ m$, $H = 5\ m$, $\frac{d}{H} \simeq 0.03$, and $S = 2.37\ m^2$) provided by TREDI company. Flat filters were made from the same media used for the bag filter with the size of 275 x 275 mm and total surface filtration of 0.0756 m^2.

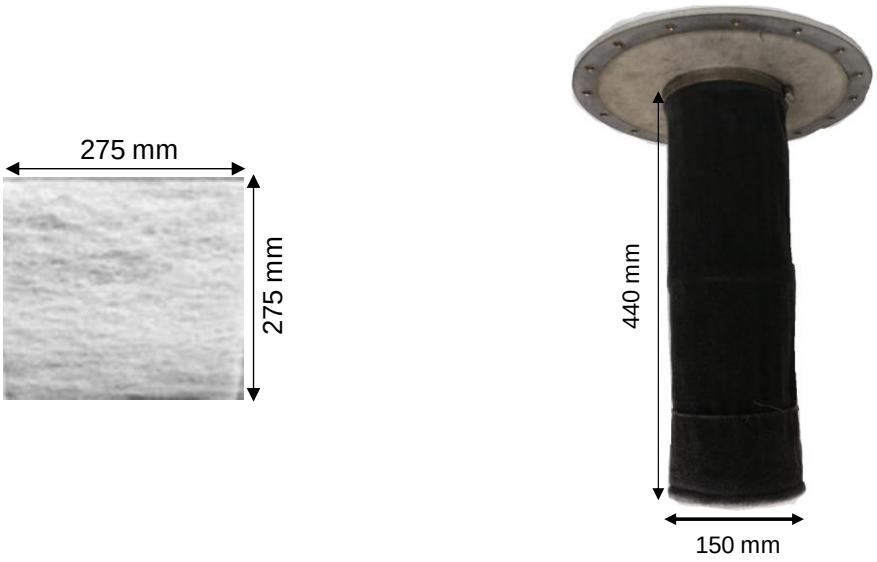

Figure 34: Dimensions of tested filters

The 2 used bag filters were dismantled from air pollution control device in the industrial gas treatment unit and sent for a special washing before receiving it in the laboratory.

The 2 tested bag filters were received in 5 m of height and reduced to 0.44 m to adapt the experimental setup in laboratory. The extra length was cute out into several parts of flat geometry (total surface filtration of 0.0756 m^2) in order to test the filter performance at two different filtration velocities (1.4 and 1.9 $cm.s^{-1}$) with reproducibility of the results.

IV.2 Structural parameters of the filtering media

The structural properties of the filtering media (thickness, fiber median diameter, porosity and basis weight) are presented in **Table 5.** These values were estimated from experimental measurements.

The media is a non-woven structure composed of Teflon fibers (Polytetrafluoroethylene PTFE). **Figure 35** presents pictures of the surface and a transversal cross-section of the filter from Scanning Electron Microscope (SEM) observations. The pictures were carried out using the SEM JEOL 5800-LV. Before microscope observation, the samples were degassed under vacuum and metalized by deposition of gold-palladium layer.

Table 5: Main structural parameters of the filtering media (Le Bihan et al. 2014)

Parameters	Value	Method
Thickness (µm)	1256 ± 31	Scanning electron microscope
Fiber median diameter (µm)	19.5	Scanning electron microscope
Total porosity (-)	0.64	Mercury porosimetry
Basis weight ($g.m^{-2}$)	750	NF EN 12 127

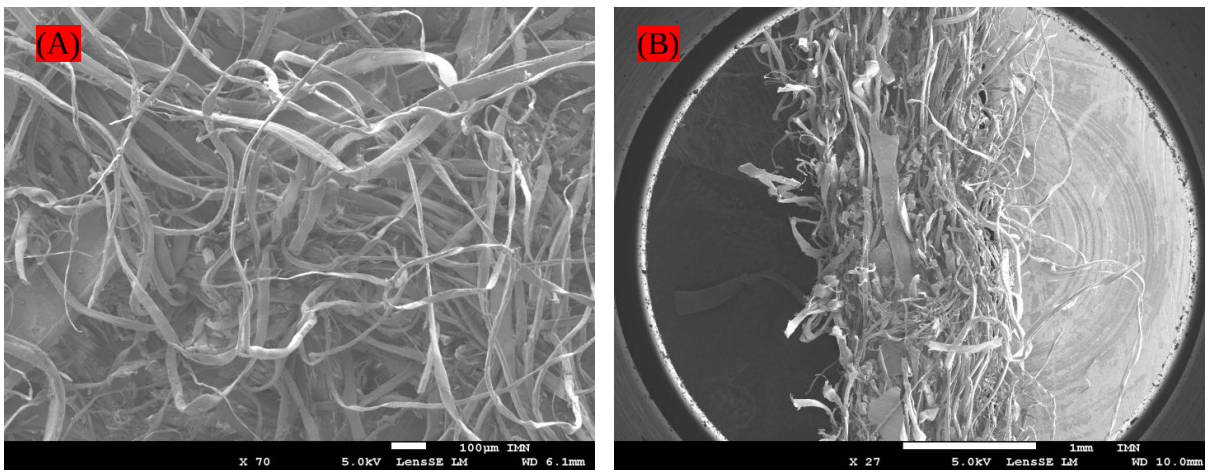

Figure 35: SEM observation of the surface (A) and the slice (B) of the filter media

IV.2.1 Fiber nature

PTFE (brand name Teflon (R)) is used in several industrial applications, such as aerosol sampling, air venting, and gas filtration. The main properties of PTFE filter during filtration is the hydrophobic characteristics, which makes the media water non-absorbent (Jornitz et al.

2007). Additionally, PTFE has high chemical resistance and good thermal resistance which makes this material a frequent choice for the membrane material in the industrial field (inert to most chemically aggressive solvents, strong acids and bases), and has a very low coefficient of friction which avoid particle sticking and allow an easy on-line cleaning.

IV.2.2 Fiber diameter

The geometrical diameter of the fibers was measured by image analysis of the fiber diameters from the SEM observations using the Image J software. More than 100 fibers were analyzed from 3 different samples of the media. As the results showed in the **Figure 36**, the fibers distribution is mono-modal with modal diameters observed at 15-20 µm.

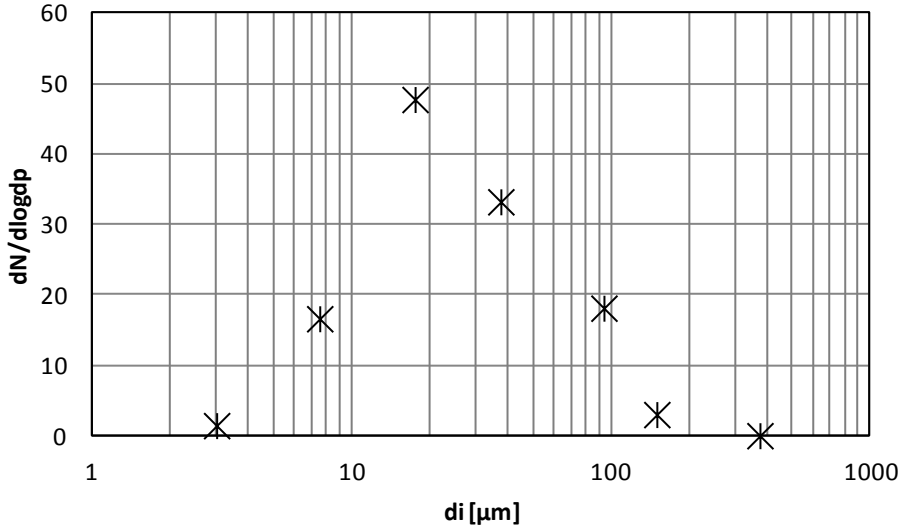

Figure 36: Size distribution of the Teflon fibers constituting the filter media (obtained by SEM image analysis)

IV.2.3 Filter media porosity

There are several methods to characterize the porosity of a filter media such as extrusion flow porometry, extrusion porosimetry, mercury intrusion porosimetry, non-mercury intrusion porosimetry, vapor adsorption, vapor condensation. In our study, mercury porosimetry was chosen because of its efficiency to provide information about the porosity and the inter-fiber porous distribution, i.e., the pore size distribution of the media at the inter-fiber scale of the material. For this purpose, the following equation allows to estimate the equivalent diameter of the fibers, as a function of the porosity and the hydraulic diameter of the pores:

$$S_f = \frac{\mathbf{4}\boldsymbol{\varepsilon_i}}{(\mathbf{1}-\boldsymbol{\varepsilon_i})\,\boldsymbol{d_{pores}}} \qquad (58)$$

S_f [m^{-1}] is the specific surface area of the fibers which corresponds to the ratio between the external surface of a fiber and its volume. $\boldsymbol{\varepsilon_i}$ [-] is the inter-fiber porosity and d_{pores} is the mean diameter of the pores media. Considering the fiber as cylindrical, the specific surface area of a fiber can be used to determine its diameter $S_f = \frac{4}{d_f}$

IV.2.4 Surface treatment of fabric filter

In order to enhance the life period and resistance of fabric filters, the latter must be treated (finished) to withstand various conditions, especially moisture and abrasion. A different way of surface filter finishing exists, for instance, mechanical and chemical treatment of either the entire fabric or just the fabric surface. The main objectives of surface treatment are: capturing fine particulate, improving filtration efficiency, improving the dust cake formation on the filter and efficiency of filter cleaning. This can be achieved by common mechanical treatment such as: singed, eggshell, glazed, calender and ePTFE membrane (Hutten 2007). For this work, used media is a used calendered PTFE fabric.

Calendaring is the high pressure pressing of the filter media by rollers to flatten or smooth the material in order to compress the fibers to smooth the surface. This type of treatment surface is efficient to prevent the clogging of filter media and improve the cake release and rectify its permeability for stabilization of the filtration efficiency (Hardman et al. 2003).

IV.2.5 Filter media permeability

The permeability is a widespread quantity used to control the filter performance (Seville 1997). Each filter has a specific air permeability value (K), which differs according to its properties and characteristics. According to the Darcy's equation, one of the overall approaches used to describe pressure drop (ΔP) across a filter, the expression of the air permeability (K) can be determined by the following formula already presented in **Chapter I**:

$$K = \mu \frac{U_f . L}{\Delta P} \quad (59)$$

Air permeability (**Figure 37**) was determined from measuring the variation in the pressure drop generated by tested filters as a function of flow velocity passing through it. These measurements were carried out for flat and bag filter in different filtration conditions. The permeability was performed for air velocities between 0.001 and 0.12 $m.s^{-1}$.

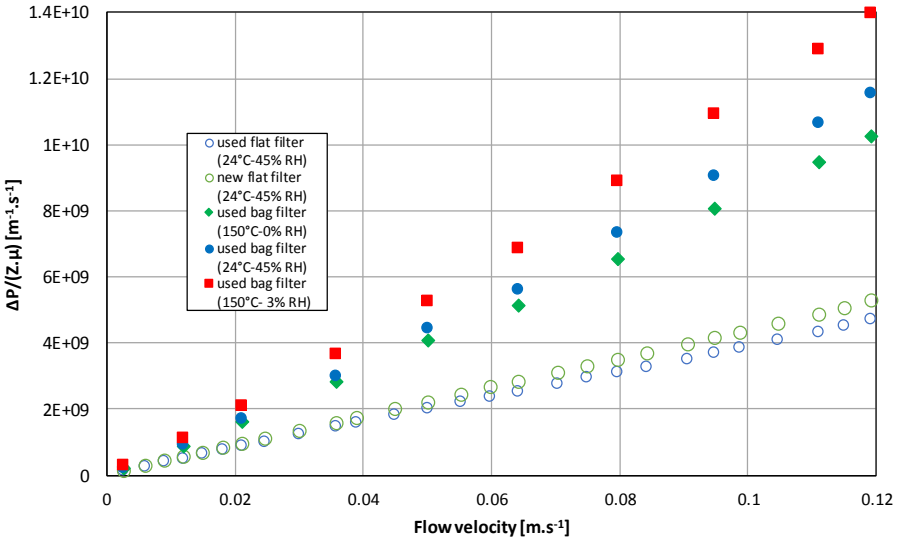

Figure 37: Evolution of pressure drop of the filter media as a function of the flow velocity for flat and bag filter at different operating parameters of filtration conditions

The air flow across the filter was gradually increased and measured its pressure drop accordingly. The results show a linear relationship between pressure drop (ΔP) and air flow velocity for flat filters, while for bag filter the curve is slightly rising in parabolic shape. This difference in behavior is certainly due to the influence of the filter geometry where important pressure is applied on the inner face of the bag filter. The filter resistance changes as well with changing the filtration conditions. The resistance of bag filter is higher at incineration conditions (150°C - 3% RH) than ambient conditions (24°C - 45% RH); the resistance of bag filter increases as well in presence of humidity (150°C - 3% RH) than dry conditions (150°C - 0% RH). On the other hand, Miguel et al. (2003) showed that non effect of relative humidity was observed on clean filter media permeability. Nevertheless, this difference with our results can be explained by the fact that the amount of water at 150°C and 3% RH (almost 100 g water/kg air) is significant in comparison to the water content tested by Miguel et al. (2003).

According to the Darcy's law, the filter resistance decreases with increase of air viscosity. From the other hand, the air viscosity decreases with increase of humidity. Thus, the filter resistance is important at higher value of humidity.

V Methodology

V.1 Overall Methodology

As filter presented in this chapter, PTFE filter of two different geometries (bag and flat configurations) were studied at laboratory scale in terms of pressure drop (ΔP) and particle

collection efficiency (E%) for sequential clogging/unclogging cycles. The experimental methodology and corresponding objectives for performance investigation of flat and bag filter are shown in **Figure 36**.

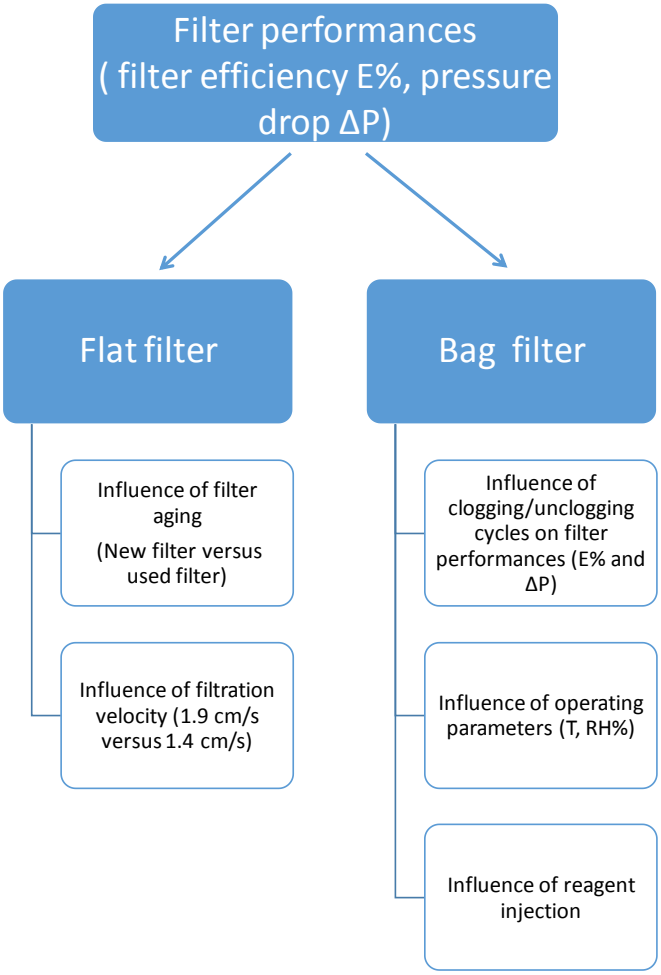

Figure 38: Diagram illustrator of main experimental objectives

V.2 Operating conditions for experimental campaigns

Filtration performance of bag filter was evaluated at the laboratory for 10-15 cycles of clogging/unclogging. The experiments were conducted from one side at ambient conditions of temperature and humidity (24°C - 45% RH) for clean and used bag filters and from the other side two used bag filters were clogged at incineration temperature conditions (150°C - 3% RH and 150°C – 0% RH). For all filtration conditions, filtration velocity was fixed at 1.9 $cm.s^{-1}$ representative of that encountered in incineration plants.

The results are presented considering the evolution of filter pressure drop during 10 cycles of clogging/unclogging and considering the fractional efficiency (particle collection efficiency versus particle diameter).

For the flat filters, each test was repeated three times with different filter samples clogged at room conditions (24°C – 45% RH) for a maximum pressure drop of 120 Pa. The **Table 6** and **Table 7** resume all test made for different filters:

Table 6: Experimental campaigns at ambient conditions

	Used flat filter		**New flat filter**		**Used bag filter**	**New bag filter**
Operating conditions	Ambient conditions: 24°C - 45% RH					
Aerosols	BC NPs (0.01 to 0.315 µm)					
Filtration velocity ($cm.s^{-1}$)	1.9	1.4	1.9	1.4	1.9	1.9
Number of tested filter	3	3	3	3	1 (10 filtration cycles)	1 (10 filtration cycles)
Maximum pressure drop (Pa)	120	120	120	120	120 per filtration cycle	120 per filtration cycle
Clogging time per one tested filter (h)	8-9	10	8-9	10	39-40	39-40

Table 7: Experimental campaigns at 150°C temperature conditions

	Used bag filter	**Used bag filter**	**Used bag filter**
Operating conditions	150°C - 3%RH	150°C - 0%RH	150°C - 3%RH
Aerosols	BC NPs	BC NPs	BC NPs + Reagents
Filtration velocity ($cm.s^{-1}$)	1.9	1.9	1.9
Number of tested filter	1 (10 filtration) cycles)	1 (10 filtration)	1 (10 filtration) cycles)
Maximum pressure drop (Pa)	150	150	150
Clogging time/cycle (h)	30	50	16

V.3 Aerosol preparation and generation protocol

Preparation of aerosol samples in laboratory-scale undergoes two separate steps: homogenization and pre-drying. The reagents sample is prepared by mixing a definite amount of activated carbon and sodium bicarbonate (respectively 2.5 $g.m^{-3}$ and 0.2 $g.m^{-3}$) that was previously determined from TREDI conditions on real incineration plant. Pre-drying of the samples was performed for 48h inside the oven at 100°C. The pre-drying is currently widely used for particle samples; it keeps the texture of the sample and eliminates the absorbed humidity. Before the particle injection, the setup was periodically cleaned from the inside via a particle vacuum. The cleaning was ensured before each test to avoid particle contamination that can vary the concentration of injected aerosols. The cleaning of nozzles and tubes for injection and particle sampling are performed by blowing with compressed air.

The prepared reagent particles were then injected by the powder dispersed generator SAG 420, TOPAS. Meanwhile the carbon agglomerates were emitted from graphite monoliths (generator DNP 2000, Palas). Before starting the particle generation inside the set-up, the generator DNP was started outside of the experimental setup for a period of 90 min to stabilize the mass flow rate of generated particles and ensure their homogeneous dispersion in the flow.

V.4 Aerosol dilution

The measurements of the particle concentrations under incineration conditions (150°C - 3% RH and at 150°C – 0% RH) were carried out with the implementation of a VKL diluter before the particle counter SMPS, to avoid exceeding the maximum allowed operating temperature and humidity for the SMPS.

VKL is a dilution system employed to reduce aerosol concentration for a given gas flow. The dilution occurs by homogeneous mixing of a definite amount of clean air with a definite amount of aerosol (**Figure 39**). The ratio of the mixed amount of aerosol and clean air is predetermined and stable during dilution.

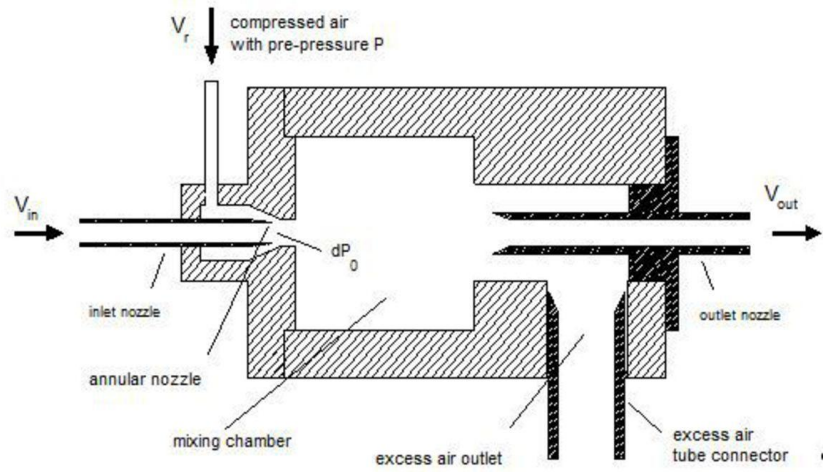

Figure 39: Pneumatic control panel

Different nozzle diameters must be adopted according to the outlet flow rate in order to prevail in isokinetic sampling and to avoid the divergence of flow lines around the sampler inlet.

V.5 Pressure drop measurement

The measurement of the pressure drop evolution generated by the gas flow through the filter during clogging is ensured using a pressure sensor made by the company FCO (model332), their characteristics are:

- Pressure measuring range: 0-200 Pa;
- Measuring accuracy: <0.5%;
- Configuration of 2, 3 or 4-wires;
- Voltage or current output: 4 - 20 mA.

The pressure measuring wires are placed upstream and downstream of the filter.

V.6 Efficiency measurement

V.6.1 Flat filter

V.6.1.1 Fractional efficiency of particle filtration

The fractional efficiency $E_{d_p}(t_n)$ is the filter collection efficiency measured at the time (t_n) for a given particle diameter d_p. The collection efficiency of particle d_p is determined by the ratio of number concentration measured upstream $N_{upstream,dp}$ to downstream $N_{downstream,dp}$ of the tested filter. For the flat filter, the filtration efficiency for a given particle diameter d_p is calculated according to the following equation (60):

$$E_{d_p}(t_n) = \frac{\left[N_{upstream,d_p}(t_{n-1}) + N_{upstream,d_p}(t_{n+1})\right]/2 - N_{downstream,d_p}(t_n)}{\left[N_{upstream,d_p}(t_{n-1}) + N_{upstream,d_p}(t_{n+1})\right]/2} \quad (60)$$

An initial value of fractional efficiency, that we can determine by the Most Penetrating Particle Size (MPPS), which represents the size of particle for which the collection efficiency is the lowest.

Figure 40, indicates the methodology of aerosol sampling with flat filter setup during clogging time. The protocol is used for particle sampling upstream and downstream the flat filter. The time duration of each sample takes 5 min, including 2 min of the "break time", i.e the gas sampling pass through the particle counter without data acquisition to stabilize flow of the sampled gas and to avoid measuring the particle concentration measured in the previous gas sample. The next 3 min of sampling is the overall time that takes the particle counter to measure the particle concentration.

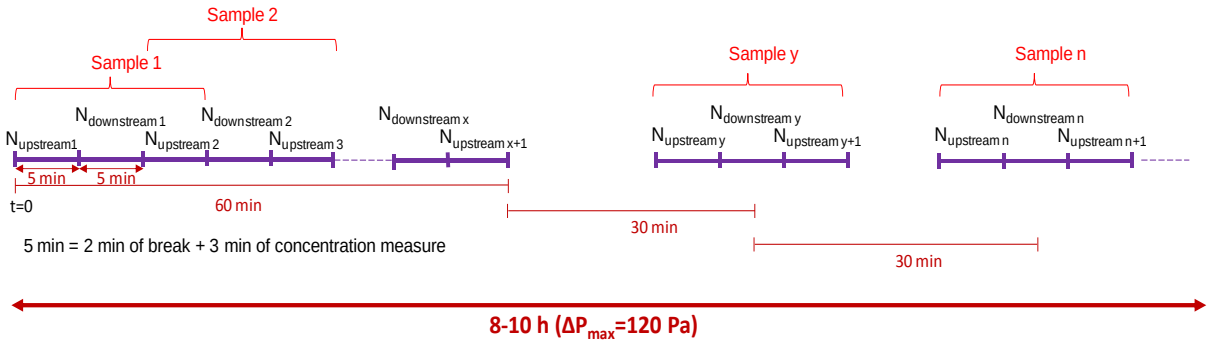

Figure 40: Schematic illustration of aerosol sampling methodology

V.6.1.2 Overall filtration efficiency

The overall filtration efficiency E(t) at the time t, is determined from the difference of the total measured particle numbers upstream and downstream of the tested filter. For flat filter E(t) can be determined from the following equation (61):

$$E(t_n) = \frac{\left[N_{upstream}(t_{n-1}) + N_{upstream}(t_{n+1})\right]/2 - N_{downstream}(t_n)}{\left[N_{upstream}(t_{n-1}) + N_{upstream}(t_{n+1})\right]/2} \quad (61)$$

V.6.2 Bag filter

Regarding the bag filter efficiency, a significant amount of particles carried by the gas is deposited on the walls of the filter holder upstream of the filter media and downstream of the particle sampling gauge. Thereby, the deposited particle concentration must be taken into

account in order to avoid a systematic error of calculated filtration efficiency. Thus, particles were generated in the bag filter experimental setup for the same experimental conditions without bag filter (as illustrated in **Figure 41**) in order to measure the particle concentration downstream of bag filter holder location as representative of the upstream effective particle concentration to be considered for tests performed with bag filter.

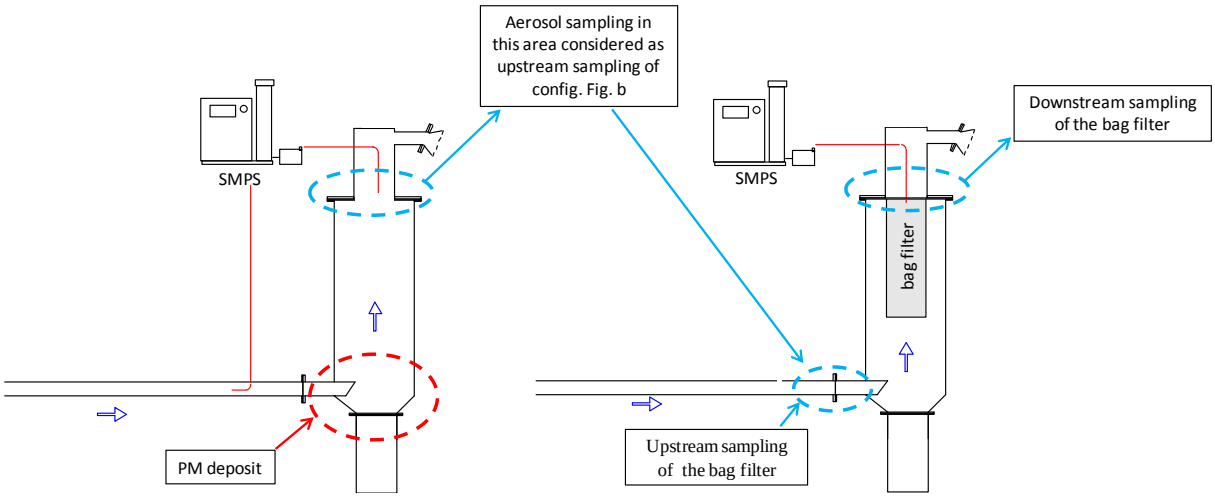

a) setup without bag filter b) setup with bag filter

Figure 41: Schematic illustration of particle concentration measuring upstream of bag filter

The measured particle concentrations at ambient conditions, without bag filter are presented in the **Figure 42**. The curves are the average of 6 aerosol samplings carried out on two different days. The results indicate a difference between particle concentration measured upstream and downstream of the filter holder in absence of bag filter. A significant amount of particles is deposited before reaching bag filter (see location of deposited in (**Figure 41-a**). This difference in concentration represents the particle collection efficiency of the filter holder.

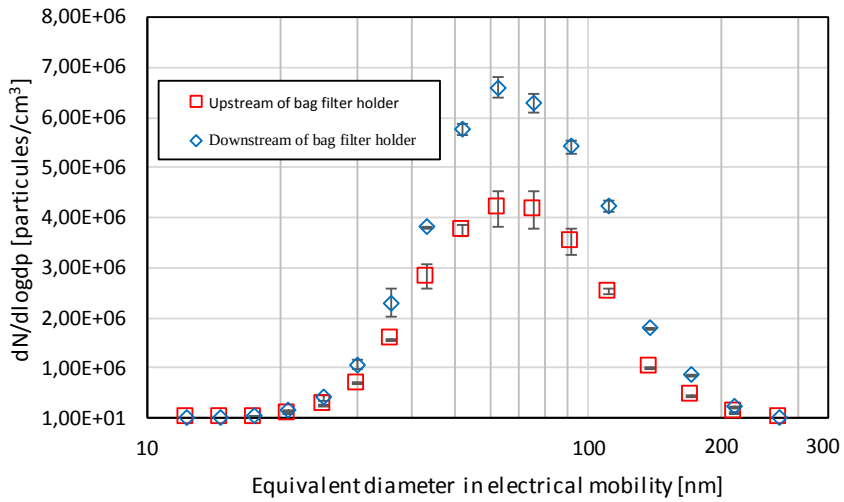

Figure 42: Difference of particle concentration upstream and downstream of filter holder in absence of bag filter

V.6.2.1 Fractional efficiency of particle filtration

As explained in the above section, the particle number upstream ($N_{upstream,dp}$) of the bag filter cannot be taken into account in the efficiency equation because of deposited particle in bag filter holder. In this case, the particle number measured downstream ($N_{downstream,dp}$) of the filter is varied as a function of filtration, while upstream particle number is a constant value pre-determined before the filtration testing ($\overline{N_{upstream,dp}}$). Thereby, the fractional efficiency is determined as:

$$E_{d_p}(t) = \frac{\overline{N_{upstream,d_p}} - N_{downstream,d_p}(t)}{\overline{N_{upstream,d_p}}} \quad (62)$$

V.6.2.2 Overall filtration efficiency

Similarly to fractional filtration efficiency, the overall efficiency was calculated according to the following equation (63):

$$E_t(t) = \frac{\overline{N_{upstream}} - N_{downstream}(t)}{\overline{N_{upstream}}} \quad (63)$$

VI Conclusions of the chapter

In this chapter, we presented filter characteristics and the experimental setups used for testing the filter performance. The first experimental setup was developed for bag filter geometry in order to be as representative as close as possible to the bag filter unit in waste incineration flue gas treatment. The device was equipped with pulse-jet cleaning system, which allowed us to test the filters during several clogging/unclogging cycles. The second experimental setup was used for testing the filter in flat geometry at ambient temperature but for different velocity. Several flat filters were clogged until the maximum fixed pressure drop without cleaning.

The injected particles in the flue gas were also described in this chapter. Two different aerosols with different size were used to clog the filters: black carbon nanoparticles representative of the particle size distribution (PSD) emitted from nano-waste incineration, and reagent particles, i.e. a mixture of activated carbon and sodium bicarbonate for dioxin/furan and acid gas removal. Particle size distribution of the aerosols and their electrical mobility median diameter were presented as a function of operating parameters measured at different experimental setup.

The particle sampling protocol and the protocol for collection efficiency measurement and pressure drop were presented in this chapter.

Chapter III Pulse-jet bag filter performance for treatment of submicronic and nanosized particles at waste incineration conditions

I Introduction

The main objective of this chapter is to evaluate the clogging/unclogging tests behavior of single baghouse fabric filter regarding the filtration of submicronic and nanosized particles. The operating conditions of filtration were fixed as close as possible to those of waste incineration plants in terms of gas filtration velocity, concentration of particle reagents, gas temperature and humidity, pressure and duration of the cleaning pulse-jet. The performance of the bag filter along 11 clogging/unclogging cycles were evaluated regarding the filtration of aerosol which particle size distribution is representative of nano-waste incineration emissions at the outlet of the boiler (Le Bihan et al. 2014; Tran et al. 2014). The airflow and the bag filter were heated to 150°C, the water content was maintained in the airflow in the range of 10-12% (i.e. 3% RH), while the filtration velocity throughout the bag filter was 1.9 $cm.s^{-1}$. Activated carbon and sodium bicarbonate, used in flue gas treatment lines mainly for dioxins/furans and acid gas removal, were generated simultaneously in air flow in submicronic size.

The study aimed to characterize the evaluation of the filtration performance at the beginning of the bag filter lifetime that is to say before stabilization of the residual pressure drop resulting from the previous filtration cycles. The maximum pressure drop was set at 150 Pa for all filtration cycles. Once the maximum pressure drop was reached, the filter was regenerated using the pulse-jet system for 0.3 s. The filtration is then continued until reaching again the maximum pressure drop.

The performance of the studied bag filter will be presented in terms of evolution of pressure drop, fractional and total particle collection efficiency.

II Bag filter pressure drop

Figure 43 shows the evolution of the used bag filter pressure drop (ΔP) as a function of time over 11 successive cycles of clogging/unclogging (C1 to C11). It should be noted that the error bars related to the experimental points have not been represented in the figure since the measuring accuracy of the pressure sensor is small (less than 0.5%) and did not allow a readable representation on the graph.

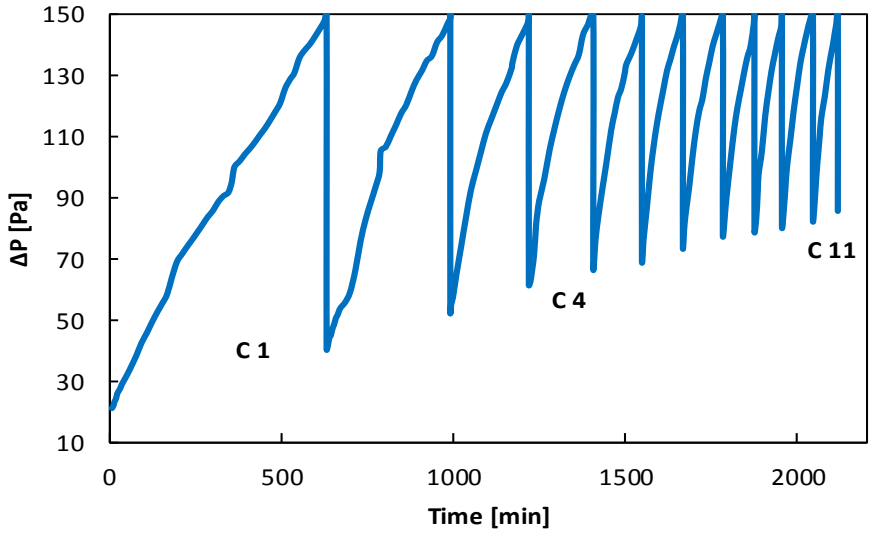

Figure 43: Bag filter pressure drop (ΔP) evolution versus time for 11 clogging/unclogging cycles (from C1 to C11) during clogging with reagents and nanoparticles

In agreement with the literature (Park 2012), the experimental results show the decrease of cycle time from the first cycle C1 (630 min) to the cycle C6 (100 min) as illustrated in the **Figure 44**. Moreover, it can be noted a stabilization of clogging time once reached the cycle 6, cycle time ranging between 100 and 70 min. The observed behavior is associated with the penetration of particles in the thickness of the filter media, while the pulse-jet cleaning is unable to remove these trapped particles (Saleem et al. 2011). Moreover, the residual particulate cake on the surface of filter media also affects the minimum pressure drop, which increases gradually with filtration cycles (from around 20 to 84 Pa) in accordance with the literature (Saleem et al. 2011). Cirqueira et al. (2017) showed almost the same behavior regarding unclogging filtration tests conducted with treated fibrous filter (calendared) clogged at the maximum pressure drop of 100 Pa with the filtration velocity of 4 $cm.s^{-1}$. In their tests, the duration of pulse-jet was fixed at 0.2 s. Their results showed the increase of residual pressure drop from 20 Pa to 60 Pa during the first 10 filtration cycles. Lee et al. (2015) also reported the decrease of unclogging efficiency with the sequential filtration cycles. According to Petean & Aguiar (2015), the unclogging efficiency can be affected by the adhesion forces between the cake and the filter which depend of the chemical and physical proprieties of collected particles and the filter media. Note that the residual cake after cleaning and the increasing filter pressure drop baseline (i.e. the filter pressure drop at the beginning of each cycle), are strongly dependent on the efficiency of the unclogging system. The cleaning of bag filter is considered efficient when the pressure drop after unclogging remains constant and

equal to the original minimum value of conditioned bag filter after numerous pulse-jet cleaning. Hence, the residual particles can affect seriously the performance and lifetime of bag filter (Mukhopadhyay 2010 and Bao et al. 2014).

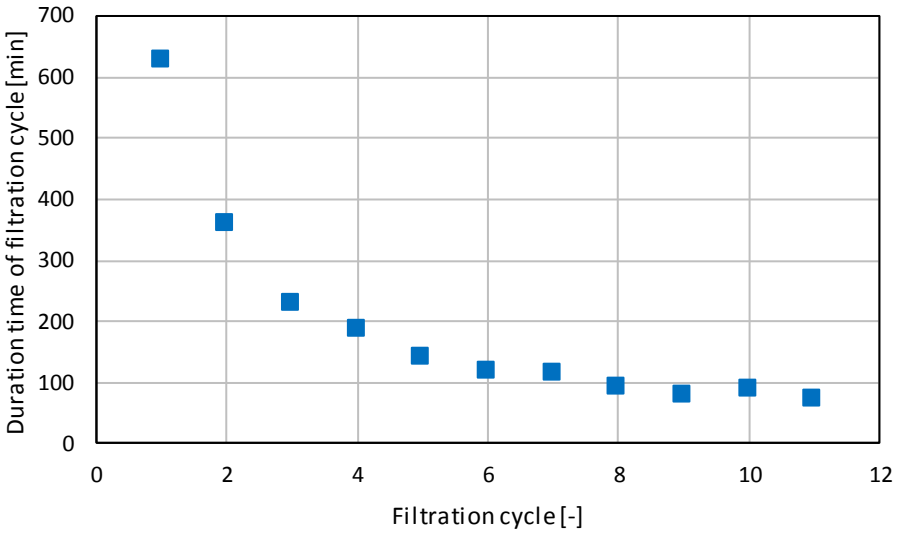

Figure 44: Evolution of cycle time as a function of filtration cycle

From the **Figure 43** we can clearly observe that the shape pressure drop curve becomes more concave as the number of filtration cycle increases. The concave rise can be due to the following phenomenon:

- the non-uniform distribution of the aerosol concentration at the filter media surface which leads to a non-uniform distribution of the cake area load,
- the incomplete removal of the particulate cake from the media surface, leading to a heterogeneous media surface mixing residual cake zones with totally clean zones (Saleem et al. 2011).

The first phenomenon can be neglected in this study because of the stabilized concentration and particle size distribution of the aerosols measured during repeated experiments. Hence, the concave rise can be mainly attributed to the incomplete removal of the particulate cake (**Figure 45-c**). As a consequence, during the next filtration cycle, the local gas flow through the filter becomes higher through the clean area as compared to the area holding residual cake (**Figure 45-d**). At constant dust concentration, the cake thickness builds up faster for cleaned areas than for the residual cake laden areas (**Figure 45-e**). This means that the overall pressure drop may increases rapidly until the cleaned areas are filled in with particles forming a cake leading to a homogeneous cake on the media surface. Indeed, overall pressure drop is a linear combination of pressure drop through cleaned areas and pressure drop through residual

cake laden areas (**Figure 45**). At this point, the flow resistance becomes balanced over the media surface and a linear rise of pressure drop is observed.

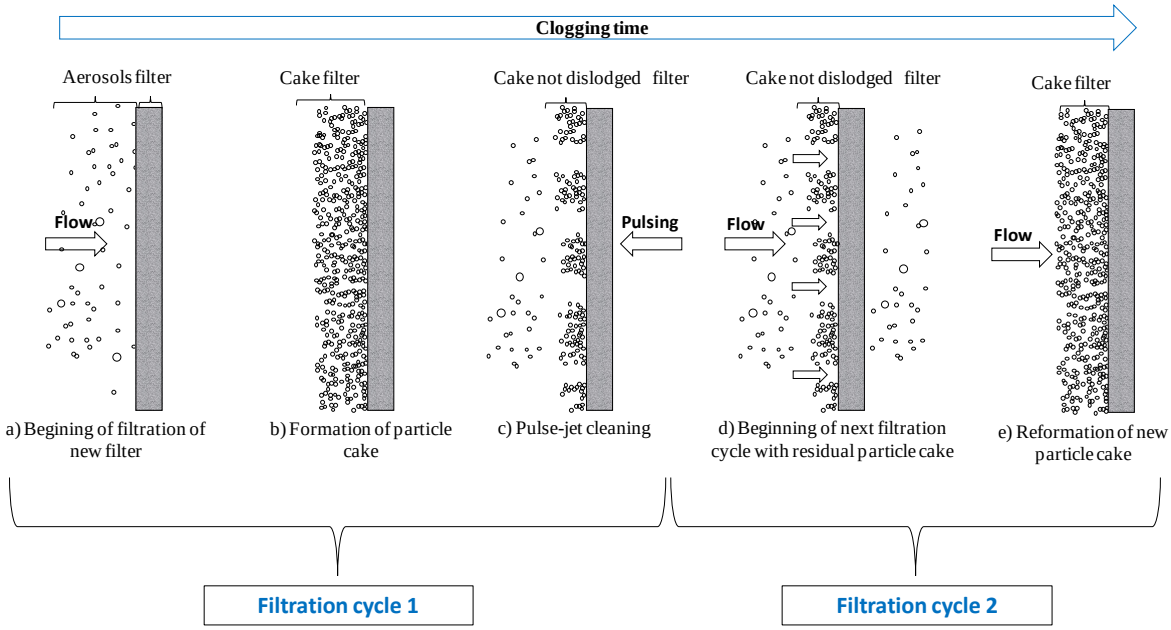

Figure 45: Illustration scheme of incomplete detachment of cake filter and reformation of new dust cake

SEM observations of the filter media surface of the unclogged bag filter were presented in the **Figure 46**. These photographs must be taken with some cautions, because during the sampling of unclogged filter, a part of the residual cake can be destroyed during the cut of the filter into small pieces and also during their transportation to the scanning electron microscope laboratory. As the photographs show, the detachment of the dust cake from the media surface is not complete, we can clearly see an important residual cake emerged on the filter media. Our assumption of non-homogeneous cake distribution on the surface of the regenerated filter may be confirmed by analyzing theses pictures, where cleaned areas can be distinguished from area clogged with particles. Across the obstructed area, the permeability of the filter decreases with clogging and the pressure drop increases gradually. As we can see from the **Figure 46**, areas on the filter surface are not yet completely clogged, this part of filter media constitutes preferential pathways for the airflow, where the interstitial velocity increases because of the increase of pressure on the filter surface.

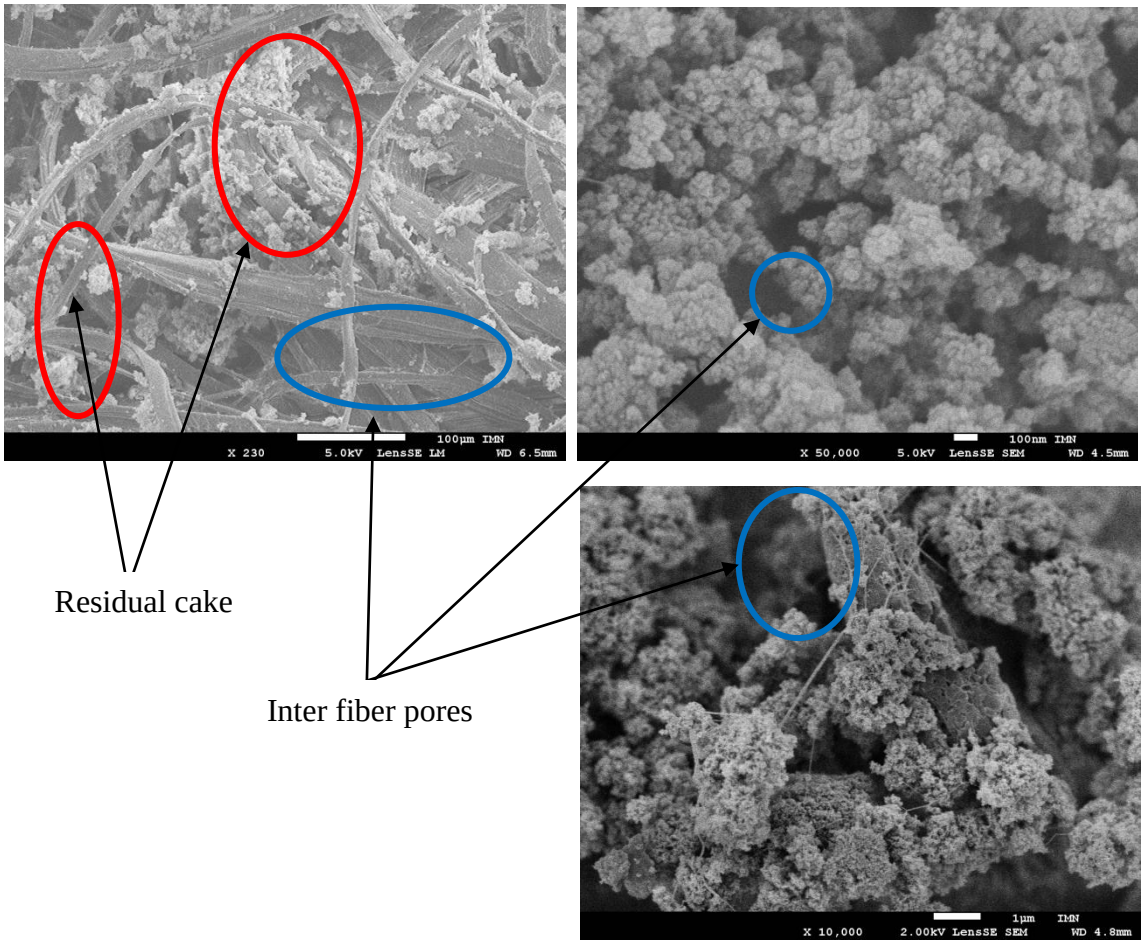

Figure 46: SEM photographs of the unclogged bag filter

III Bag filter efficiency for cycle 1

III.1 Total efficiency

The evolution of efficiency as a function of collected particle mass is depicted in the **Figure 47** during the first filtration cycle. The rise of pressure drop is also plotted in order to link the evolution of both parameters.

First of all, the determination of agglomerates density is necessary to calculate the collected particle mass. In fact, the particles generated by combustion are fractal agglomerates of small primary spheres, which lead to a change of particles properties, including density (Maricq & Xu 2004). The effective density of the primary particles can vary between 0.1 and 0.7 times during the aggregate formation (Fuchs 1964). Thus, two most popular methods are used in the literature to measure the effective density of agglomerates: (1) combination of measurement of aerodynamic and mobility equivalent diameter (2) combination of measurement of mobility equivalent diameter and particle mass (Ristimäki et al. 2002; Charvet et al. 2014).

In the present study, the effective density values are determined from Lee (2014) which measured the effective density of black carbon generated by the same instrument used in the present study (DNP 2000, Palas). Lee (2014) estimated the effective density from the mass concentration and the mobility diameter for carbons ranged from 50 nm to 600 nm of diameter.

However to calculate the total mass of collected particle, the effective density as a function of particle diameter was generalized for the entire particles sampling which constituted of a mixture of reagents and nanoparticles. In fact, as illustrated in the figures of particle size distribution (Chapter II, **Figure 32**) the number concentration of the generated reagents is not significant in comparison with the generated nanoparticles. Moreover, the densities of reagents and nanoparticles are almost similar (2.1 - 2.3 g.cm^{-3}).

The collected particle mass $w(t)$ was then calculated using mass balance at different time t:

$$w(t) = \dot{m}_p \times E \times t \times S^{-1} \quad (64)$$

Where $\dot{m}_p$ is the total mass flow rate of generated particles which is calculated from the mass flow rate according to the following equation (65):

$$\dot{m}_p = \sum \left(C_i \times m_{pi}\right) \times Q \quad (65)$$

Where C_i is the number concentration of generated particles of diameter d_i [#.cm^{-3}], and Q is the gas flow rate [l.min^{-1}]. E is the total efficiency of the tested filter at the time t, and S is the filter total surface.

m_{pi} is the particle mass calclated from the effective density ρ_{eff} which is defined as the mass divided by the volume of a sphere of the same diameter according to the following equation (66):

$$m_{pi} = \rho_{eff}(d_i)\frac{\pi d_i^3}{6} \quad (66)$$

For calculation purpose, the cake mass is considered uniform over the filter media.

The error of the measurement which represents the difference between the measured value and the exact value is taken into account in the present study. Thus, the uncertainties related to the filter efficiency measurements in this study are given by:

$$\Delta E = \frac{\Delta C_{downstream}}{C_{upstream}} + \frac{C_{downstream}}{\left(C_{upstream}\right)^2} \times \Delta C_{upstream} \quad (67)$$

With $\Delta C_{downstream} = 5\% \times C_{downstream}$

5% is the particle concentration accuracy of the SPMS for single particle counting according to the technical notice.

As $C_{upstream}$ is a constant value determined from preliminary experiments, $\Delta C_{upstream}$ is obtained from the experimental uncertainty of the particle counting measured upstream of the filter for 6 sampling carried out on two different days. $\Delta C_{upstream}$ depends on the particle size range.

The error bars plotted on figures of efficiency and collected mass of particle per surface unit correspond to the maximum and minimum values.

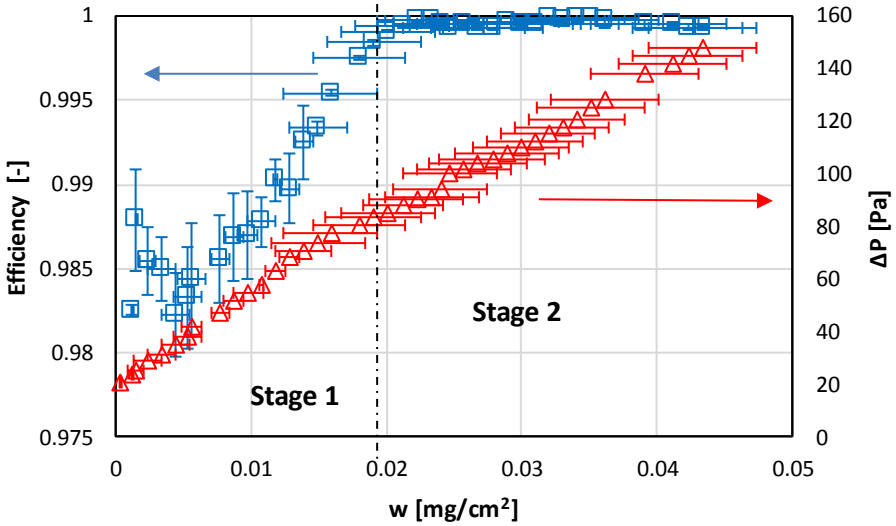

Figure 47: Evolution of overall efficiency and pressure drop during the first filtration cycle as a function of the collected mass of particles per surface unit for particle size range of 16-750 nm and median diameter of 45 nm

The collection efficiency illustrated in the **Figure 47** can be described in two stages. During the first stage, the total efficiency increases with loaded particles, from 98.5 ± 0.5 % at the beginning of clogging to 99.98 ± 0.02 % at 0.02 mg.cm^{-2}. Considering the overall particle concentration of 5.45.10^{6} part.cm^{-3}, this means that, at the end of stage 1, 110 particles.cm^{-3} passed through the filter (corresponding to 0.02% of the upstream particles concentration). The pressure drop varies from 20 Pa to 82 Pa from the beginning to the end of the stage 1.

In the second stage (from 0.02 to 0.045 mg.cm^{-2}), the collection efficiency keep constant at its maximum value of 99.98% ± 0.20% while pressure drop increases from 82 to 150 Pa with a less sharp slop than during stage 1 (4.1 Pa.cm^{2}.mg^{-1} during stage 1 against 2.7 Pa.cm^{2}.mg^{-1} during stage 2). This can be explained by the incomplete regeneration of cake filter from media surface as illustrated in the **Figure 45-c**. Indeed, the air flow is higher through the

regenerated area as compared to the areas holding thick cake (Saleem et al. 2011). Hence, the rate of clogging of regenerated area is fast which leads to form quickly a cake filter as compared to the area holding residual cake, by consequence, fast increase of pressure drop in the stage 1 (**Figure 47**). Once the new cake filter is reformed and important regenerated areas start to be full of collected particles (**Figure 45-e**), the air flow begins to be balanced throughout the filter surface, which leads to reduce the velocity of pressure drop rise (**Figure 47**, stage 2).

The high value of collection efficiency in the second stage can be explained by the accumulation of collected particles on the upstream surface of the filter, which forms gradually a cake of particle while contributes to particle capture (Thomas 2001). During the dust loading, the porosity of deposited particles decreases as pressure drop increases (Wang et al. 2016) which in turns reduces the penetration of particles through the filter media. The relation between the filter efficiency and the pressure drop as a function of mass of loaded particles was also studied by Thomas (2001) during the clogging of fibrous filters with solid aerosol. The results showed an important effect of particle loading on the filter performance, with linear increase of filter efficiency. These results are in good agreement with the present study.

III.2 Fractional efficiency

The evolution of bag filter efficiency as a function of particle diameter for different levels of clogging (i.e. different values of bag filter ΔP) during the first filtration cycle is presented in the **Figure 48**. The results show a minimum particle collection efficiency of 98.5±0.5 % at 75 nm for ΔP=25 Pa. They also reveal, in accordance with the filtration theory and the literature, a gradual increase in particle collection efficiency with the filter loading (Leung & Hung 2008; Park 2012; Förster et al. 2016). This can be explained by the effect of deposited particles on the filter surface which contributes to the collection of incoming particles. We can notice that, the error bars of the efficiency are significant in the range of 75-110 nm due to the high aerosol concentration downstream of the filter because of the MPPS range.

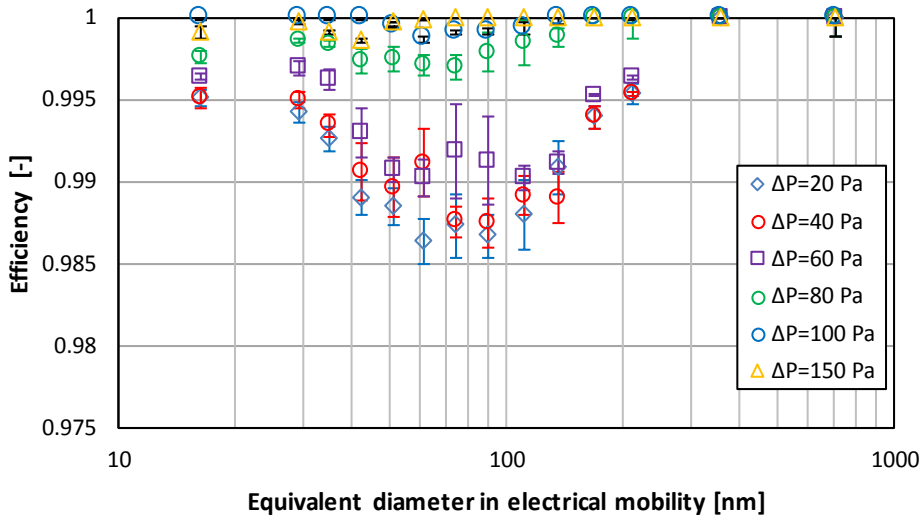

Figure 48: Evolution of filtration efficiency as a function of particle diameter for the first filtration cycle (C1) at different values of filter pressure drop (ΔP)

The difference in fractional efficiency as a function of particle diameter can clearly be seen in the figure. The influence of particle diameter on the filtration efficiency is explained by the filtration mechanisms responsible for particle collection by fibers. At the beginning of clogging ΔP=25 Pa, three areas of particle diameter can be distinguished in the **Figure 48:**

(1) For small particles of 16-35 nm, the efficiency is 99.5 ± 0.1%. This high collection efficiency is in agreement with the experimental work of Förster et al. (2016) obtained at the same temperature conditions as our study (150°C) during the filtration of nanoparticles with fibrous bag filter. In this particle size range, the dominant particle collection mechanism is the Brownian diffusion. According to the literature (Brown 1993; Kulkarni et al. 2011), the effect of filtration mechanism by Brownian diffusion decreases with increasing of particle diameter. Moreover, according to Saleem et al. (2011), the retention time of nanometric particles at the vicinity of fibers is important at low filtration velocity (1.9 $cm.s^{-1}$) because those nanoparticles are less influenced by the gas stream, the fact that increases their chance to be collected on the fibers by the Brownian diffusion.

(2) The second area of particle size range is between 40 and 170 nm. This particle size range is the most penetrating through the filter media, and the efficiency achieves the lowest value of 98.5% (most penetrating particle size MPPS close to 70-80 nm at the beginning of clogging). The main reason of this particle penetration is due to the non-predominant collection mechanism for this particle size.

(3) For particles higher than 200 nm in diameter, the efficiency is higher than 99.5 ± 0.1% even at the beginning of filtration. Interception is the dominant filtration mechanism responsible for particle size collection in the range of 200 nm and 750 nm.

III.3 Evolution of MPPS as a function of clogging

The **Figure 49** illustrates the evolution of Most Penetrating Particle Size at different levels of filter clogging during the first filtration cycle (for different values of pressure drop). The results show a decrease of the MPPS with filter loading from 76 ±15 to 39 ± 4 nm particle diameter. In this zone of lower filtration efficiency, the Brownian diffusion mechanism is neglected due to size of particles leading to the Pe number ranging between 34 to 423 at the given condition of flow, while the interception and impaction mechanisms are less efficient because of too small particle sizes (Liu. et al. 2011) (Stokes number is ranging between $4.4.10^{-5}$ to $6.8.10^{-4}$).

According to the literature, numerous studies showed that the range of MPPS can vary as a function of the clogged filter model and the operating filtration conditions (Lee & Liu 1980; Leung & Hung 2008; Agranovski 2010). In the present investigation, the measured values of MPPS (76 ±15 to 39 ± 4nm) are lower than those usually mentioned in the literature (between 0.1 and 0.5 µm according to Podgórski et al., 2006).

The increase of interception mechanism contribution to particle capture with filter loading may be a reason of decreasing of MPPS. According to Leung & Hung (2008), the size of fiber diameter has a significant influence on the collection efficiency. Indeed, the study shows that the nano-fibrous media exhibiting higher surface area per unit volume of fiber is more efficient regarding particle collection than the micro-fibers filter. The mechanism of interception is responsible of this decrease of MPPS and increase of the collection efficiency. According to these results it can be assumed in our study that the nanoparticle agglomerates forming dendritic network at the surface of the filter media are equivalent to a nanofibrous network contributing to collect the incoming particles.

However, these values of MPPS must be taken with some cautions because in some curves the diameters corresponding to the minimum filtration efficiency is not clear from the curves, this can be due to the effect of the cake formation which contributes to the collection of particles.

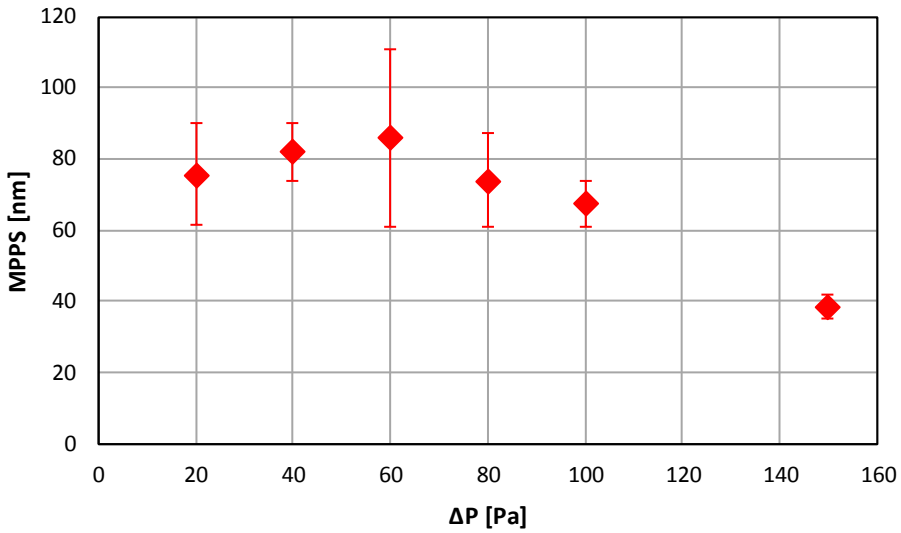

Figure 49: Evolution of MPPS as a function of clogging during filtration cycle 1

IV Influence of filtration cycles on bag filter total efficiency

Evolution of collection efficiency of the bag filter as a function of time is presented in the **Figure 50**. Indeed, the operation of bag filter consists of a sequence of 11 filtration cycles (C1, C2,…, C11). One filtration cycle represents the overall time of clogging and unclogging of the filter media.

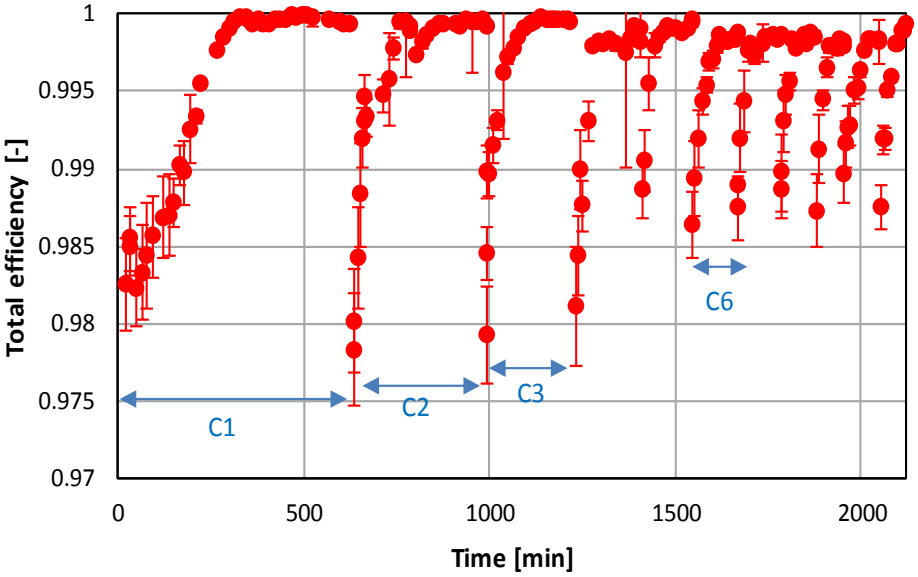

Figure 50: Evolution of filtration efficiency during the 11 filtration cycles

Regarding the efficiency at the beginning of each clogging/unclogging cycle, except for the first cycle C1, the results tend to reveal a first stage with a gradual increase in the efficiency at the minimum pressure drop values of filtration cycles. They then seem to indicate a second

stage with a stabilization of the filtration efficiency evolution for the last filtration cycles at residual pressure drop (almost 98.6%).

Regarding the efficiency at the end of clogging of filtration cycle C1, C2, and C3, the values are close to 99.9%. However, we can notice a slight but significant decrease of the maximum collection efficiency from the filtration cycle number 4. The reason can be attributed to the residual cake as explained in the previous section. The airflow may follow preferential pathways inside the loaded filter leading to an increase of the interstitial velocity. By consequence, the effect of Brownian diffusion, the main mechanism responsible of nanosized particle collection, decreases with increasing of interstitial velocity.

For more investigation, we will discuss in the following section the evolution of fractional efficiency as a function of clogging and filtration efficiency.

V Fractional efficiency as a function of filtration cycles

Figure 51 and **Figure 52** represent the filtration efficiency measured respectively at the minimum and the maximum pressure drop of the filtration cycles C3, C5, C7, and C9.

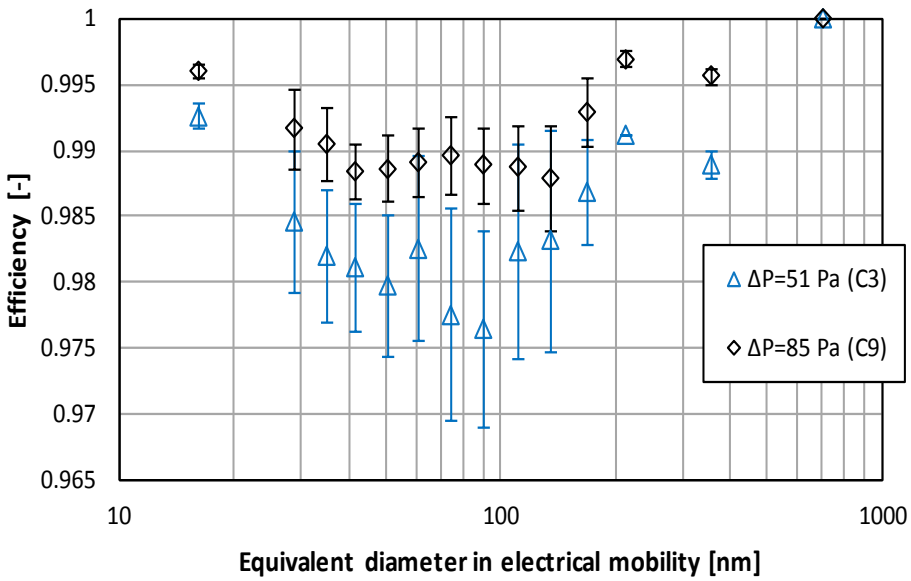

Figure 51: Evolution of fractional efficiency measured at the minimum pressure drop for different filtration cycles as a function of particle diameter

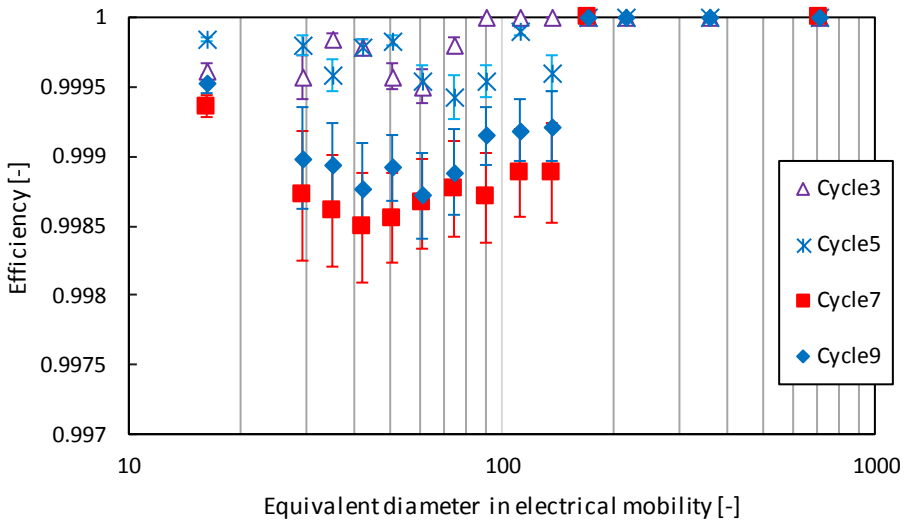

Figure 52: Evolution of fractional efficiency at the maximum pressure drop (150 Pa) for different filtration cycles as a function of particle diameter

As a function of filtration cycles, the fractional efficiency at residual pressure drop in the **Figure 51** increases from 97.5% to 99% for particles in the size range of 35-170 nm (MPPS range). While, the collection efficiency of the particles lower than 30 nm and above 200 nm in diameter is less influenced by the sequence of clogging/unclogging cycles. The residual cake from previous filtration cycles becomes a part of filter media and contributes to increase the collection efficiency.

As illustrated in the **Figure 53** the remaining particle cake from the media surface increases with filtration cycles, the fact that leads to increase the overall surface of residual cake ($L_{cake\text{-}3} < L_{cake\text{-}9}$) , which will contribute to collect important number of the incoming particles ($N_{\#3} < N_{\#9}$).

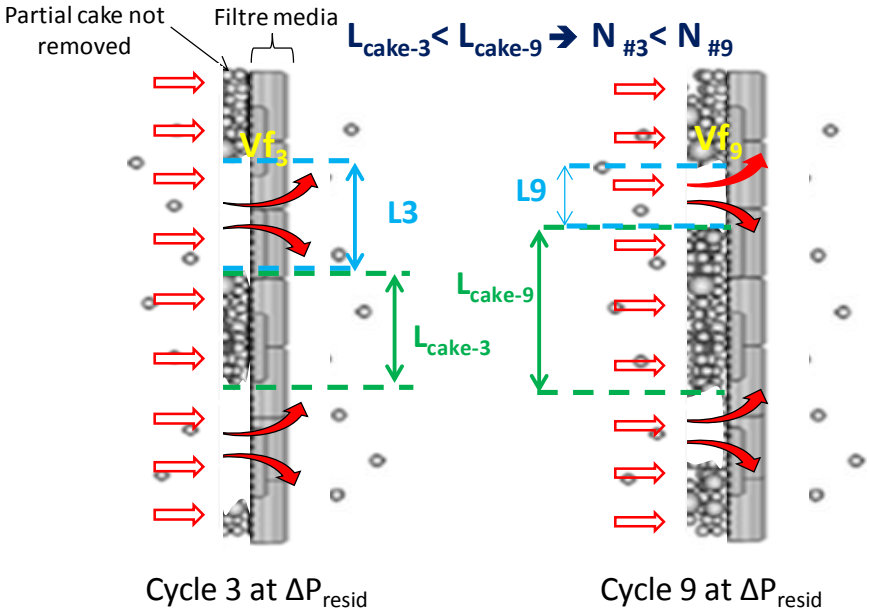

Figure 53: Illustration scheme of the increase of residual particle cake with filtration cycles

Regarding the fractional efficiency at the maximum pressure drop (**Figure 52**), the results show that the collection efficiency is close to 100% for all filtration cycles (between 99.85% and 99.99%). However, a slight decrease of fractional collection efficiency can be observed for the couple of efficiency curve (C7 & C9) as compared to the filtration cycles (C3 & C5).

As illustrated in the **Figure 54**, the non-homogeneous particle cake at the maximum pressure drop leads to preferential pathways with local increase of filtration velocity. Indeed, the surface areas of lower cake thickness (L') decrease with filtration cycles. Thus, L'3>L'9 which create local increase of interstitial velocity through these preferential pathways of the airflow, with $Vf'_3 << Vf'_9$. Thus, the increase of interstitial velocity affects the collection efficiency by the mechanism of Brownian diffusion. The fact that can explain the decrease of filtration collection between C3 and C9 at the maximum pressure drop.

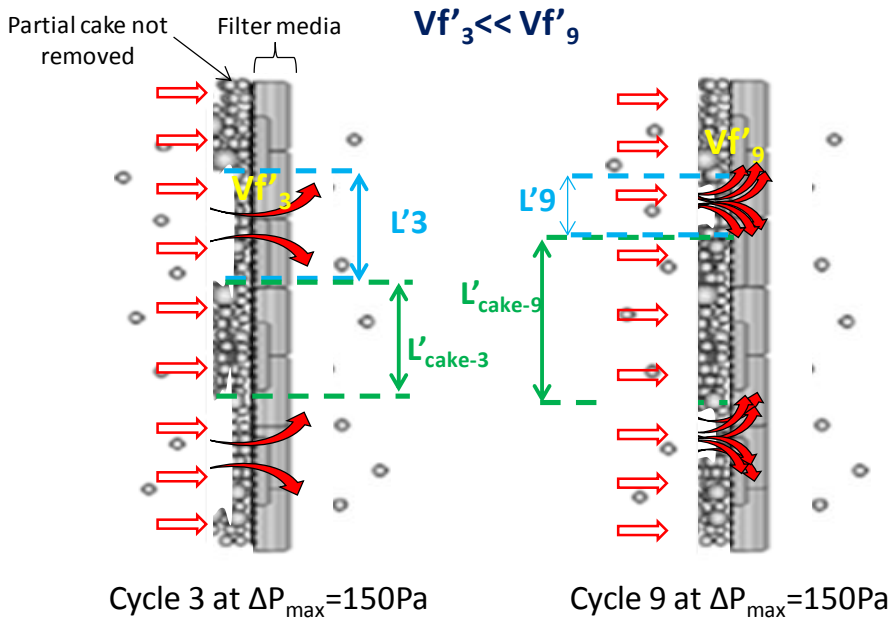

Figure 54: Illustration scheme of increase of local filtration velocity at maximum filter pressure drop with filtration cycles

The evolution of the MPPS as a function of filtration cycles was investigated in the following section. **Figure 55** shows the particle diameter where the minimum filtration efficiency was measured at the beginning of each filtration cycle. In contrast of what obtained regarding the evolution of MPPS during the first filtration cycle, the results illustrate an increase of MPPS during the 11 cycles of clogging/unclogging. The MPPS over filtration cycles is ranged between 76 ± 15 and 136 ± 11 nm. The increase of MPPS can be explained by the change in the filter media structure. Changes in the physical properties of filter media are largely governed by the cleaning frequency of bag filter. Indeed, the residual cake resulting from the filtration cycles quickens the rise of pressure drop which increases the frequency of cleaning. By consequence, the structure of filter media is influenced by pulse-jet cleaning, so that the porosity increases because of the high volume and the pressure of injected air flow in a very short time 0.3 s. Hence, the size of penetrating particles increases with increase of media porosity, especially at the beginning of filtration cycle.

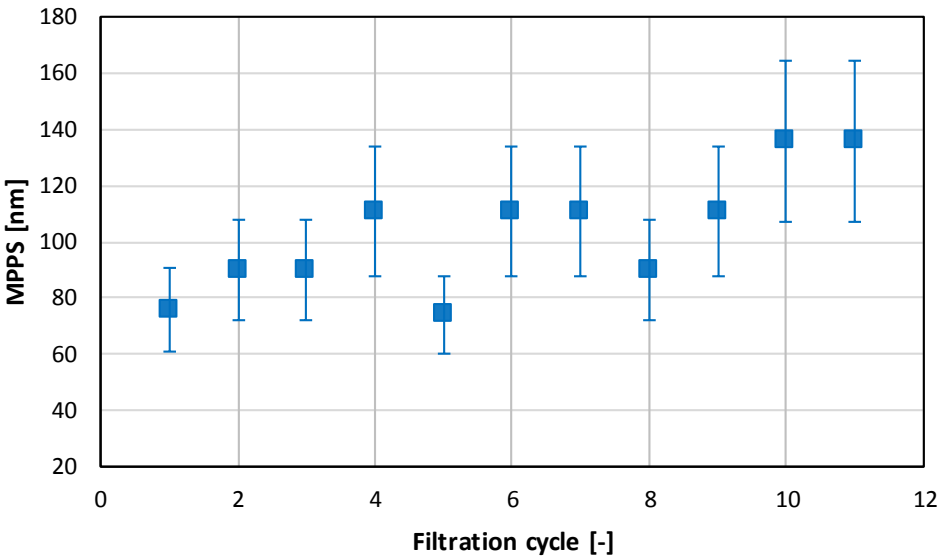

Figure 55: Evolution of MPPS as a function of filtration cycles at residual ΔP (pressure drop after regeneration for a given filtration cycle)

VI Evolution of cake filter and filter media resistance after cleaning

Evolution of media and dust cake filter resistance is important to understand the dust cake formation and cake detachment as a function of filtration cycle.

The dust cake resistance can be determined based on experimental data of collecting particles by the filter. In fact, the specific cake resistance K_c [m.kg^{-1}] is calculated from the slope of the curve describing the increase in the pressure drop of the filter as a function of the collected particle mass per unit area w, considering the gas viscosity (μ), and the filtration velocity (V_f), as determined in the following equations:

$$\Delta P(t) = \Delta P_{\text{residual after unclogging}} + \Delta P_{\text{cake}}(t) \quad (68)$$

$$\Delta P(t) = \Delta P_{\text{residual after unclogging}} + \Delta P_{\text{cake}}(t) \quad (69)$$

With

$$\Delta P_{\text{cake}}(t) = w(t).V_f.\mu.K_c \quad (70)$$

And

$$K_c = \frac{\frac{\Delta(\Delta P)}{\Delta(t)}}{w.V_f.\mu} \quad (71)$$

The evolution of pressure drop as a function of collected particle per unit area for 10 successive filtration cycles is plotted in the **Figure 56** in order to calculate the specific cake resistance. The slope of the curves was $U_f . \mu . K_c$.

As the results illustrate, the pressure drop curves are concave initially and become linear afterwards. The intensity of the concave rise increases with residual pressure drop, thus with filtration cycles. Note that, the specific cake resistance is calculated from the linear part of the pressure drop curve (**Figure 56).**

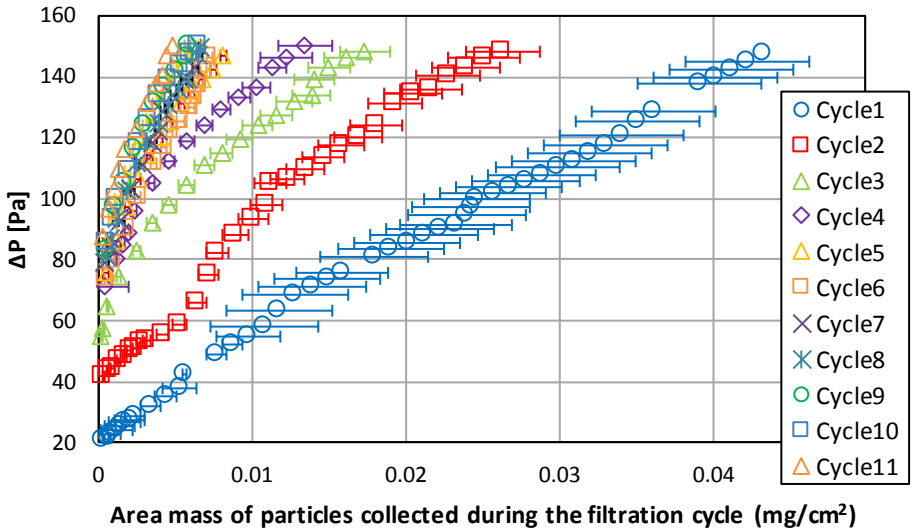

Figure 56: Pressure drop evolution across used bag filter against collected particles mass per unit area

The filter media resistance immediately after cleaning, i.e. the residual resistance K_m [m^{-1}], was determined after unclogging of the bag filter according to the following equation (72):

$$K_m = \frac{\Delta P_{\text{residual after unclogging}}}{V_f . \mu} \qquad (72)$$

The **Figure 57** shows the evolution of the residual resistance and the specific cake resistance build up on the used bag filter as a function of filtration cycle. In general, the cake resistance increases gradually with filtration cycle, a similar behavior is also reported by Saleem & Krammer (2007). The slight increase of the residual resistance was also observed and seems to be leveled off from the filtration cycle C6.

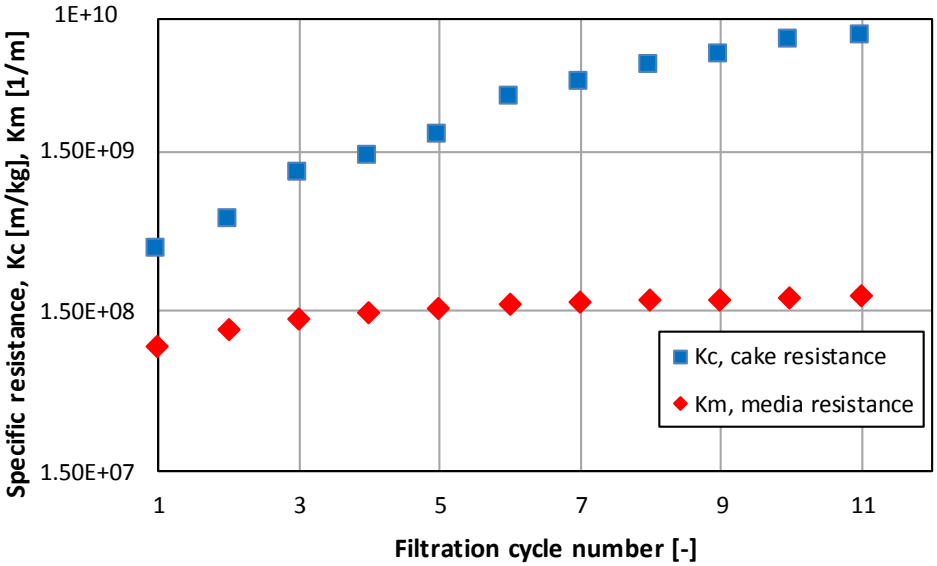

Figure 57: Evolution of specific cake resistance and media filter resistance as a function of filtration cycles

According to the literature, the increase of filtration velocity leads to the increase of the specific resistance of the dust cake (Silva et al. 1999; Cheng & Tsai 1998). Moreover, the cake porosity is also affected by the filtration velocity, where the dust cake becomes less porous with filtration velocity (Cheng & Tsai 1998). Thereby, these results can be explained by two main reasons:

1. The first reason is due to the assumption that the non-uniform distribution of the cake filter formation leads to non-uniform distribution of the filtration velocity on the cake surface, and an increase of filtration velocity locally through the filter media. Hence the increase of cake resistance can be explained by the decrease of cake porosity which leads to a filtration velocity increase locally and so gradually favors increase of cake resistance. Indeed, for higher filtration velocity, the coarse particles are more compressed deeper into the cake when fluid drag force overcomes particle adhesion force (Cheng & Tsai 1998).

2. The second reason can be explained by the effect of the pulsed air of the cleaning system on the residual cake. Indeed, with filtration cycles, the residual cake becomes more compacted because of the pressure of pulse-jet. Hence, the resistance of residual cake filters increases with filtration cycles (**Figure 58**, inspired from Park 2012).

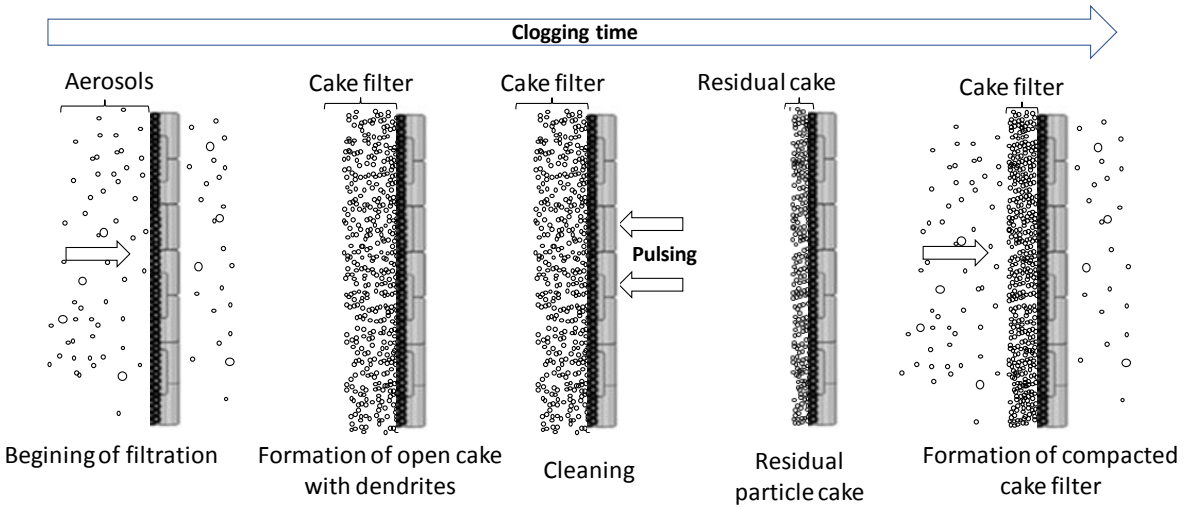

Figure 58: Effect of pulse-jet cleaning on residual dust cake structure

VII **Conclusions of the chapter**

The present chapter focused from the one hand on the filtration performance of bag filters used for the treatment of flue gas from waste incineration. The study aimed to quantify the filtration performance of a pulse-jet bag filter at the laboratory-scale regarding submicronic particles with a nanosized fraction during clogging/unclogging cycles. The bag filter was operated in realistic conditions, as close as possible to those found in flue gas treatment lines of waste incineration, in terms of temperature, humidity, filtration velocity and injection of sorbent reagents. From the other hand, the resistance of the bag filter was investigated as a function of filtration cycles. The main conclusions of this experimental study are:

(1) The high performance of the industrial pulse-jet bag filter during submicronic and nanosized particle filtration. The overall efficiency of the bag filter increases rapidly with clogging from a minimum value of 98.5% to a maximum of 99.98%.

(2) The fractional efficiency varies with particle size. Three areas with significant differences in efficiency can be distinguished. Particles with a diameter of 76 ±15 nm are the most penetrating through the filter, for which the efficiency reaches a minimum value of 98.5%. As a function of clogging, the decrease of MPPS was observed from 76 ±15 to 39 ± 4 nm particle diameters. However, the evolution of MPPS at residual pressure drop during 11 filtration cycles was different, the results showed the increase of MPPS over filtration cycles from 76 ± 15 to 136 ± 11 nm. The increase of MPPS was explained by the change in the filter media structure.

(3) Clogging duration decreases from 630 min for the first filtration cycle to around 70 min for the last one, as a result of the residual pressure drop increases with unclogging cycles.

(4) The residual cake and the non-uniform distribution of the cake filter are the main reasons of non-uniform distribution of filtration velocity on the media surface, which contributes to increase the interstitial velocity through the area less loaded with particles. The investigation showed that the increase of the interstitial velocity can lead to decrease the collection efficiency of nanoparticles and increase the cake resistance.

In general, these results demonstrated the effectiveness of bag filters for submicronic and nanosized particle filtration in industrial conditions for the treatment of waste incineration fumes.

Chapter IV Influence of operating parameters on filtration performance of bag filter and flat filter

I Introduction

In the **chapter III** we have studied the performance of the bag filter in operating conditions as close as possible to those found in real-scale waste incineration plants (150°C - 3% RH). In the following chapter we will discuss experimentally and theoretically the influence of different parameters on the bag and flat filter performance based on the reference condition (150°C - 3% RH). The investigation will be in terms of the influence of operating parameters such as humidity (3% RH versus 0% RH), temperature (150°C versus 24°C), filtration velocity (1.9 $cm.s^{-1}$ versus 1.4 $cm.s^{-1}$) and the dust characteristics (reagents versus nanoparticles). The loading of the media will be discussed as well in order to investigate the influence of filter aging and the residual dust cake on the filter performance.

II Influence of humidity

To illustrate how the bag filter performance change with clogging/unclogging cycles during nanoparticle filtration at 150°C, the following section describes the variation of pressure drop and the filtration efficiency over 10 successive cycles of clogging/unclogging. The bag filter was clogged at maximum pressure drop of 150 Pa for two different values of humidity: 0% RH (dry gas) and 3% RH (humid gas) which correspond respectively to 0 and 100 g water/kg air.

The concentrations of NPs at (150°C - 3% RH) and (150°C - 0% RH) were respectively $5.09.10^6$ and $5.79.10^6$ $particles.cm^{-3}$ with particle mode respectively of 50 and 45 nm. For both experimental conditions, the same bag filter was used for clogging test. In fact, filtration test was performed at (150°C - 0% RH) for several clogging/unclogging cycles in order to remove the residual cake and reduce the pressure drop before a new filtration step. The clogging/unclogging test was then performed for next filtration condition (150°C - 3% RH). The main purpose of this assessment is to investigate the influence of humidity on experimental pressure drop and efficiency evolutions and to study the behavior of the filter regarding cake detachment.

II.1 Filtration efficiency

II.1.1 Experimental results

Figure 59 shows the evolution of fractional efficiency at different pressure drop during the first filtration cycle in humid (3% RH) and dry (0% RH) conditions. At the same level of

pressure drop, the fractional efficiency is lower at (3% RH) as compared to (0% RH) whatever the particle diameter (in the studied range) with minimum efficiency of 96.7% ±1% in humid conditions (3% RH) against 98.5% ±0.5% for dry conditions (0% RH). For the two conditions, the increase of fractional efficiency with pressure drop is clearly observed.

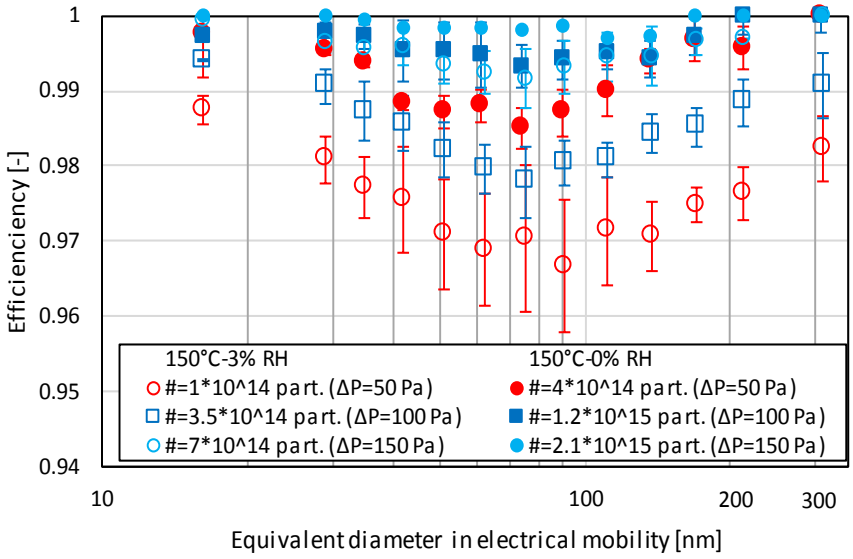

Figure 59: Fractional efficiency of bag filter for different pressure drop level at 150°C - 3% RH and 150°C - 0% RH with carbon nanoparticles for the first clogging cycle

This difference in fractional efficiency can be explained by the difference in the number of collected particles. Indeed, at the same level of pressure drop (ΔP=50 Pa), the number of collected particles at 3% RH is 1.10^{14} against 4.10^{14} of collected particles at 0% RH. According to the literature (Leung & Hung 2008; Park 2012; Förster et al. 2016) the deposited particles on the filter surface contributes to the collection of incoming particles.

The evolution of fractional efficiency as a function of the same collected particle number in humid (3% RH) and dry (0% RH) conditions is plotted in the **Figure 60**.

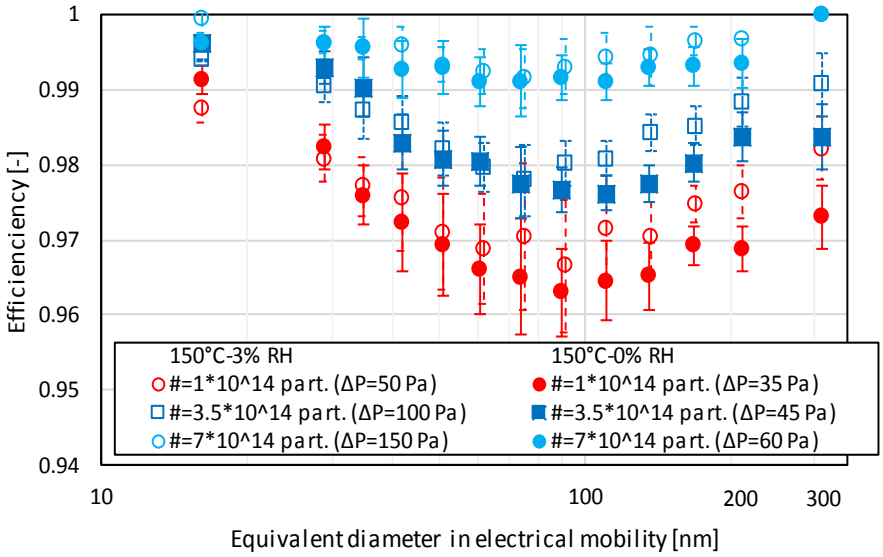

Figure 60: Evolution of fractional efficiency for different collected carbon nanoparticle number - 150°C in humid (3% RH) and dry (0% RH) conditions for the first filtration cycle

Two ranges of particle diameter can be distinguished from the **Figure 60**. First, for particle size range 16-100 nm, no significant difference of filtration efficiency is observed for the two relative humidities. Second, for submicron particles higher than 110 nm, higher filtration efficiency is reported at 3% compared with 0% RH, for collected particle numbers equal to 10^{14} and $3.5.10^{14}$.

II.1.2 Theoretical investigation

Theoretically, the influence of humidity on the filter efficiency is investigated in the present section based on the three main filtration mechanisms, mainly Brownian diffusion, interception, and impaction. The theoretical study takes into account the filtration conditions (T, humidity), gas characteristics (air density, mean free path, viscosity), filter characteristics (filter thickness, compactness, fiber diameter) and particles proprieties (diameter and density). In the **Figure 61**, the fractional efficiency estimated from the Kasper model (Kasper et al. 1978) is plotted at 150°C for 3% and 0% of relative humidity. The values of gas viscosity at 150 °C for different humidities were taken from the experimental study of Melling et al (1997): 2.4×10^{-5} and 2.3×10^{-5} $kg.m^{-1}.s^{-1}$ respectively for 0% and 3% RH.

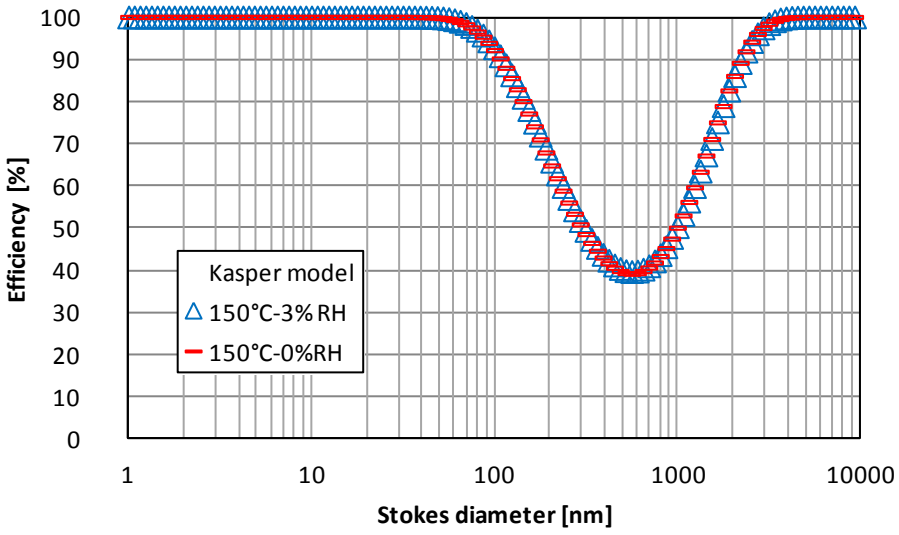

Figure 61: Influence of humidity on theoretical filtration efficiency

No significant difference of collection efficiency was observed comparing the two filtration conditions. The model predicts very high collection efficiency for particles lower than 70 nm in diameter (~100%), while the MPPS is identified at 550 nm. Regardless the difference of fractional efficiencies between the theoretical simulation and the experimental findings, the main conclusion is that the theoretical filtration mechanisms cannot explain the influence of humidity on the filtration efficiency observed from experimental results. The difference between experimental and theoretical studies in terms of minimum fractional efficiency and MPPS can be explained by the influence of humidity on particle size distribution and shape of aggregated particles which is not considered in the model. Moreover, the difference between the structural parameters of the tested non homogeneous used filter media and its corresponding ideal theoretical filter can partly explain the discrepancy between the results.

Then it can be assumed that the humidity has a direct influence on the structure of the deposited particles which in turns can affect the filtration efficiency.

The investigation of pressure drop evolution in the following section may be useful to understand the influence of humidity on bag filter performance.

II.2 Filter pressure drop

Figure 62 shows the evolution of bag filter pressure drop with filtration time. The total filtration time of bag filter clogging at 3% RH is 1850 min against 5000 min at 0% RH. For both filtration conditions, the time of the filter clogging decreases gradually with number of filtration cycles.

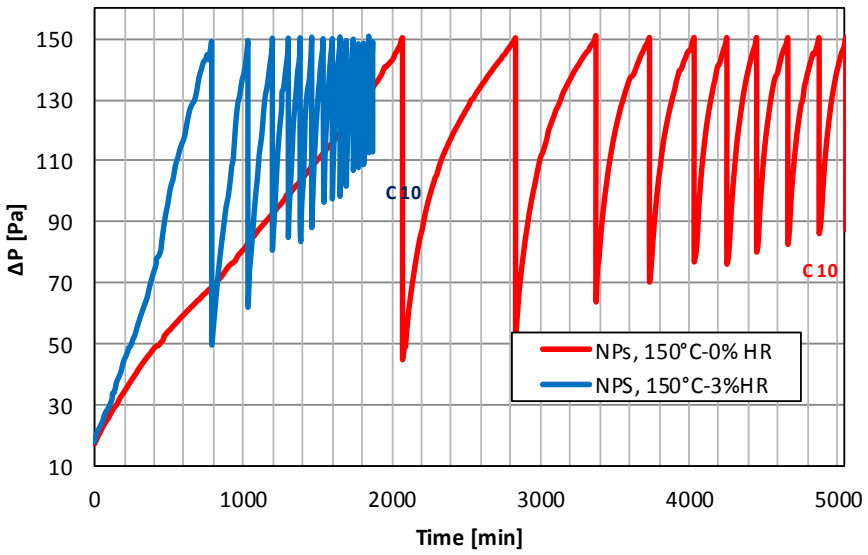

Figure 62: Influence of humidity on change in bag filter pressure drop during clogging/unclogging cycles

In the following section, the filter resistance ξ [m^{-1}] is expressed as the ratio of the measured pressure drop ΔP minus the initial pressure drop ΔP_0 of the filter (clean media) over the filtration velocity V_f times air viscosity μ: $\xi = (\Delta P - \Delta P_0)/(V_f.\mu)$.

Figure 63 shows the evolution of filter resistance ξ during particle loading at 150°C for dry (0% RH) and humid gas (3% RH) during the first filtration cycle. As can be seen, the increase of the filter resistance is identical during the first short number of collected particles (0- 5.10^{13} part), then a sharp increase of filter resistance can be clearly observed at 3% RH as compared to 0% RH indicating different structural properties of the deposited particle. At the maximum value of filter resistance ($\xi=3.25.10^{8}$ m^{-1}), the number of collected particles is significantly higher at 0% RH as compared to 3% RH, respectively 7.10^{14} and $2.5.10^{15}$ particles. Hence, significant effect of humidity can be observed on the evolution of filter resistance.

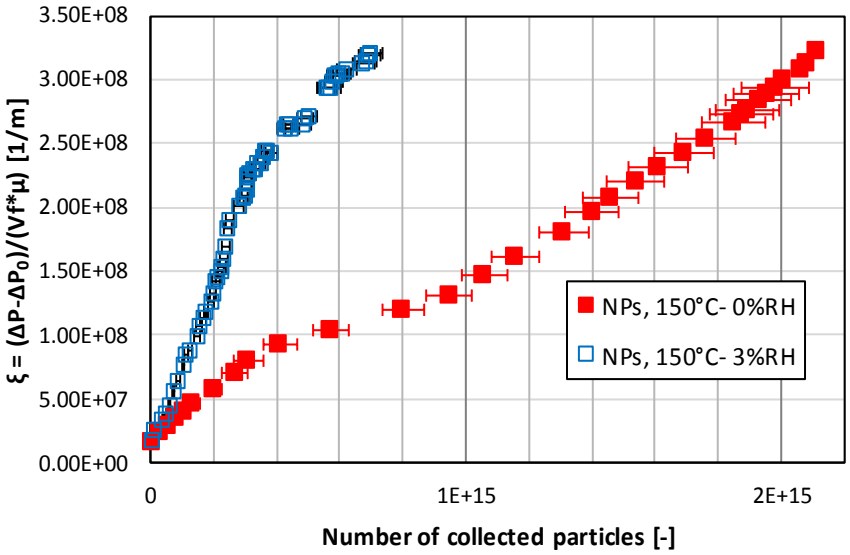

Figure 63: Evolution of ΔP as a function of collected particle number at (150°C - 3% RH) and (150°C - 0% RH)

Considering literature review on the influence of humidity on filter resistance, different findings were observed in terms of pressure drop evolution as a function of humidity. Joubert et al. (2010) and Gupta et al. (1993) showed that the pressure drop decreases with the presence of humidity during clogging of HEPA filters for a given mass of submicron hygroscopic aerosols collected at ambient temperature. The difference between literature and the present study regarding the influence of humidity can be explained by the difference of filtration conditions in terms of temperature (150°C), humidity, and also the aerosol nature and their size. Indeed, due to the important amount of gas humidity (around 100 g water/ kg air) in the present study, and to the small size of particles (16-310 nm) with high specific surface area which increases the ability of water absorption, the particles have tendency to attract water molecules at (3% RH).

II.3 Discussion of performance results

According to the literature, the presence of humidity between two solid surfaces causes an attractive force called the capillary force (Butt and Kappl 2009). This adhesion force is the main reason to reduce the distance between deposited particles and form a compact dust cake on the surface media as illustrated in the **Figure 64**. Hence, this can explain the fast increase of pressure drop in the presence of humidity than dry gas (0% RH) as observed in the **Figure 63**.

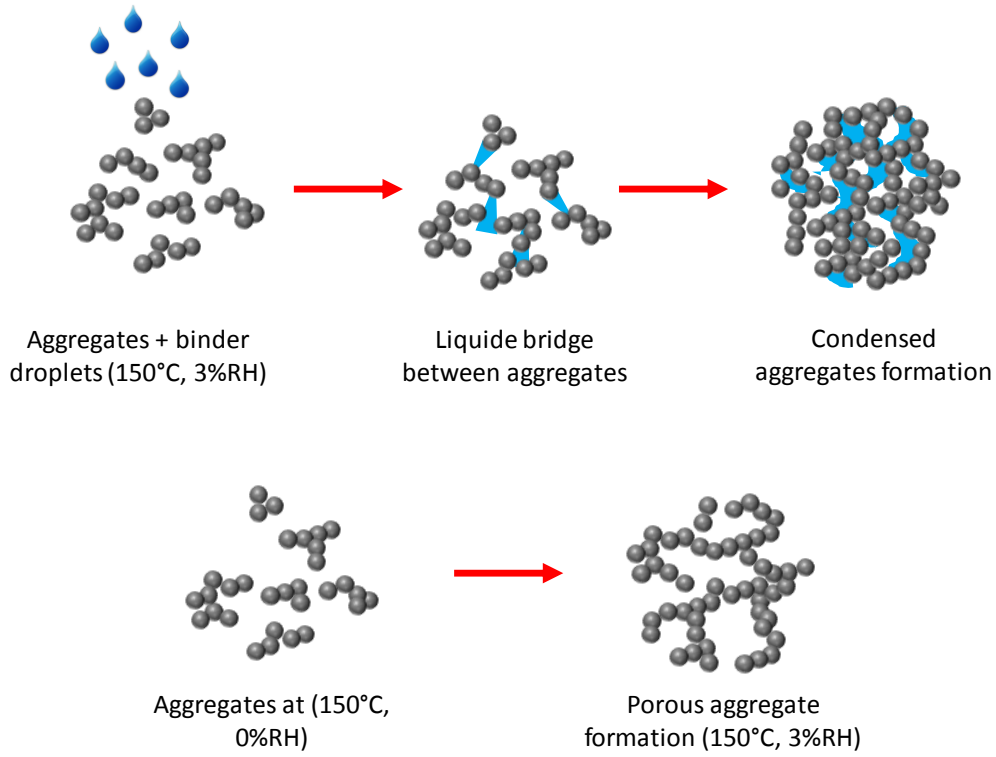

Figure 64: Effect of humidity on aggregates

According to the literature, two solid spheres of rough surface get into contact by the capillary bridges formed between asperities (**Figure 65**). The asperities of solid surface can highly influence the capillary force between the two particles. In this regard, three regimes can be distinguished as a function of vapor pressure between particles (Butt and Kappl 2009):

- At low vapor pressure, the two solid surfaces are linked by only one capillary bridge formed at the outmost asperity. Thus, the capillary force will be low because of the small formed curvature radius. The formed capillary bridge creates a gap between the two particles and prevents the capillary condensation between the remaining asperities.
- At intermediate vapor pressure, the number of formed capillary bridges increases between asperities of the two solid surfaces.
- At high vapor pressure, the capillary bridges between asperities are more important and interact with each other to form a continuous capillary bridge.

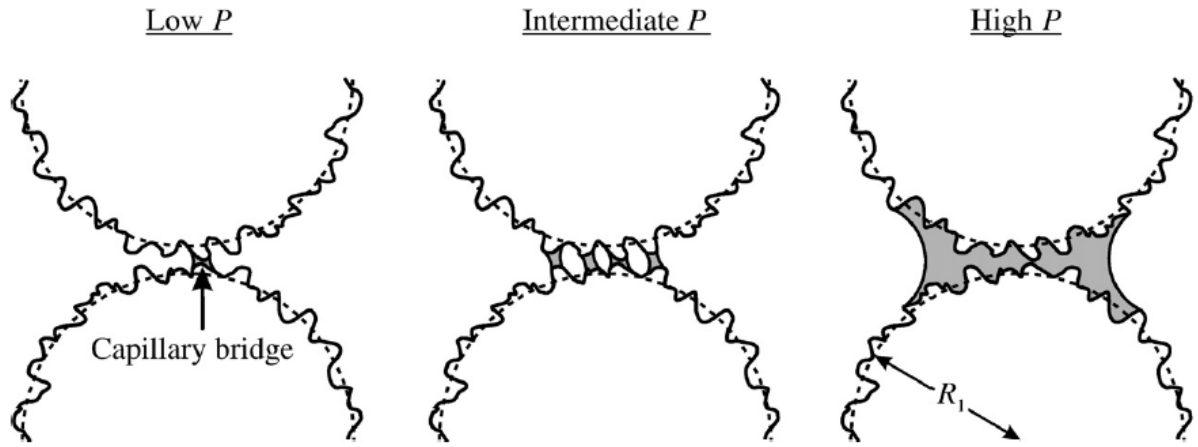

Figure 65: illustration scheme of two solid particles of radius R1, in contact at different vapor pressure (Butt and Kappl 2009)

In the **Table 8**, the vapor pressure and absolute humidity is calculated at the three experimental filtration conditions for (24°C, 45% RH), (150°C, 3% RH), and (150°C, 0% RH).

Table 8: Vapor pressure and absolute humidity at different filtration conditions

Operating parameters	**Absolute humidity [g.m^{-3}]**	**Vapor pressure [Pa]**
24°C - 45% RH	10	1347
150°C - 0% RH	0	0
150°C - 3% RH	73	14285

The results show that the vapor pressure increases with increase of absolute humidity, so that for 150°C-3% RH, the vapor pressure is 10 times higher than at (24°C, 45% RH), thus the formation of capillary bridges is more important at (150°C - 3% RH). The fact that leads to increase the capillary condensation between the deposited particles. Thus, in presence of humidity, the capillary condensation leads to decrease the porosity of the particulate cake and thus it leads to increase the filter resistance to air flow. This is in accordance to the curves of evolution of bag filter pressure drop during 10 cycles of clogging/unclogging at three different conditions (150°C - 3% RH; 150°C - 0% RH; and 24°C - 45% RH) plotted in the **Figure 66**.

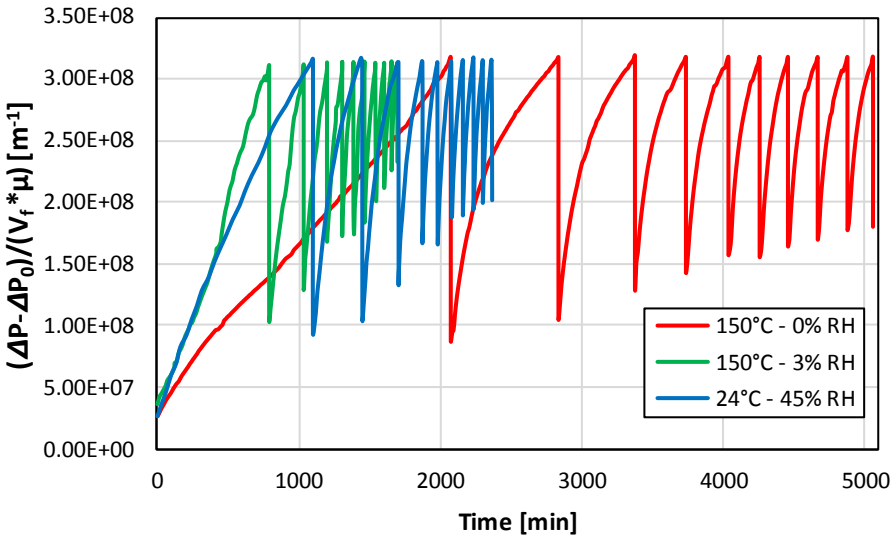

Figure 66: Influence of humidity on raw flow resistance through the bag filter

The difference of filtration efficiency observed in the **Figure 60** at 3% and 0% RH as a function of the particle size, can be then explained by the direct consequence of the capillary condensation. In fact, the capillary force has a direct consequence to increase the adhesion forces between the aggregates and decrease the distance between them, which means that the particle cake porosity decreases and become more compact at (3% RH) as compared to 0% RH **Figure 64**.

This can be confirmed according to the particle size distribution measured at the upstream of bag filter at (150°C, 3%RH) and (150°C, 0%RH) (Chapter II, Figure 32), the distribution shows, for particles higher than 100 nm, a slight decrease of concentration at (150°C, 3%RH) as comprised to (150°C, 0%RH). Thereby, the decrease of particle concentration in the range size of 100-300 nm can be explained by the clusters of aggregates due to the capillary force at 3% RH. Thus, the more the cluster is important, the more the size of agglomerates increases, by consequence the particle concentration decreases in presence of humidity.

Particle size ranging between 100 and 300 nm are mainly submitted to interception and inertial impaction mechanisms. As the particle density is a key parameter influencing inertial impaction mechanism, it can explain that collection efficiency is higher at 3% RH than 0% RH for particle size range 100-300 nm.

According to the literature, Kim et al. (2006) tested the filtration of hygroscopic sodium chloride (NaCl) nanoparticles with diameters ranged between 3 and 70 nm at filtration velocity of 2.5 $cm.s^{-1}$ by a fiberglass filter for different values of humidity (0.04; 1.22 and 92% of RH). The results showed that no influence of humidity was observed on the filter

performance. However, Miguel (2003) has studied the influence of humidity on the filtration of non-hygroscopic aluminum particle (Al_2O_3) in the size range of 0.8–6 µm by fiberglass media. The results show that the efficiency of fibrous filter increases with the increase of humidity at filtration velocity of 2, 5 and 15 $cm.s^{-1}$. Regardless the nature of particles, the obtained results of this study is consistent with the literature findings regarding the influence of humidity on fiber filter efficiency.

II.4 Effect of humidity on unclogging efficiency

In order to investigate the influence of humidity on cleaning efficiency of bag filter, the evolution of filter resistance $\xi' = (\Delta P_{res}-\Delta P_0)/(V_f.\mu)$ after the pulse cleaning is plotted in the **Figure 67** as a function of filtration cycles at (150°C - 0% RH) and (150°C - 3% RH).

The residual pressure drop ΔP_{res} indicates the overall pressure drop across the filter media (ΔP_0) and the residual cake remaining on the filter surface after the pulse cleaning, originating from insufficient filter cleaning. The evolution of residual pressure drop ΔP_{res} as a function of filtration cycles at 3% and 0% RH increased respectively from 22 to 111 Pa and from 19 to 87 Pa (**Figure 62**). Thus, the filter resistance (ξ') plotted in, shows that in presence of humidity (3% RH) the residual cake non-released after cleaning is quite important in comparison to 0% RH, which means that the pulse-jet cleaning system is more efficient to release the cake filter formed in dry gases (0% RH) than dust cake in humidity conditions (3% RH). It is obvious that the main reason of this difference of cleaning efficiency is due to the difference in the formed cake structure. As explained before, in the case of humid gas (3% RH), the capillary condensation between the particles increase the particle-particle adhesion forces and thus, it leads the cake is more difficult to remove from pulse-jet method.

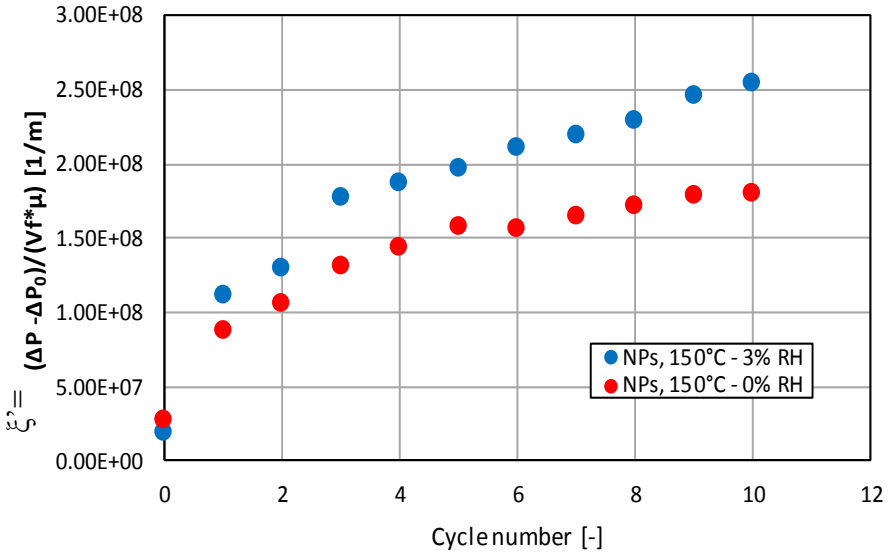

Figure 67: Filter resistance evolution of bag filter at the beginning of each filtration cycle - (150°C - 0%RH) and (150°C - 3%RH)

II.5 Filtration cycles

II.5.1 Fractional efficiency at residual pressure drop

To investigate the influence of clogging/unclogging cycles on filtration efficiency, we plotted in the **Figure 68** the fractional efficiency measured at residual pressure drop of each filtration cycle.

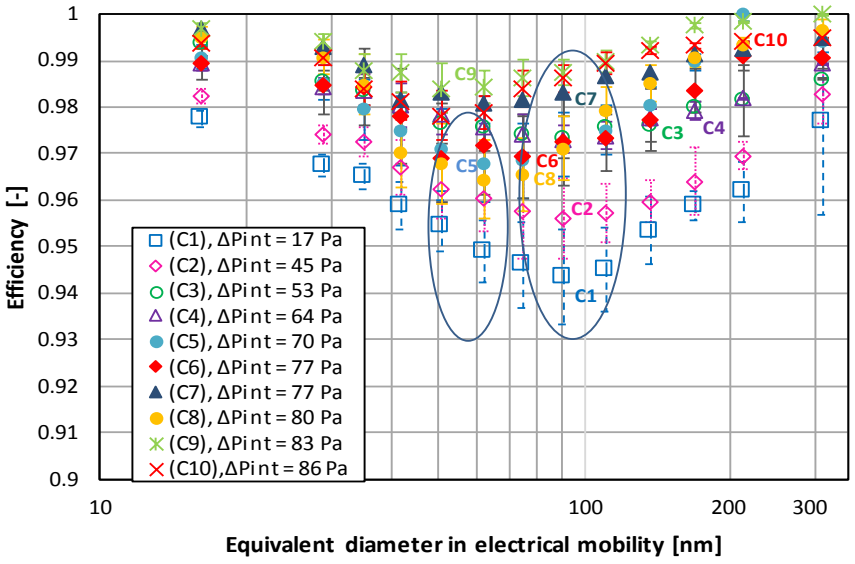

Figure 68: Influence of clogging/unclogging cycle and residual ΔP on filtration efficiency and MPPS (150°C - 0%RH)

As the results illustrated, the initial pressure drop of the bag filter was 17 Pa at first filtration cycles, where the minimum measured collection efficiency was 94.4% at MPPS of 92 nm.

Until the filtration cycle number 4, the efficiency increased and reached almost 97.2% for the same value of MPPS. However, from the filtration cycle number 5, we can notice a decreasing of the MPPS, from 92 to 64 nm. This change can be explained by the increase in residual dust cake which can be considered as loaded particles from previous cycles. The results are in accordance with Leung & Hung (2008) who observed MPPS decrease from 203 nm to 128 nm, during the loaded of nano-fibrous filters with NaCl particles of size ranging from 41 to 514 nm in electrical mobility diameter.

At the last filtration cycle (cycle 10) where the clogging filter started with high value of residual pressure drop (86 Pa), the efficiency was estimated at 98.2%.

In terms of comparison to the results of influence of filtration cycles on bag filter efficiency at 150°C and 3% RH, presented in the chapter III, the measured collection efficiency at minimum residual pressure drop of 25 Pa was 98.5% for the MPPS of 74 nm. Since the second filtration cycle the efficiency at residual pressure drop was varied between 97.5 and 99% with decreasing in the MPPS from 90 to 42 nm as a function of filtration cycles.

II.5.2 Fractional efficiency at maximum pressure drop

The filtration efficiency was also monitored (**Figure 69**) at the maximum pressure drop of 150 Pa as a function of filtration cycles. At this stage, an important cake filter was formed on the surface of filter media, which in turn plays an important role in collection efficiency.

At 150°C - 0% RH, the fractional efficiency is higher than the one at 150°C - 3%RH, for the all particle size range and for each cycle. Indeed, the fractional efficiency is higher than 99.9% in all cases and the efficiency increases gradually to achieve maximum value of almost 100 % at the filtration cycle 10. Moreover, considering the maximum pressure drop of 150 Pa which does not correspond to a sufficiently thick dust cake on the surface of filter media, the fractional efficiency obtained in both conditions still different. As illustrated in the **Figure 60**, for the same level of pressure drop (150 Pa), the number of collected particles is important at 150°C - 0% RH than 150°C - 3% RH.

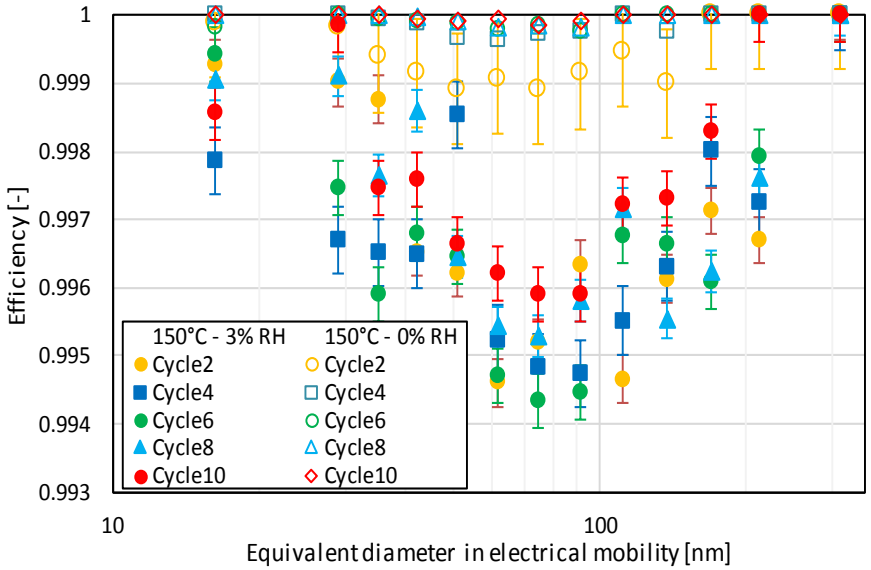

Figure 69: Collection efficiency at maximum ΔP (150 Pa) over 10 filtration cycles at (150°C - 3% RH) and (150°C - 0% RH)

Similar figure was presented in the chapter III in order to investigate the influence of filtration cycle on the filtration efficiency at 150 Pa for bag filter clogged with NPs + reagents at 150°C - 3% RH. In order to compare this result with the efficiency presenting in the **Figure 52**, the minimum efficiency obtained at pressure drop of 150 Pa during 10 cycles of clogging/unclogging was 99.85% at the SMPS of 40 nm, while in the **Figure 52**, the minimum efficiency is lower (99.4%) at the MPPS of 74 nm which then increases gradually with filtration cycle to reach maximum value of 99.6% at the filtration cycle 10.

III Influence of operating conditions driven by temperature

In the following section, the experiments were carried out in order to investigate the performance of bag filter at two different filtration conditions, i.e. (150°C - 0% RH) and (24°C - 45% RH) where the corresponding specific humidity of each condition is respectively 0 and 10 g water/kg air. In order to take into account, the variation of gas viscosity with operating parameters, especially with temperature, the maximum pressure drop was set at 150 Pa and 120 Pa respectively for 150°C and 24°C. To compare the different experimental tests, the deposited particle number has to be approximately the same for a similar filtration velocity (1.9 $cm.s^{-1}$). Thus, filtration efficiency and pressure drop are plotted as a function of the number of collected particles.

III.1 Bag filter efficiency

III.1.1 Experimental results

In order to study the influence of temperature on the collection efficiency measured at 150 °C and 24°C, the fractional efficiency for each temperature at 3 levels of filter clogging (number of collected particles) is plotted in **Figure 70.**

The 3 values of collected particles number (respectively 0.2, 0.8, and $1.6.10^{15}$ particles) corresponds to the pressure drop of 26, 54, and 80 Pa for the filtration experiments at 24°C and 36, 60, and 110 Pa for 150°C.

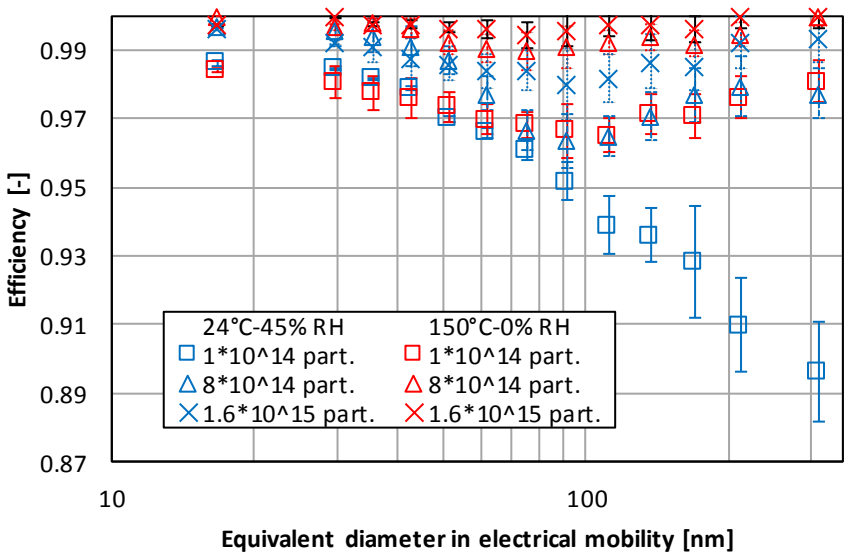

Figure 70: Bag filter fractional efficiency as a function of particle diameter for different collected particle numbers at 24°C - 45% RH and 150°C - 0%RH

As expected, for the same number of collected particles, the fractional efficiency is higher at (150°C - 0% RH) than at (24°C - 45% RH) for the entire particle size range which is respectively in the range of 97.4 - 99.9% and 90.5 - 99.9 %. For both conditions, the filtration efficiency depends on the particle sizes, which lie in a range from 10 to 310 nm. A special attention must be paid to the very different fractional efficiency behavior for particle size higher than 100 nm considering the measures obtained at 1.10^{14} particles for the two filtration conditions. Indeed, for the experiment at 24°C, for a number of particles collected of 1.10^{14}, the fractional efficiency slowly decreases from 100 nm to 310 nm particle diameter. On the contrary, for a temperature of 150°C and for the same size range, the collection efficiency increases slowly with the increase of particle size. As a consequence, MPPS equals to 90 nm at 150°C while MPPS seems to be higher than 300 nm at 24°C.

Regarding the fractional efficiency for particles lower than 100 nm, the curves are re-plotted in the **Figure 71** in order to clarify the influence of temperature in the size range of 16-111 nm. At the same number of collected particles, the fractional efficiency of particles higher than 52 nm (52-111 nm), at 150°C, is higher as compared to 24°C. Thereby, the measured filtration efficiency curves are in good agreement with the expected behavior for Brownian diffusion mechanism. While for particle lower than 35 nm, no significant influence of temperature was observed, although the Brownian diffusion is the mechanism predominant which is not consistent with filtration theory.

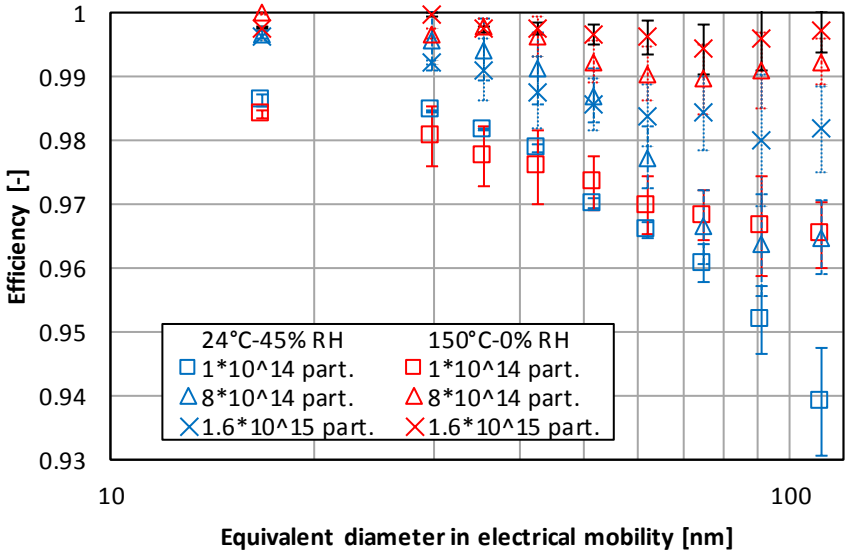

Figure 71: Bag filter fractional efficiency as a function of particle diameter for different collected particle numbers at 24°C - 45% RH and 150°C - 0% RH for nanopartcile size range

The findings are consistent with the recent work presented by Förster et al. (2016) during nanoparticles filtration with fibrous filter. The study showed that the collection at 200°C was 95% against 93% at ambient temperature (20°C). The low content of humidity at 24°C (45% RH corresponding to 10 g water/kg air) can be considered as not influential factor in comparison to the temperature.

III.1.2 Theoretical investigation

The effect of temperature on the fractional filtration efficiency was investigated by a numerical approach based on Kasper model (**Figure 72**). The numerical fractional efficiency is plotted for the two filtration conditions (24°C - 45% RH) and (150°C - 0%RH).

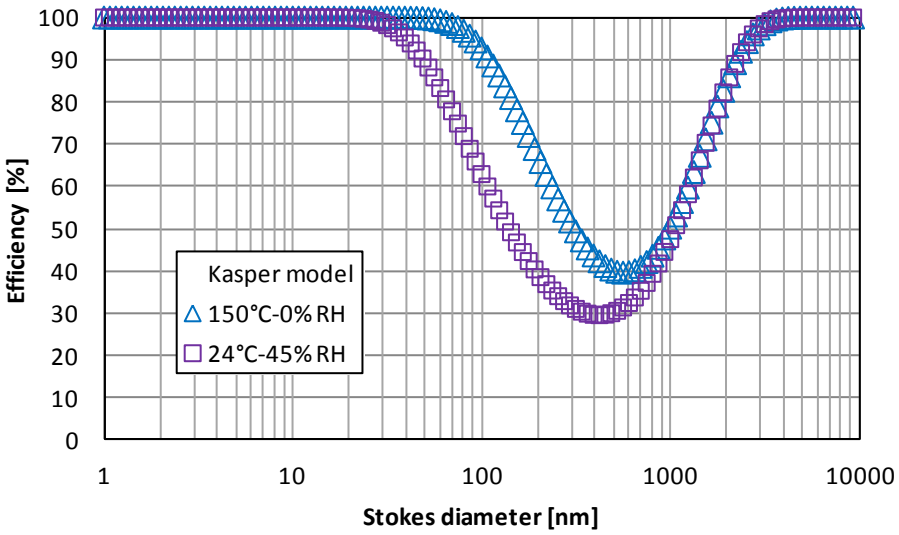

Figure 72: Influence of temperature and humidity on Initial fractional efficiency according to Kasper et al. (1978) model

In both conditions, fractional efficiency as a function of particle size exhibits a V shape as showed by Richard (1993); Hinds (1999); Lee & Mukund (2001) and Liu et al. (2011). As shown in the **Figure 72** (for 150°C - 0% RH and 24°C - 45% RH) for size ranges higher than 700 nm and lower than 30 nm, the fractional efficiency is not influenced by temperature. The influence of temperature is observed between 30 and 700 nm where the MPPS is identified. These results can be explained by the influence of temperature on same filtration mechanisms that we will discuss in the following section.

Figure 73 exhibits the fractional efficiency (η) calculated for each capture mechanisms from the Kasper model at 150°C and 24°C. The Kasper model is determined taking into account the diffusion (η_d), the direct interception (η_i), and the inertial impaction (η_r), mechanisms given as following:

$$\eta=1-(1-\eta_d)(1-\eta_i)(1-\eta_r) \quad (73)$$

As expected, the results show that temperature influence is observed on Brownian diffusion for particle size range between 30 and 700 nm in diameter. In fact, considering molecular description of the fluid, the increase of temperature leads to increase air molecules motion, leading to collision with the carried particles (nano and submicron particles) and enhancing their fluctuation around air flow path.

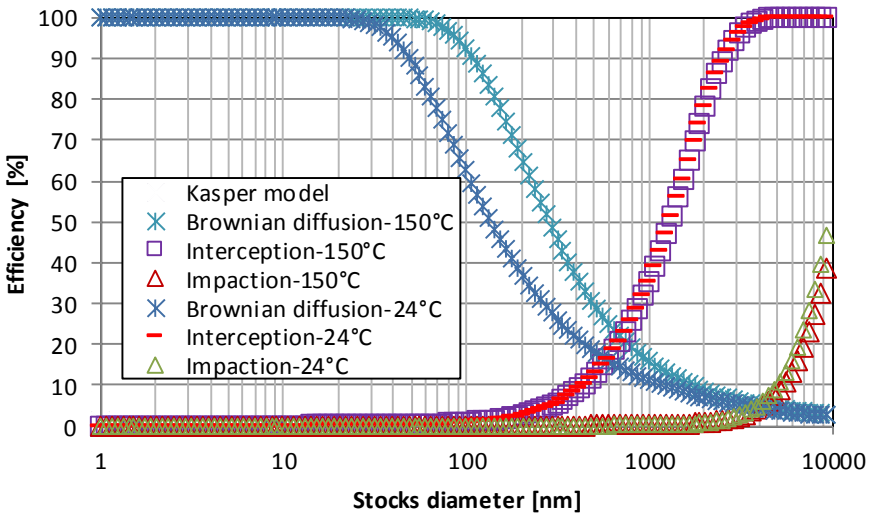

Figure 73: Efficiency of collection mechanisms by the model of Kasper et al. (1978) at 150°C and 24°C

III.2 Filter pressure drop

To investigate the influence of filtration temperature on the bag filter pressure drop, the ratio of relative pressure drop over velocity times viscosity $\xi = (\Delta P - \Delta P_0)/(V_f \times \mu)$ is plotted in the **Figure 74** as a function of collected particles number for the experimental results at 24°C and 150°C during the first filtration cycle. The evolution of filter resistance can be distinguished in two stages, in the first stage, the increase of filter resistance (ξ) at 24°C and 150°C is identical and linear from the beginning of filtration until the collected particles number of 2×10^8. The proportional increase of filter resistance to the number of collected particles can be explained by the influence of temperature on filter resistance. Indeed, from the **Figure 74**, the identical curves allow considering that:

$$\frac{(\Delta P^{150} - \Delta P_0^{150})}{\mu^{150}} = \frac{(\Delta P^{24} - \Delta P_0^{24})}{\mu^{24}} \quad (74)$$

The gas viscosity increases with temperature $\mu^{150} > \mu^{24}$ which means that $\mu^{150}/\mu^{24} > 1$, by consequence:

$$(\Delta P^{150} - \Delta P_0^{150}) > (\Delta P^{24} - \Delta P_0^{24})$$

In the second stage, from the collected particle number of 2.10^{15}, the curve of filter resistance at 150°C increases in parabolic shape and the slope enhances with loading particle number, while the filter resistance curve at 24°C still rises linearly. This change in the filter resistance at 150°C can be explained by the change in the structure of particle cake. Indeed, the porosity

of particle cake is lower at 150°C as compared to the particle cake formed at 24°C. This is a direct consequence of the difference of particle size distribution at 150°C and 24°C as explained in the chapter II. Indeed, important particles are deposited on the experimental set-up because of the thermophoresis phenomena which leads reducing the particle concentration and their size received on the filter media at (150°C) as compared to 24°C. The particle modes at 150°C and 24°C are respectively 45 and 62 nm. According to Thomas (2001), the resistance cake filter increases with decreasing of particle size because of their large specific area.

Considering literature review on influence of temperature on pressure drop, (Kim et al. 2008) have been studied experimentally the evolution of the pressure drop across dust cake of ash aerosol deposited on ceramic filter clogged at different values of temperature (Room temperature – 673 K). The study showed that the pressure drop of the filter increases with filtration temperature. The main reason of this increase was due to the change of fluid viscosity which increases with temperature. This is consistent with the obtained results in the **Figure 74**.

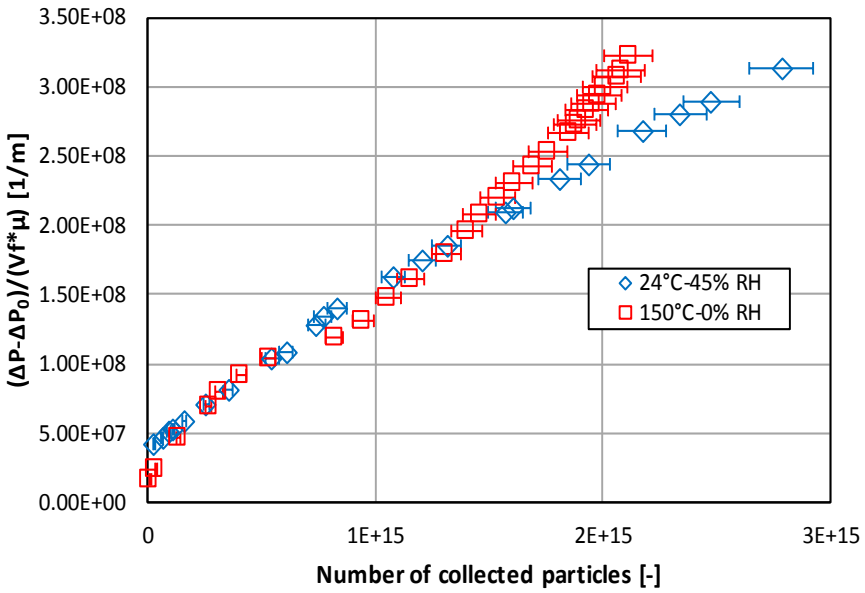

Figure 74: Evolution of filter resistance as a function of collected particle number at 24°C - 45% RH and 150°C - 0%RH for cycle 1

The evolution of bag filter pressure drop at 150°C and 24°C, is plotted in **Figure 75** as a function of time during the filtration cycles. **Figure 75** is not appropriate to compare the rise of ΔP in terms of time because of the change in aerosol concentration, as explained in the **chapter II**, important particles are deposited on the experimental setup because of the thermophoresis phenomena which leads reducing the particle concentration received on the

filter media at (150°C) as compared to 24°C). However, the curves can be analyzed in terms of filter resistance $\xi'' = (\Delta P_{res} - \Delta P_0)/(V_f.\mu)$ at residual pressure drop (ΔP_{res}) of each filtration cycle.

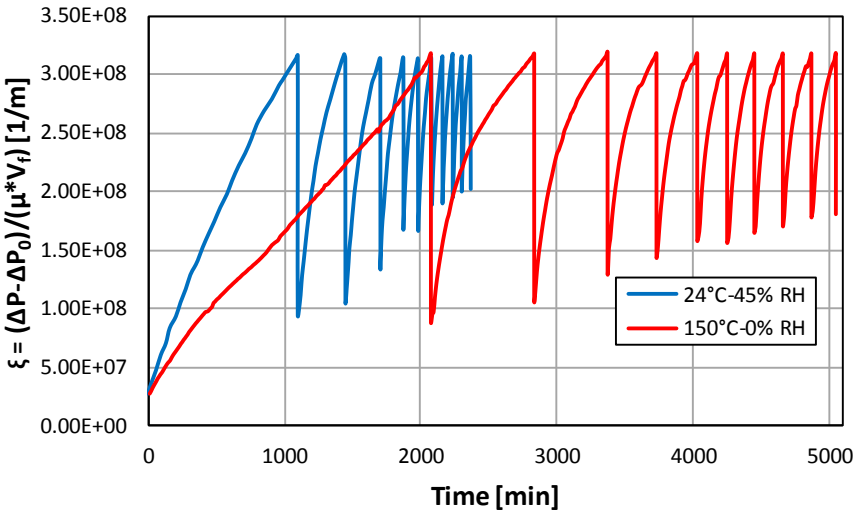

Figure 75: Bag filter resistance as a function of time – (24°C - 45%RH) and (150°C - 0% RH)

The results (**Figure 76**) show the evolution of filter resistance ξ'' as a function of filtration cycles. In all cases, the resistance (ξ'') increases with filtration cycles and seems to reach an equilibrium value gradually as the number of filtration cycle increases.

For the first 5 cycles, the filter resistance (ξ'') at 150°C is almost similar as compared to the 24°C. However, a slight divergence can be observed from the filtration cycle 6. According to Mukhopadhyay et al.(2016) the efficiency of unclogging filter decreases with increasing of gas temperature because of the change of the air characteristics retro-pulsed in the bag filter, hence, the temperature effect was deeply related to the fluid viscosity. However, the study was occurred at a temperature of 400°C which is much higher to than the filtration temperature of 150°C of the present study.

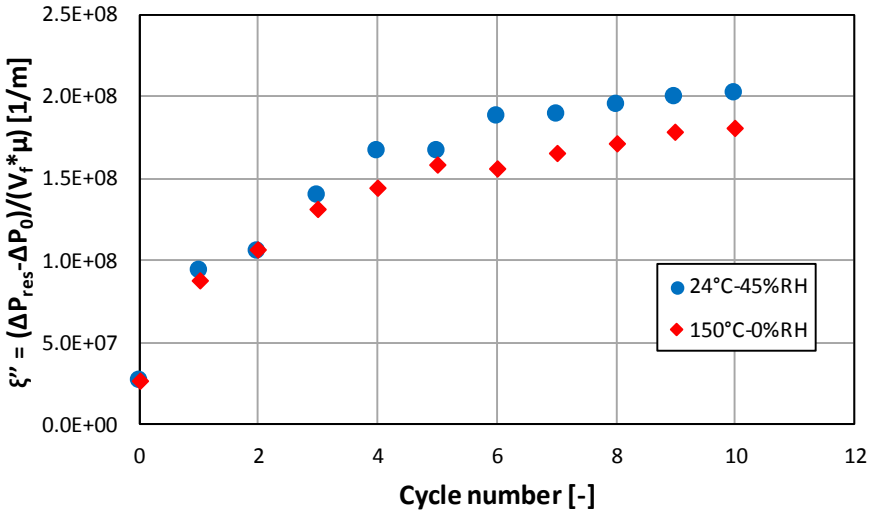

Figure 76: Residual pressure drop evolution of bag filter as a function of filtration cycles at (24°C - 45%) RH and (150°C - 0% RH)

IV Influence of added reagents

Used bag filter was clogged in waste incineration conditions (150°C - 3% RH) from one side with carbonaceous nanoparticles (NPs) at total concentration of $5.09.10^6$ particles.cm^{-3}, from the other side with NPs + reagents (sodium bicarbonate and activated carbon) with particle concentration of $5.45.10^6$ particles.cm^{-3}. For both filtration conditions, the same bag filter was tested in the present investigation. Indeed, the bag filter was de-clogged several times to remove the residual cake and restart the experiments with almost the same initial residual pressure drop for both filtration conditions. For the simplicity of results presentation, the bag filter clogged with NPs is named (F1) while the bag filter clogged with NPs + reagents is named (F2).

For both filters the concentration of NPs aerosol was similar in order to investigate the influence of particle size on bag filter performance over 10 filtration cycles.

IV.1 Filtration efficiency

The fractional collection efficiency of the tested bag filters was plotted in the **Figure 77** as a function of particle diameter for different level of filter clogging. The minimum collection efficiency at the initial value of pressure drop was measured at 98%. At this value of pressure drop the difference of collection efficiency for particles smaller than 70 nm was not significant for both filters. In general, the remarkable difference that can be revealed from the collection efficiency curves is the faster increase of fractional efficiency with clogging in the

case of nanoaprticles in comparison with NPs + reagents, especially for pressure drop equal or higher than 60 Pa. To understand the filtration efficiency difference, we investigated in the following section the evolution of pressure drop and the cake structure of deposited particles as a function of dust loading.

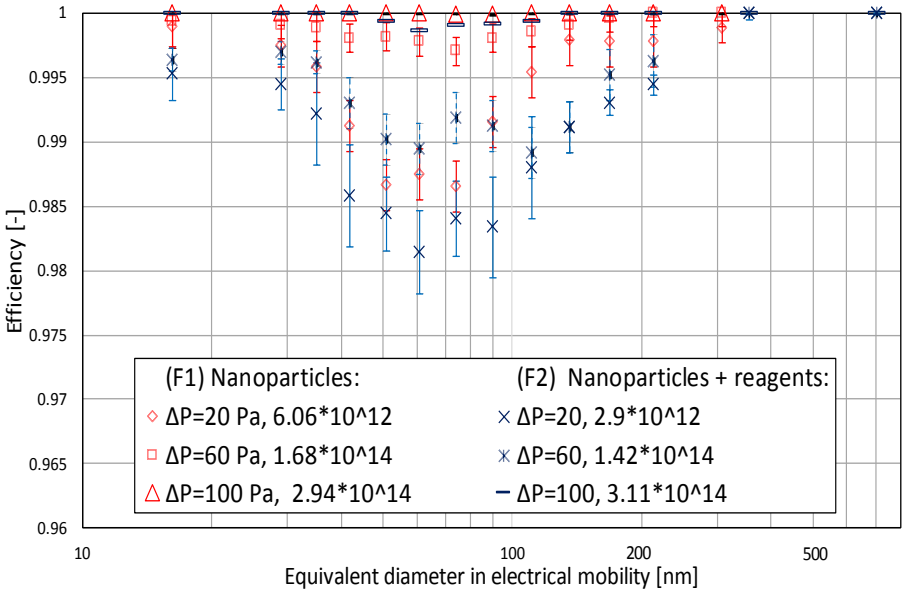

Figure 77: Filtration efficiency versus particle diameter for the first filtration cycle of used bag filter, at different values of ΔP and collected particles number for the two particles: NPs and NPs + reagents

IV.2 Influence of particles on pressure drop

The evolution of bag filters pressure drop as a function of the collected particle number during the first filtration cycle is presented in the **Figure 78** for both particles: NPs and NPS+ reagents. For the filter (F2), clogged with NPs + reagents, the results show a gradual increase of pressure drop with particles loading, pressure drop increases with slight concave rise from ΔP = 80 Pa, while for the filter (F1), after a linear increase of pressure drop, a concave rise is detected for ΔP ≥ 110 Pa, this sudden change in the pressure drop rise can be explained by the clogging of all the inter-fibers pores with compact agglomerates resulting from nanoparticle collection.

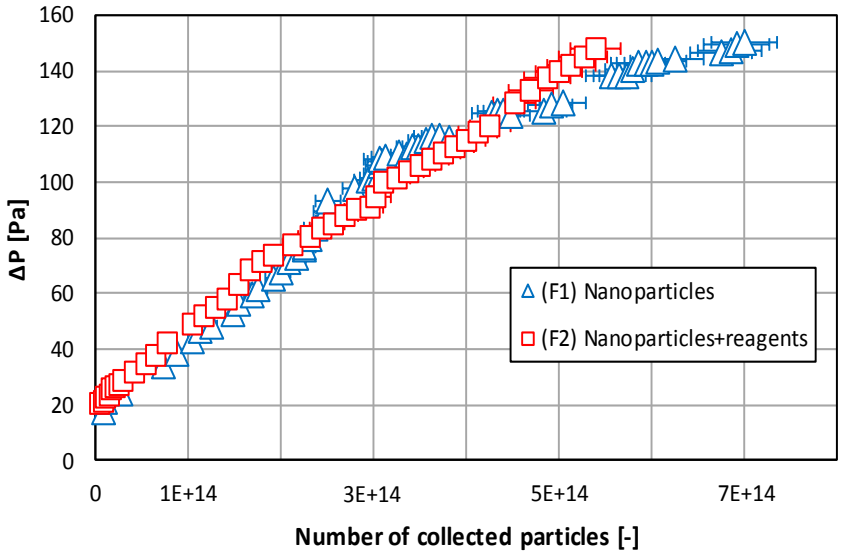

Figure 78: Evolution of pressure drop versus collected particles number at 150°C and 3% RH for the two particles (NPs and NPs + reagents) for first clogging cycle

The **Figure 79** illustrates the pressure drop evolution with clogging cycles as a function of time for the tested particles. The results show an important influence of particle size on unclogging efficiency. During the first filtration cycle, the clogging time of the bag filter (F1) clogged with NPs agglomerates (800 min) is longer than the bag filter (F2) clogged with NPs + reagents (620 min), which can be explained by the difference in total particle concentration: respectively ($5.09.10^6$ particles.cm^{-3}) and ($5.45.10^6$ particles.cm^{-3}). However, for the second filtration cycle and the following ones (cycle 3 to 10) the clogging time of the filter (F1) becomes shorter in comparison to the bag filter (F2) as illustrated in the (**Figure 80**).

This can be explained by the porosity and the structure of the filtration cake. In fact, the deposited nanoparticles form a resistant cake with high porosity, while the larger particles of reagents added to the NPs build up a cake exhibiting lower porosity. The results are in agreement with the experimental works of Thomas (2001) dealing with the clogging of fibrous filters by solid aerosol particles. Thomas (2001) observed an increase of the pressure drop of the filter with the decreasing of the size of loading particles. According to Thomas (2001) the main reason is the specific area of particles which is larger for smaller particles that leads to form a cake filter with higher pressure drop.

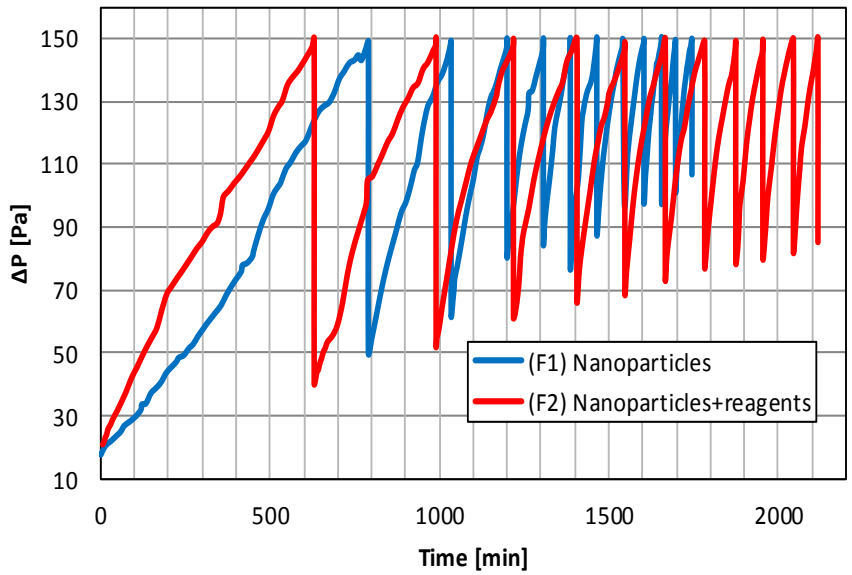

Figure 79: Evolution of pressure drop (ΔP) of bag filter versus time for 10 clogging/unclogging cycles for two loading particles at 150°C, 3% RH

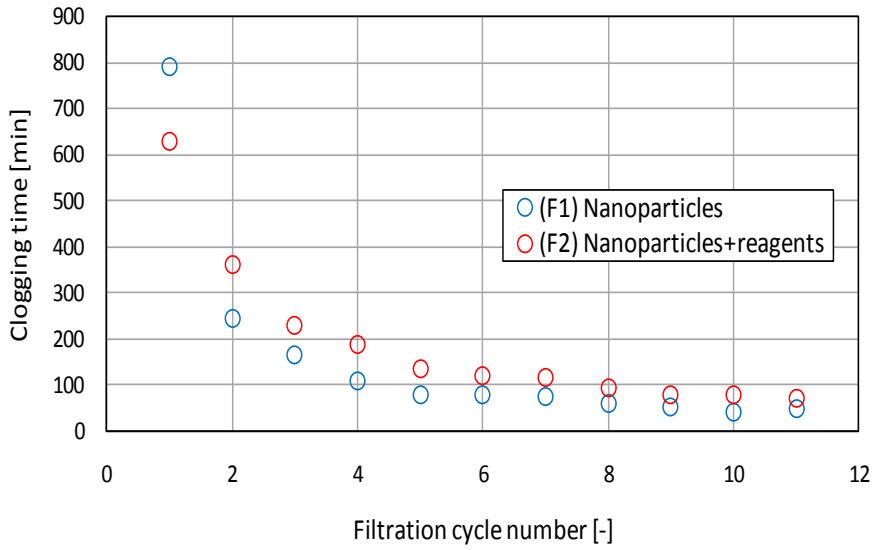

Figure 80: Clogging time as a function of filtration cycles for the two particles: NPs and NPs + reagents

For more investigation, an extensive study of deposited particles structure was performed by using scanning electron microscope (SEM). Two flat filters, used for deposited particle sampling, were clogged respectively with NPs and reagents in order to investigate the structure of deposited particles for the same concentration and operating parameter conditions as the bag filter clogging.

Figure 81 shows photographs performed at different locations on the filter surface. In the photographs (a), the filter is loaded only with reagents, while in the photographs (b) the filter is clogged with NPs agglomerates. It can be seen from the figure the difference of deposited particles structure. The reagents particles form a structure more homogeneous with high porosity leading to lower pressure drop. This is probably the reason which makes the dislodgement of particle cake easier. While, the deposited nanoparticles form a resistant cake.. Despite the increase of cleaning efficiency with reagents particles, the residual pressure drop still not yet stabilized. Most probably, this is due to the low value of maximum pressure drop of bag filter (ΔP_{max}=150 Pa). According to Saleem et al. (2012), ΔP_{max} is one of the key factors that affects cake filter detachment. In fact, with thicker cake filter (higher ΔP_{max}) the cleaning filter must be improved.

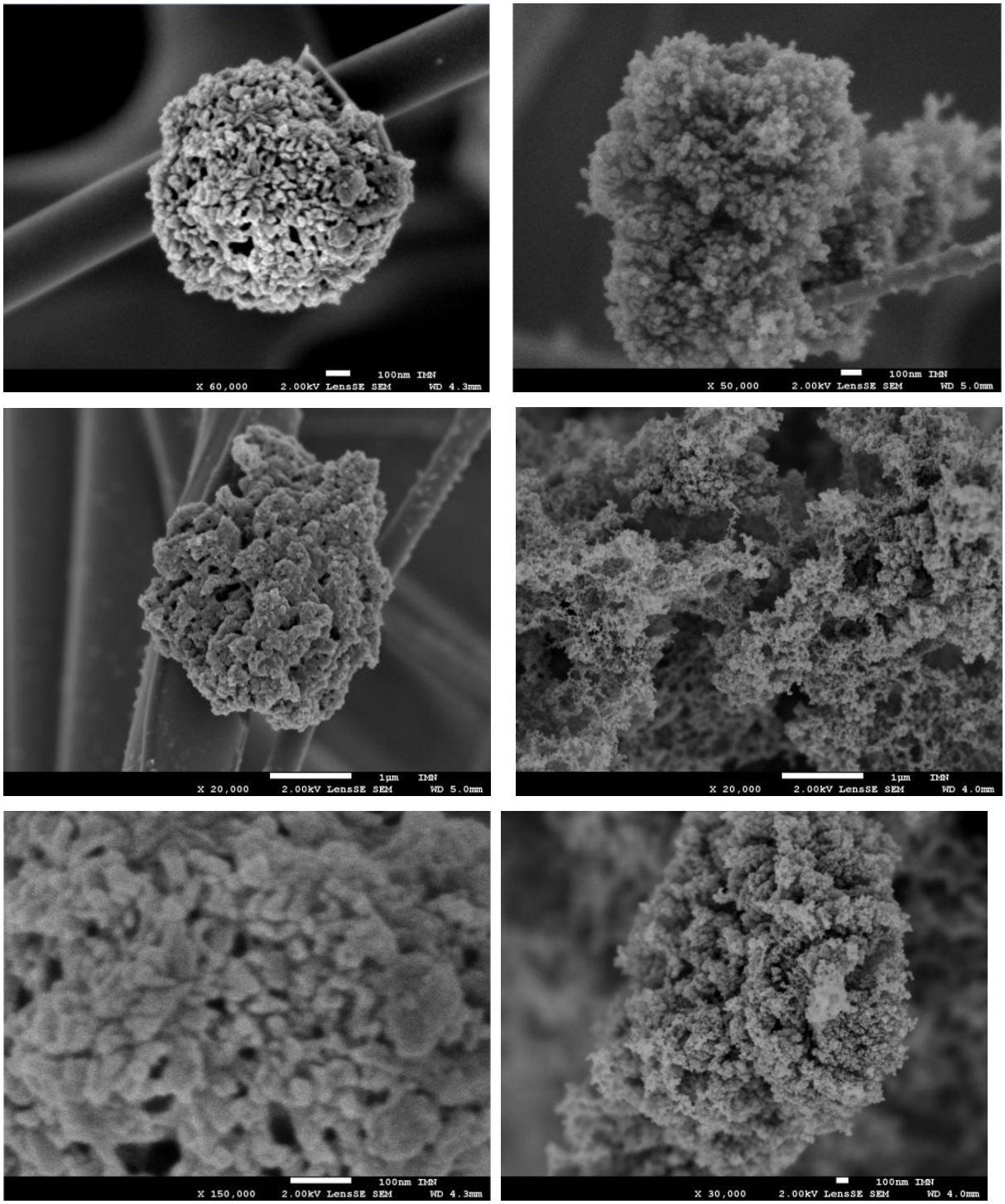

a) Reagents (sodium bicarbonate and activated carbon).

b) BC Nanoparticles

Figure 81: SEM images of particles (reagents and nanoparticles) captured at the surface of tested filter for the two particles

V Influence of filter aging

V.1 Filter efficiency

To investigate the efficiency of fibrous media exposed to particle loading, used and new filters are implemented in the experimental device presented in **chapter II** allowing testing filter in flat configuration perpendicular to air flow. Operating conditions are filtration velocity of 1.4 $cm.s^{-1}$ and ambient conditions (24°C - 45% RH) for carbonaceous nanoparticles at $3.2.10^{7}$ $particles.cm^{-3}$ concentration.

The total collection efficiency is plotted in the **Figure 82** as a function of pressure drop ratio for new and used filter.

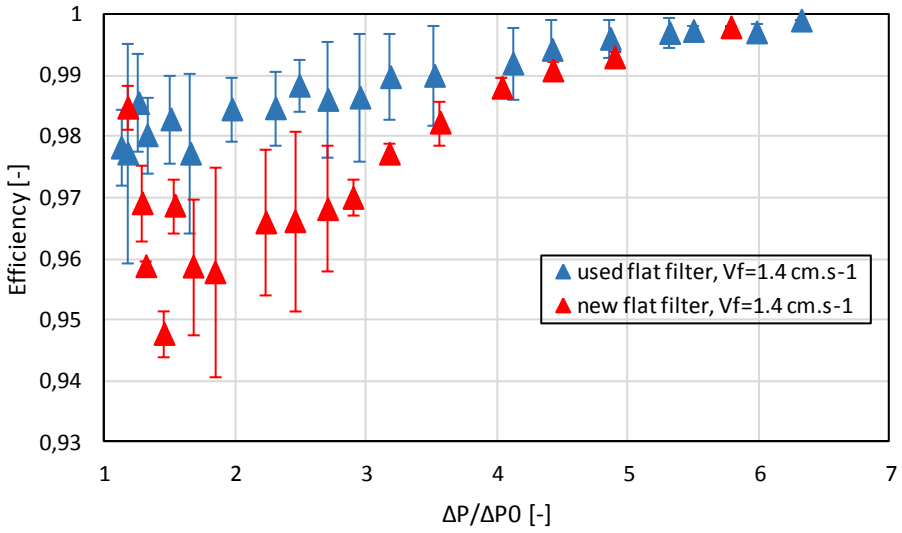

Figure 82: Evolution of total efficiency as a function of $\Delta P/\Delta P_0$ for used and new flat filters at filtration velocity of 1.4 $cm.s^{-1}$

For used filter the total efficiency increases gradually with clogging from 97.8 to 99.75%. While, for new filter, the efficiency was higher at the beginning of clogging for total efficiency of 98.5%, suddenly, a sharp decrease of efficiency is observed from 98.5 to 95.6% until ΔP/ΔP0=2. This fast decrease in filtration efficiency can be explained by the variation of interaction between particles and clean filter fibers. Indeed, the particles are collecting by clean fibers because of the filtrations mechanisms (Brownian diffusion, interception, and impaction) until the total recovery of fibers by the collected particles. In the some phase of filtration (deep filtration) the deposited particles will play the role of fibers and collecting the incoming particles. However, the efficiency of fibers to particle collection is important than the collect by deposited particles. Hence the gradual decrease of filtration efficiency can be

explained by the gradual increase of fiber coverage with deposited particles. At the formation of cake filter on the surface of filter media, the filtration efficiency start to increase from 96% at ΔP/ΔP0=2 to 99.75% at ΔP/ΔP0=6.

Figure 83 presents the fractional efficiency for 3 levels of clogging (ratios ΔP/ΔP0). As expected, the fractional efficiency decreases with increasing of particle size in the range of particle diameter 10-310 nm. At lower value of pressure drop (ΔP/ΔP0=2), the used filter is more efficient than the new filter for collecting particles higher than 90 nm in diameter.

This difference in the fractional efficiency between new and used flat filter for particles higher than 100 nm, decreases with clogging until the particle collection efficiency of 99.2 % corresponding to ΔP/ΔP0=6. While, the collection efficiency of particles lower than 90 nm was higher for both filters from the beginning of filtration. Furthermore, the most penetrating particle size is influenced by the ageing process, especially for the new filter as used filter exhibit a MPPS of 150 nm compared with 120 nm for the new filter, at ΔP/ΔP0=2. This can be explain by the increase of interception effect, during filter clogging, which is considered as one of the main mechanism responsible for particle collection which diameters higher than 100 nm.

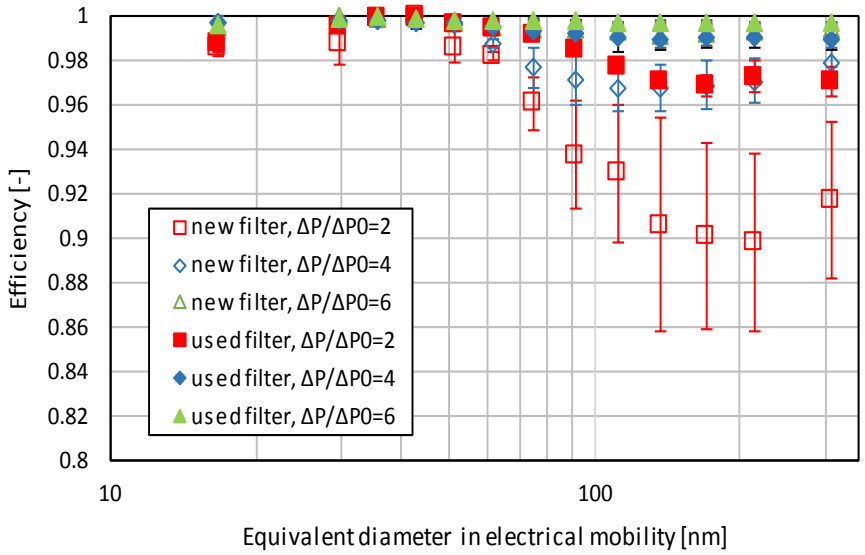

Figure 83: Evolution of fractional efficiency as a function of particle size for used and new flat filters and for different level of clogging ΔP/ΔP0 – Filtration velocity=1.4 cm.s^{-1}

V.2 Pressure drop evolution

Pressure drop evolution of new and used bag filter as a function of time is plotted in the (**Figure 84-a**). At ambient conditions (24°C - 45% RH), the filters were tested over 10

filtration cycles, clogged with carbonaceous NPs (16-315 nm in diameter). The used bag filter was previously precoated (in conditions representative of industrial ones) by a thin layer of reagents (sodium bicarbonate + activated carbon). Before the test, the filter was unclogged several times by pulse-jet system to remove the residual cake and reduce the pressure drop.

The maximum pressure drop ΔP_{max} for all filters and during 10 filtration cycles was set to 120 Pa at which point the process of dust cleaning is encaged.

In agreement with the previous results of this study, the experimental results showed that the clogging time of the filtration cycles decreases from the first cycle (1090 min) to the last one (~55 min). The increase of residual pressure drop (ΔP_{min}) with filtration cycles, from 20 to 80 Pa for used filter and from 10 to 60 Pa for new filter is due to the residual cake of the previous filtration cycles in accordance to (Saleem et al. 2011). The residual cake contributes strongly to ageing process and leads to reducing the life of filters (Bao et al. 2014).

Different curves are plotted in the (**Figure 84**) in order to compare the new and the used bag filter in terms of pressure drop rise as a function of filtration cycles. The aim of this section is to investigate the influence of filter aging on bag filter performance.

During the first filtration cycle (**Figure 84-b**), the initial pressure drop for new and used bag filter are different (respectively 10 and 22 Pa) because of the residual particles on used bag filter (clogged particles by depth filtration and the presence of fragmental particle cake on the filter media surface). This can explain the difference in pressure drop rise between both filters during the cycle time. Indeed, during clogging of clean filter (**Figure 84-a**), three stages can be distinguished (**Figure 84-b**): (1) depth filtration, (2) transition filtration, and (3) cake filtration. Over the first 200 minutes of clogging, the rise of new filter pressure drop was not important as a function of time which is explained by the occurrence of depth filtration (1) (Mukhopadhyay et al. 2016), indeed, as the filter media was clean, the particle penetrates the filter media and captured only through the fibers. The rise of pressure drop was then followed by the change of curve slope (2) where a slight increase of pressure drop is observed, which means that the filtration is in transition area from deep filtration to the surface filtration. The third phase of filtration (3) is characterized by a linear and sharp rise of pressure drop, which corresponds to the formation of the particle cake on the media surface (Song et al. 2006). The results are in good agreement with previous studies investigating clean fibrous filters clogged with monodisperse aerosols (Japuntich et al. 1994 and Thomas 2001).

In comparison to the used bag filter, it can be seen that the curve shape of new bag filter pressure drop is different during the first filtration cycle. In contrast to the new bag filter, the

rise of pressure drop of used bag filter is faster from the beginning of filtration (especially for ΔP =20 Pa to ΔP = 55 Pa), which can be explained by the occurrence of deep filtration. As compared to the overall time of filtration cycle 1, a gradual transition from concave to linear rise can be observed for used bag filter pressure drop. This leads to slight decrease of pressure drop rise from ΔP = 55 Pa.

From the second filtration cycle (**Figure 84-c, d, e, f**), the evolution of pressure drop of new and used filter is important immediately after regeneration process. While a small deviation of pressure drop curve is observed, for both filters, during a gradual transition from concave to linear rise. The time of concave rise of pressure drop is important for new bag filter as compared to the used bag filter. This transition in pressure rise is due to the residual particle cake on the media surface. Indeed, the absence of this deviation can be observed at the cake filtration regime for new bag filter during the first filtration cycle, where no residual particle cake was formed on the filter surface. Moreover, although the difference in residual pressure drop for both filters (about 20-30 Pa) during all filtration cycles (from cycle 2 to cycle 10), both filters reach the maximum pressure drop (120 Pa) in almost the same duration time. Hence, the more residual cake is important, the more the concave rise of pressure drop is faster.

This can confirm the assumption discussed in the chapter 3, where the non-uniform distribution of cake filter leads to increase the interstitial velocity through the preferential pathways, which means large amount of small particles (<100 nm) pass through the filter without collection. By consequence, the particle cake on the surface of used filter media is formed with large particles as compared to the cake filter build-up on the new filter. As a result, the resistance of particle cake of used filter is less important than the formed on the new bag filter which increases its clogging time as compared to the used bag filter.

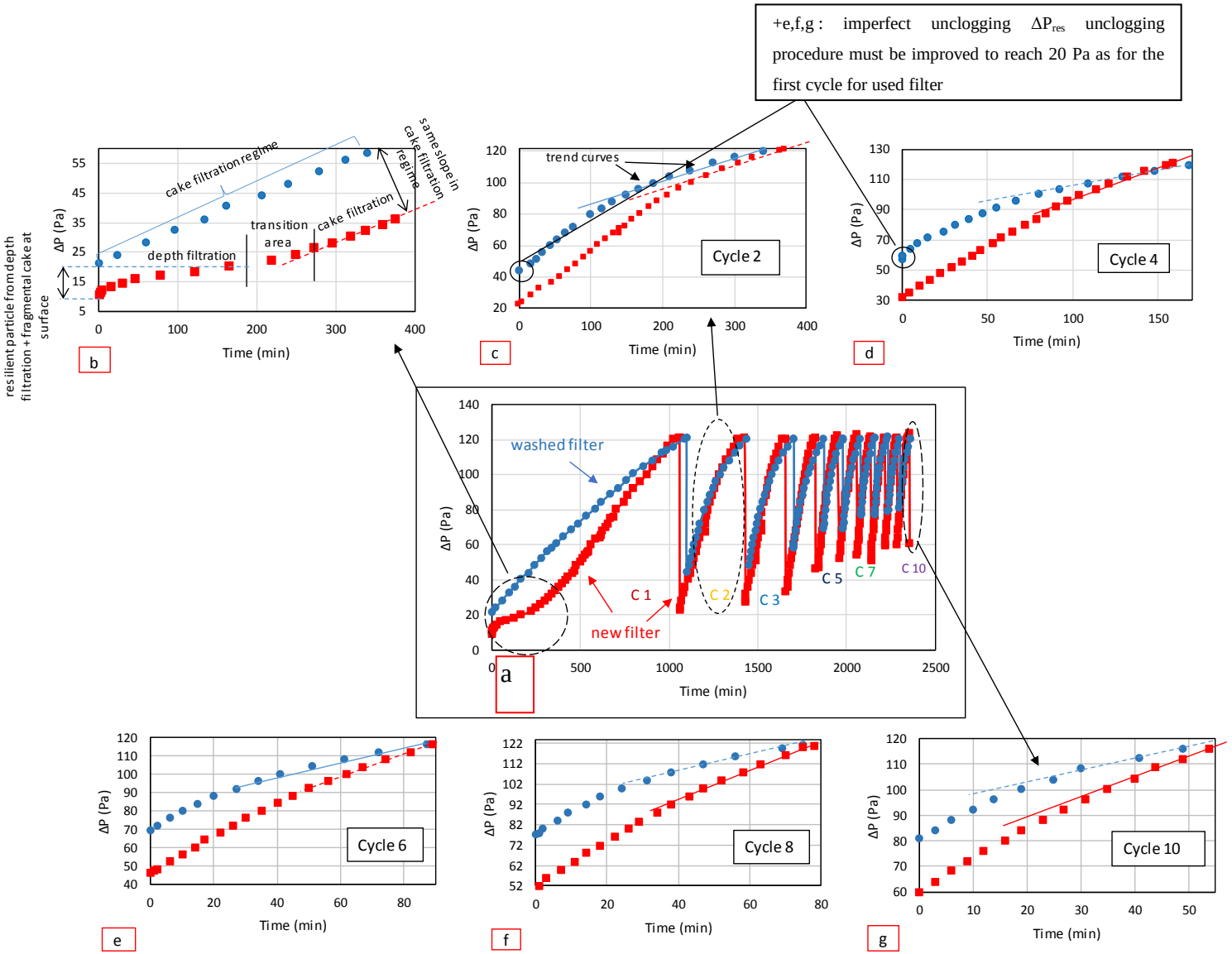

Figure 84: Pressure drop across new and used bag filter against time for 10 clogging/unclogging cycles at (24°C - 45% RH)

VI Influence of filtration velocity

VI.1 Collection efficiency

Figure 85 shows the fractional collection efficiency of used flat filters clogged at 2 different filtration velocities (1.4 and 1.9 $cm.s^{-1}$) for different level of clogging (ratios ΔP/ΔP0). As seen previously in the (**Figure 83**) and in accordance with the filtration theory, the efficiency increases with clogging for both filtration conditions. For ΔP/ΔP0=2 (corresponding to a filtration regime before the formation of cake), the efficiency is higher at filtration velocity of 1.4 $cm.s^{-1}$ than at 1.9 $cm.s^{-1}$ for particle size ranging from 50 to140 nm (i.e. below the MPPS). This result is in good agreement with filtration theory: for particle size smaller than the MPPS, the Brownian diffusion is the dominant particle collection mechanism and its efficiency increases as filtration velocity decreases. In fact, as described in the chapter 1 of state of art, the particle collection is governed by the relative importance of the diffusion movement with respect to the fluid convective motion, which is called the Peclet number, expressed by the following equation (75):

$$P_e = \frac{V_f . d_f}{D} \qquad (75)$$

Thus, as the filtration velocity (V_f) is not important, as the Peclet number is negligible, this means that the diffusion movement of particles is significant. By consequence, the interactions particles/fibers become important and increase the chance of nanoparticle collection by fibers. These results are in agreement with previous studies, conducted on clogging of fibrous filters with nanoparticles (Wallace et al. 2010) and (Chen et al. 2001).

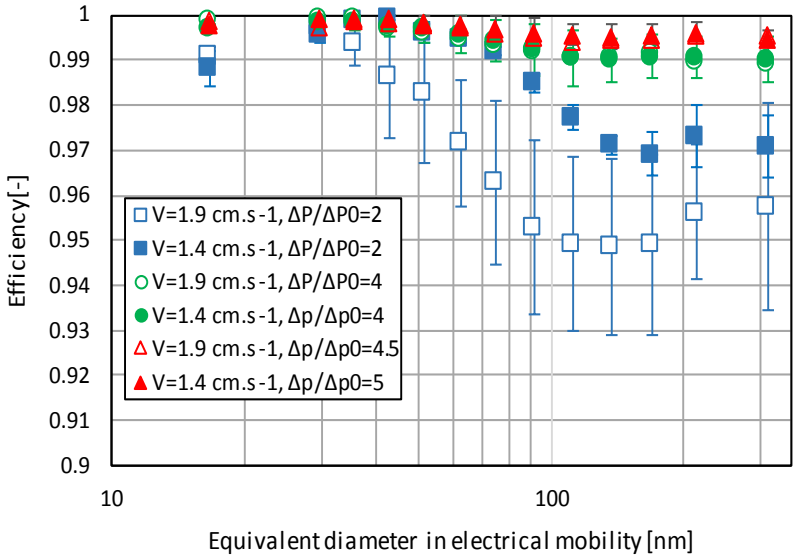

Figure 85 : Evolution of fractional efficiency, as a function of equivalent diameter in electrical mobility, of used and new flat filters at two filtration velocities (1.4 and 1.9 cm.s^{-1}) and at different values of ΔP/ΔP0 under continuous loading

VI.2 Pressure drop

Figure 86 shows the evolution of flat filter pressure drop as a function of time. The used filters were clogged at two filtration velocities (1.4 and 1.9 cm.s^{-1}).

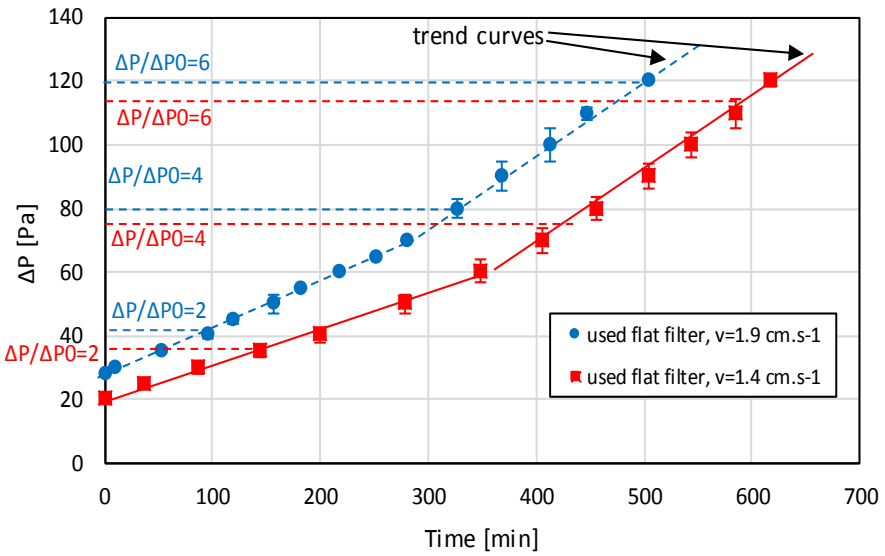

Figure 86: Pressure drop filtration time for used flat filter at 1.4 and 1.9 cm.s^{-1}

The results show that the duration of filter clogging increases with decreasing of filtration velocity for the same upper-pressure drop limit of 120 Pa. At the some and constant filtration condition, the filter clogged at 1.9 cm.s^{-1} reaches the upper-pressure drop limit faster than filter clogged at 1.4 cm.s^{-1} (500 and 600 min respectively).

The initial relative pressure drop for used filter clogged at 1.9 cm.s^{-1} is important as compared to the filter clogged at 1.4 cm.s^{-1} (respectively 20 and 28 Pa), this indicates the influence of velocity on pressure drop for air flow through the porous media.

The evolution of pressure drop for both conditions can be distinguished in two stages. First, a linear rise of pressure drop for both filtration velocities is observed from the beginning of filtration to the pressure drop of 60 and 70 Pa, respectively at 1.4 and 1.9 cm.s^{-1}. During the evolution of pressure drop a slight divergence between curves is observed with important slope at 1.9 cm.s^{-1} as compared to 1.4 cm.s^{-1}, this stage corresponds to the transition area from the deep filtration to the surface filtration. In the second stage, an important increase of the curves slop is observed for both filters, with almost similar rise of pressure drop at 1.9 cm.s^{-1} and 1.4 cm.s^{-1}. Hence, the influence of filtration velocity on filter pressure drop is depending on the different stage of deposited particles, with remarkable influence at transition area of filtration regime.

Moreover, to investigate whether the gap between the pressure drop curves (1.9 cm.s^{-1} versus 1.4 cm.s^{-1}) is due to the variation of the filtration velocity or due to the quantity of the collected particles, the ratio of pressure drop and the filtration velocity times viscosity are plotted in the **Figure 87** as a function of collected particle number. The results show that for the same level of filter resistance the number of collected particles is higher at filtration velocity of 1.4 cm.s^{-1} than 1.9 cm.s^{-1}.

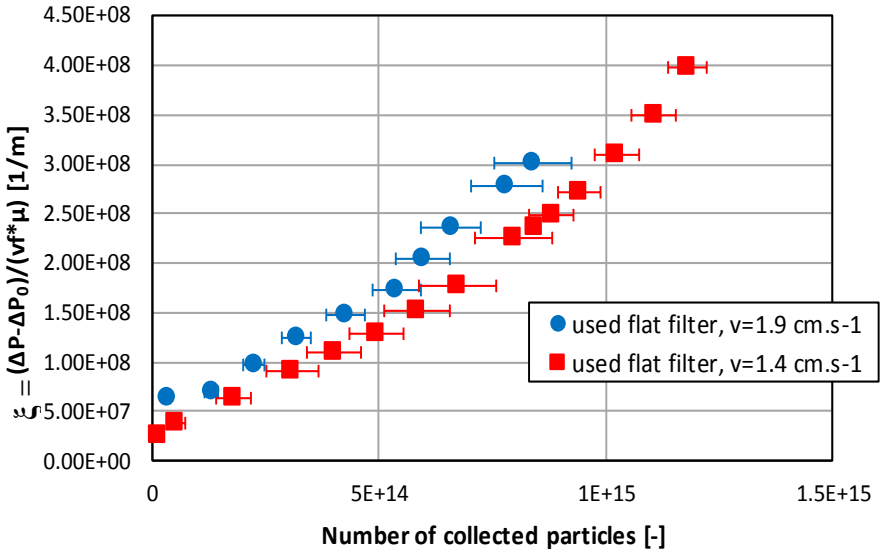

Figure 87: Pressure drop as a function of collected particles for used flat filter at 1.4 and 1.9 cm.s^{-1}

VII Mathematical and numerical modeling of nanoparticles transport

VII.1 Introduction

In the following section, an overview study based on numerical simulation on nanoparticle transport in gas stream is presented. The simulation of nanoparticles movement was carried out on a filter fiber within a control cell which is considered as the basic unit and delimited area of the studied particles. The purpose of this work is to assess the effect of temperature, particle size and fluid velocity on nanoparticle transport around a single spherical collector which is considered as a filter media for nanoparticle filtration. The stochastic Langevin equation was used to describe the dynamic behavior of particles, taking into account the drag, gravitational and Brownian forces which acting simultaneously on these particles.

VII.2 Simulation method

The trajectory of particles moving in a gas was described by Lagrangian integration of the Langevin equation (Paul Langevin, 1908). This one dimension classical model, for the sake of simplicity, takes into account all the deterministic and probabilistic forces which are acting simultaneously on a particle and influencing the its path. These forces include the drag, gravitational and Brownian forces. In contrast, the effect of particle interaction is neglected assuming a dilute concentration, spherical particles. Similar approach is used to determine the path of particles as proposed by Gupta et al. (1984).

The trajectory of nanoparticles under the action of random and determinist forces are determined by the equation (1):

$$\begin{cases} \frac{dX_p(t)}{dt} = v_p(t) \\ \frac{d\vec{v_p}}{dt} = \frac{\vec{F}_d}{m_p} + \frac{\vec{F}_g}{m_p} + \frac{\vec{F}_b}{m_p} \end{cases} \quad (76)$$

Where F_d is the drag force. It refers to the forces acting opposite to the relative motion of particles moving with respect to the surrounding fluid. It is the fluid resistance which is proportional to the difference of fluid velocity u and particles velocity v, F_d can be expressed using the following equation (77):

$$\vec{F}_d = m_p \beta(\vec{u} - \vec{v}) \quad (77)$$

Where β is the friction coefficient related to the particle mass m_p. β is determined from the Stokes' law and is given by equation (78):

$$\beta = \frac{6\pi\mu r_p}{C_u m_p} \tag{78}$$

Where μ is the dynamic viscosity of the gas, Cu is the Cunningham coefficient.

F_g is the Gravitational force responsible for particle sedimentation. It is given by the equation (79) (Xuan et al., 2004):

$$\vec{F}_g = -\frac{\pi}{6} d_p^3 (\rho_p - \rho)\vec{g} \tag{79}$$

Where ρ_p and ρ_f are the particle and gas density, respectively, and g is the gravitational acceleration.

The Brownian force $\vec{F_b}$ resulting from the random motion, is the product of the particle mass and a random acceleration A(t). The random acceleration depends only on time and is usually represented as a Gaussian White noise process in stochastic terms. The effect of Brownian force increases with decreasing of particle size and it is assumed to be random in direction. This force can be expressed using equation (80):

$$\overrightarrow{F_b} = m_p \vec{A}(t) \tag{80}$$

Substituting equations (77), (79) and (80) into equation (76), the trajectory of nanoparticles can be defined using the following equation (81):

$$\begin{cases} \frac{dx_p(t)}{dt} = v_p(t) \\ \frac{dv}{dt} = \beta\big(u - v(t)\big) - g\left(1 - \frac{\rho_g}{\rho_p}\right) + A(t)\overrightarrow{F_b} = m_p\vec{A}(t) \end{cases} \tag{81}$$

This system of equations can be solved analytically into equations (82) and (83) (Lantermann et al., 2007):

(82)

$$\overrightarrow{F_b} = m_p \vec{A}(t)$$

(83)

Where F_d is the external force, including gravitational force, and $\Delta t = t - t_0$ is the time step.

In order to calculate the integration of the system, the time step has to be sufficiently small which enables to consider the fluid velocity and the influence of external force remains constant during the time step. Consequently, Δt should be in the order of relaxation time of particle $\tau = \beta^{-1}$:

$$\overrightarrow{F_b} = m_p \vec{A}(t) \quad (84)$$

Where τ_b is the time step between successive collisions of the fluid molecules surrounding a given particle. τ_F is the time step which could lead to appreciable change in the particle displacement due to particle-particle interaction forces which are considered negligible in this study. The time step shall not be too small, otherwise it takes very long time to run the simulation. The time step used in this study, as calculated from numerical experiments, is estimated to be 1.10^{-7} s; from the other side, time step shall not be larger than relaxation time to avoid the effect of inertia due to the particle's mass.

As the random acceleration A(t) represents a stochastic process, the bivariate distribution function is used to calculate the integration as described by (Chandrasekhar (1943) and developed by Ramarao et al., (1993) and Ermak (1994).

VII.3 **Initial condition of particles position**

In Cartesian coordinate, the movement of particles is studied within a control cell which is considered as a basic unit consisting of a single fiber, which is surrounded by a fluid envelope of radius e which is given by (85):

$$\overrightarrow{F_b} = m_p \vec{A}(t) \quad (85)$$

Where d_f is the fiber diameter, and ε is the porosity of the media.

The flow fluid which is the carrier phase is two-dimensional. Furthermore, the initial position of the entering particles is located at x=-e and the abscise is placed from y=0 to y=e. In the general case, y can be expressed according to the following equation (86):

$$y = z.e \quad (86)$$

where z is distributed random numbers*:* $0 \leq z \leq 1$

On the other hand, the initial particle velocity is determined analytically as a normal distribution using the methods described by Zarutskaya and Shapiro (2000) as shown in equation (87):

$$v_0 = u(r_0) + v_0' \tag{87}$$

Where v_0' is the Guassian random variable with the following properties:

$$< v_0' >= 0, \quad < v_0'.v_0' >= \frac{2KT}{m_p} \tag{88}$$

Where k is the Boltzmann constant.

VII.4 Results and discussion

In the **Figure 88,** the trajectory of a particle of 30 nm in diameter was studied in two different temperatures: (150°C) and (24°C) at 2.5 cm.s^{-1} of filtration velocity.

Applying the simulation of displacement equation at the same initial position, it was found that the effect of temperature on the particle motion at 150°C to be more significant than at 24°C. There is also an important fluctuation in particle trajectory at 150°C which can be explained in terms of air viscosity. The gas at higher temperature has lower viscosity as compared to cold gas, which means the air will experience less drag forces thus less gas resistance.

Vertically, the movement of particles changes in the range of 10 µm, while the fiber diameter is 20 µm. Hence, the probability that the particle contacts the fiber surface is higher at 150°C than at 24°C. This result is in agreement with the findings of Peukert and Loffler (1991) which demonstrated experimentally that the collection of nanoparticles by filter become more effective with increasing temperature.

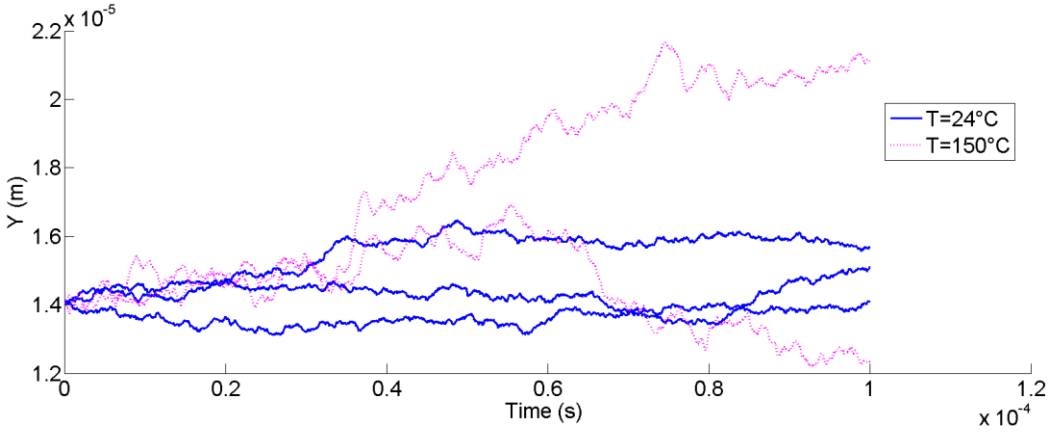

Figure 88: Particles trajectory of 30 nm size at V=2 cm.s^{-1}

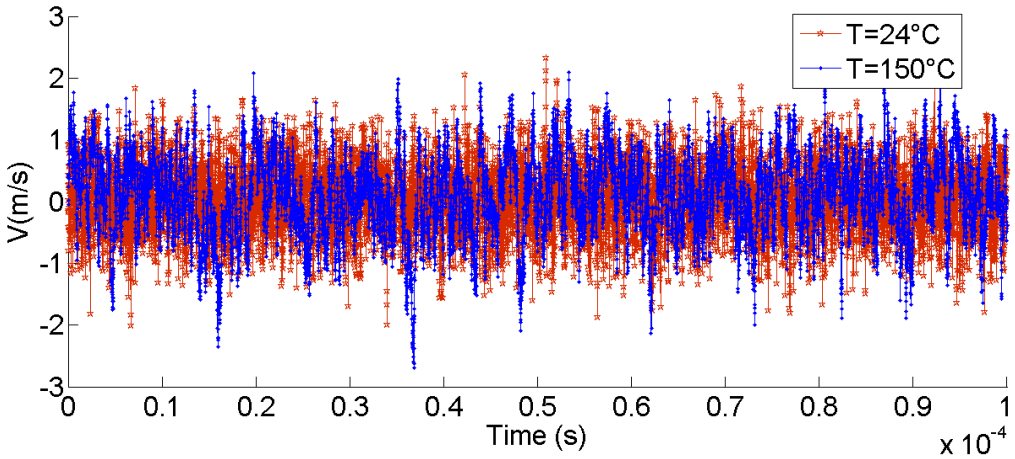

Figure 89: Particle velocity of 30 nm size at T=150°C and T=24°C

The particle collision velocity on the fiber surface, which could lead to a potential particle rebound, can be observed from the **Figure 89.** The results showed that there is no significant difference in velocity between the two operating conditions; in other words, the collision velocity of particle on the fiber surface is the same at temperature of 150°C and 24°C. According to the simulation results of Scheibel and Porstendörfer (1984) there is no thermal rebound for nanoparticles of size 3.5-130 nm. Hence the capture probability of a particle by the fiber surface is the same at both 150°C and 24°C.

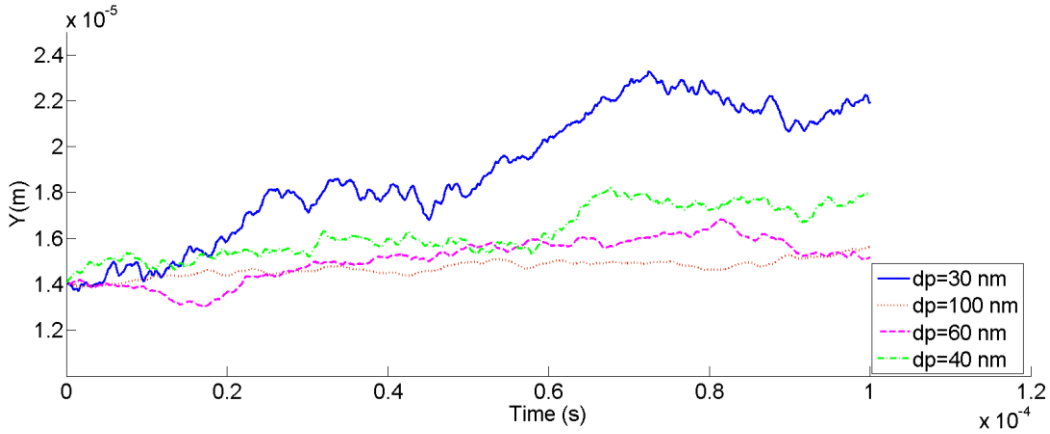

Figure 90: Particle trajectory of dp=30 nm, dp= 40 nm, dp=60 nm and dp=100 nm at T=150°C - V_f=2.5 cm.s^{-1}

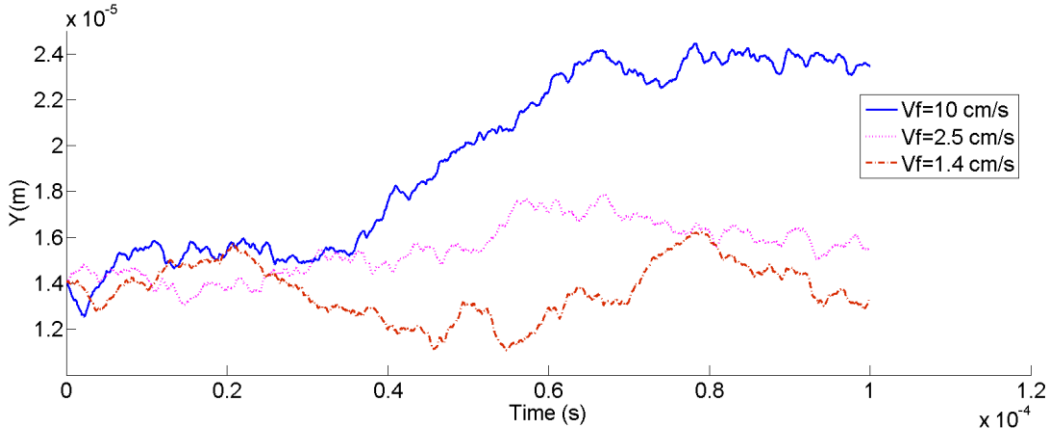

Figure 91: Particle trajectory of dp=30 nm, at T= 150°C

Furthermore, the study of particles size effect on the particle trajectory is important. The motion of particles was calculated for four different particle diameters at the same temperature and fluid velocity; **Figure 90** indicates clearly that the fluctuations of particle trajectory increase with decreasing of particle diameter.

Figure 91 illustrates the effect of fluid velocities, at T=150°C on the vertical displacement of particle with 30 nm diameter. The results show that the influence of fluid velocity variation is negligible for V_f=1.4 cm.s^{-1} and V_f=2.5 cm.s^{-1}. In contrast, the effect of fluid velocity becomes significant from 10 cm.s^{-1}.

VIII **Conclusion of the chapter**

The experimental results showed that the humidity has an important influence on bag filter performance at 150°C. At the same number of collected particles the collection efficiency increases with humidity for particles higher than 111 nm in diameter, while no effect was observed for nanoparticles (<100nm). In terms of pressure drop evolution, the humidity is a key factor that causes fast rising of bag filter air flow resistance due to the formation of compact dust cake during the clogging, the fact that makes the cleaning efficiency of bag filter with pulse-jet system less efficient in presence of humidity (3% RH) than filtration with dry gases. Briefly speaking, the humidity increases the efficiency of bag filter collection but accelerates the rise of pressure drop due to capillary condensation and reduces the cleaning efficiency which increases the residual cake filter on the filter media which is the major element that reduces the bag filter life time.

The influence of temperature on bag filter performance was also experimentally studied. In terms of filtration efficiency, the particle collection was higher at 150°C than 24°C. As a

function of time, the evolution of efficiency was faster at high temperature and reached a maximum efficiency of 99.99 % at 150°C and 99.8% at 24°C. Regardless of the variation of gas viscosity as a function of temperature, the results showed that no influence of temperature was observed on the structure of the formed cake filter.

Although the efficiency increases faster for bag filter clogged only with NPs, the dislodgement is found to be less efficient causing the residual pressure drop to increase quickly. Hence, the particle size, within the conditions of this study, is found to be a key factor that affects the unclogging efficiency of dust cake. With additional large particles (reagents), the experimental results showed that the dislodgement of cake filter is more efficient.

Theoretically, the influence of temperature and humidity on filtration efficiency was investigated at 150°C and 24°C for 1.9 $cm.s^{-1}$ of filtration velocity. The results showed that the particles less than 90 nm in diameter are most influenced by temperature with higher collection efficiency at 150°C as compared to efficiency at 24°C. This is consistent to the experimental results obtained.

Theoretically, there is no influence of the humidity on filtration efficiency at 150°C (3% RH versus 0%). However, the experimental results showed that at higher humidity, the increase in collection efficiency is significant. This may confirm the hypothesis on the combined influence of humidity on aggregates and structure of built cake filter on collection efficiency.

The filtration efficiency and pressure drop of flat filters were evaluated for black carbon particle size range of 16-315 nm. The main conclusions obtained experimentally are: (1) Nanoparticle filtration efficiency increases with clogging time; (2) Filtration efficiency decreases with increase of filtration velocity, especially for particles diameters ranging between 50-140 nm; (3) New filters are significantly less efficient than used filters in the initial values of $\Delta P/\Delta P_0$; and (4) The Most Penetrating Particle Size (MPPS) decreases with increasing of filtration across the bag and flat filter.

The results of numerical simulation show the notable effect of gas operating parameters on the particle trajectory, especially particle size and fluid temperature. Indeed, the vertical fluctuation of particles around the filter fiber at 150°C was more significant than the fluctuations at 24°C. This result indicates that the probability of nanoparticle collection by the fiber increases with an increase in temperature. On the other hand, the study showed that the particle trajectory is highly affected by particle size. In fact, the motion of small particles is significant than larger one. In contrast, the effect of velocity on the nanoparticle motion was

negligible for lower and narrow ranges of velocity (2.5 and 1.4 $cm.s^{-1}$). However, the effect is significant for 10 $cm.s^{-1}$ velocity of particle.

The present numerical simulation is a preliminary work aiming at theoretically calculations of efficiency for the filter in the same operating conditions as the experimental study. However, additional work is needed to study the mechanisms of particle capture and to calculate the filter efficiency, especially modeling of the filter structure and the fluid behavior through the filter media.

General conclusions

The results presented in this manuscript provide knowledge on assessing submicronic and nanosized particle filtration by fibrous filters. The main objectives of this study were:

- Experimental characterization of the performance of a single baghouse filter regarding the filtration of submicronic and nanosized particles. The operating conditions of filtration were fixed as close as possible to those found in waste incineration plants in terms of gas filtration velocity, concentration of particle reagents, gas temperature and humidity, pressure and duration of the pulse-jet cleaning.
- Experimental investigations of the influence of operating parameters on bag filter and flat filter filtration performance, such as humidity (3% RH versus 0% RH), temperature (150°C versus 24°C), filtration velocity (1.9 $cm.s^{-1}$ versus 1.4 $cm.s^{-1}$), filter aging, and characteristics of the particles used for clogging (reagents versus nanoparticles).
- Theoretical investigation of the influence of particle size, gas temperature, and flow velocity on particle behavior around a fiber of fibrous filter.

A literature review was first carried out and presented in the **first chapter** of this manuscript. Particular attention was paid to literature studies regarding the effect of operating parameters on: (1) filtration mechanisms, mainly Brownian diffusion, interception and impaction as a function of particle size, (2) formation/regeneration of particle cake on the surface of fibrous filter media. These informations were used to explain the obtained experimental and theoretical results.

Materials and methods used in this work were described in the **second chapter** of this manuscript. Two filters with different geometries (bag filter and flat filter) made from the same filtering media (polytetrafluoroethylene PTFE) were tested in two different experimental setups. The bag filter experimental setup was developed in order to be representative to the bag filter unit in waste incineration flue gas treatment in terms of temperature, humidity, filtration velocity and aerosol load. This setup was dedicated to clogging/unclogging cycle tests at temperature and humidity conditions of incineration plants (150°C - 3% RH) and at room temperature and humidity conditions (24°C - 45% RH). Flat filter setup was dedicated to single filtration tests (without filter on-line unclogging) at room temperature and humidity (24°C - 45% RH) for different filtration velocities (1.4 to 1.9 $cm.s^{-1}$).

The **third chapter** of this manuscript presents the performance of the bag filter for the collection of submicronic particles for 11 clogging/unclogging cycles. The operating conditions of filtration were fixed as close as possible to those found in waste incineration plants in terms of gas filtration velocity (1.9 $cm.s^{-1}$), presence of reagents (sodium bicarbonate and activated carbon), particle concentration (5.10^6 $particles.cm^{-3}$), gas temperature (150°C) and humidity (3% RH), pressure (6-7 bar) and duration of the cleaning pulse-jet (0.3 s). The performance of the tested filter was presented as a function of the evolutions of filter pressure drop and particle collection efficiency. The maximum filter pressure drop was set at 150 Pa for all filtration cycles; once the maximum pressure drop was reached, the filter was regenerated using the pulse-jet system for 0.3 s.

The experimental study showed the high collection efficiency of the bag filter for submicronic and nanosized particles. The overall efficiency increases rapidly with clogging from a minimum value of 98.5% to a maximum of 99.98%. The most penetrating particle size was 74 ± 15 nm (electrical mobility diameter) for which the efficiency reaches a minimum value of 98.5% at first filtration cycle. After 11 filtration cycles, the clogging duration decreases from 630 min to around 70 min for the last one. Indeed, the incomplete dislodgement of particle cake from the surface of the media leads to increase the residual pressure drop of the bag filter. Moreover, the investigation showed a decrease with the filtration cycles of the particle collection efficiency at the maximum filter pressure drop, especially for the nanoparticles. We assume that the residual cake at the beginning of filtration cycles lead to the formation of preferential pathways in the particulate cake formed at the surface of the media with local increase of the interstitial filtration velocity responsible for the decrease of nanoparticle collection efficiency by Brownian diffusion.

The **fourth chapter** of this study evaluates the influence of operating conditions on bag filter and flat filter performance. One of the main significant results is the influence of gas humidity. The performance of the bag filter was studied for two filtration conditions (150°C - 3% RH) and (150°C - 0% RH). The experimental results showed a significant influence of humidity on the structure of the formed particle cake at 150°C. In presence of humidity (around 100 g of water per kg of dry air), the adhesion forces between the particles are increased and the particle cake structure becomes more compact due to capillary condensation between the particles. By consequence, the increase of filter pressure drop clogged in presence of humidity is higher than in dry conditions (150°C - 0% RH). However, the results

revealed no significant influence of humidity on particle collection efficiency, especially for nanoparticles (d_p <100 nm), for a given number of collected particles.

Theoretically, the influence of temperature and humidity on filtration efficiency was investigated by particle collection mechanism models. At temperature of 150°C, the results showed no influence of humidity on collection efficiency for 3% and 0% RH, in accordance with the experimental results. In contrast, the collection efficiency at temperature of 150°C was higher than the collection efficiency at 24°C. The influence of temperature was significant especially for particles lower than 200 nm of stokes diameter, corresponding to collection by Brownian diffusion.

Experimental investigations were complete by numerical simulations of particle behavior around fiber of fibrous filter. The results showed a significant effect of particle size and fluid temperature on the particle trajectory. Indeed, the vertical fluctuation of particles around the filter fiber at 150°C was higher than the one at 24°C. This result indicates that the probability of nanoparticle collection by the fibers increases with increasing of temperature. On the other hand, the study showed the effect of particle size on the particle trajectory. In fact, the motion of small particles is higher than the one of the large particles. In contrast, the effect of velocity on the nanoparticle behavior was not significant for small particles and close values of velocity (2.5 and 1.4 $cm.s^{-1}$). However, the effect of velocity became significant from particle velocity of 10 $cm.s^{-1}$.

In general, the study permitted to quantify the bag filter efficiency for submicronic and nanosized particle filtration in realistic conditions of waste incineration fumes treatment. The results demonstrated in particular the significant influence of gas humidity on the filtration performance: the decrease of gas humidity could lead to a lower filter pressure drop by decreasing the adhesion force between particles with (i) better pulse-jet bag cleaning and (ii) formation of an open cake structure. Regarding the present numerical simulation, it was a preliminary work in order to study the trajectory of particles around fibers of filtering media in operating conditions similar as the experimental study. Additional work is needed to study the mechanisms of particle capture and to calculate the filter efficiency, especially the filter structure modeling and the fluid behavior through the filter media.

References

Agranovski, I., Lushnikov, A.A. (2010). Aerosols Science and Technology, Griffith School of Engineering. DOI: 10.1002/9783527630134.

Ahmaruzzaman, M. (2010). A Review on the Utilization of Fly Ash. Progress in Energy and Combustion Science, 36(3), 327-363.

Allen, M. D., & Raabe, O. (1982). Re-evaluation of millikan's oil drop data for the motio of small particles in air. J. Aerosol Sci. 13(6), 537-547.

Arouca, F.O., Feitosa, N.R., & Coury, J.R. (2010). Effect of Sampling in the Evaluation of Particle Size Distribution in Nanoaerosols. Powder Technology, 200,(12), 52-59.

Bao, L., Musadiq, M., Kijima, T., & Kenmochi, K. (2014). Influence of Fibers on the Dust Dislodgement Efficiency of Bag Filters. Textile Research Journal, 84(7), 764-771.

Baron, P.A, & Willeke, K. (2001). Aerosol Measurement - Principles, Techniques, and Applications.

Bémer, D., Régnier, R., Callé, S., Thomas, D., Simon, X., & Appert-Collin, J.C. (2006). Filtration des aérosols - performances des médias filtrants. Cahiers de notes documentaires ND 2241-202-06. INRS - Hygiène et sécurité du travail.

Billings, Edgar, C. (1966). Thesis of California Institute of Technology.

Bockhorn, H., D'Anna, A., Sarofim, AF., & Wang., H. (2009). Combustion Generated Fine Carbonaceous Particles, Scientific Publishing.

Boskovic, L., Igor, S., Altman, I.E., Agranovski, A., Roger, D., Toshihiko M., & Mansoo, C. (2005). Influence of Particle Shape on Filtration Processes. Aerosol Science and Technology, 39(12), 1184-1190.

Bouillard, J X., Badr, R., Moranviller, D., Vignes, A., Le Bihan, O., Ustache, A., Bomfim, J.A.S, Frejafon, E., & Fleury, D. (2013). Nanosafety by Design: Risks from Nanocomposite/Nanowaste Combustion. Journal of Nanoparticle Research, 15(4).

BREF. (2006). Incinération des déchets, Document de référence sur les meilleures techniques disponibles, Commission Européenne.

Brown, R. C. (1993). Air Filtration: An Integrated Approach to the Theory and Applications of Fibrous Filters. Oxford, UK: Pergamon Press.

Butt, H-J., & Kappl, M. (2009). Normal Capillary Forces. Advances in Colloid and Interface Science, 146(1-2), 48-60.

Chandrasekhar, S. (1943). Stochastic Problems in Physics and Astronomy. 15(1).

Chang, M. B., C. K. Huang, H. T., Wu, J. J., & Chang, S. H. (2000). Characteristics of heavy metals on particles with different sizes from municipal solid waste incineration. Journal of hazardous materials, 79 (3), 229–239.

Charitidis, Costas A., Pantelitsa Georgiou, Malamatenia A. Koklioti, Aikaterini-Flora Trompeta, et Vasileios Markakis. 2014. Manufacturing nanomaterials: from research to industry. Manufacturing Review 1: 11. doi:10.1051/mfreview/2014009.

Cheng, Y-H., & Tsai, C.J. (1998). Factors Influencing Pressure Drop through a Dust Cake during Filtration. Aerosol Science and Technology, 29(4),315-328.

Cirqueira, A. Rodrigues, S.S., Tanabe, E.H., & Aguiar, M.L. (2017). Evaluation of Operating Conditions during the Pulse Jet Cleaning Filtration Using Different Surface Treated Fibrous Filters. Process Safety and Environmental Protection, 105 (4), 69-78.

D'Ann, A., Violi, A. & D'Alessio, A. (2001). A Reaction Pathway for Nanoparticle Formation in Rich Premixed Flames. Combustion and Flame, Elsevier Science.

Davies, C. N. (1973). Air Filtration; Academic Press, 171.

Dennis, R., & Dirgo, J.A., (1981). Comparison of Laboratory and Field Derived K2 Values for Dust Collected on Fabric Filters. Filtration and Separation, 18(4), 394-417.

Dennis, R, Klemm, H. A., & Battye. W. (1979). Fabric Filter Model Sensitivity Analysis. GCAJ Technology Division,1, 40-5.

Dittler, A., Gutmann, B., Lichtenberger, R., Weber, H., & Kasper, G. (1998). Optical in situ measurement of dust cake thickness distributions on rigid filter media for gas cleaning. Powder Technology, 99(2), 177–184.

Endo, Y, Chen, D., & YH Pui, D. (1998). Effects of particle polydispersity and shape factor during dust cake loading on air filters. Powder Technology 98 (3): 241–249.

Eremin, Alexander V. 2012. Formation of Carbon Nanoparticles from the Gas Phase in Shock Wave Pyrolysis Processes. Progress in Energy and Combustion Science 38 (1): 1-40. doi:10.1016/j.pecs.2011.09.002.

Ermak, D.L., & Buckholz H. (1980). Numerical integration of the Langevin equation: Monte Carlo simulation. Journal of Computational Physics, 35(2), 169–182.

Ermak, D.L., & Buckholz H. (1994). Numerical Integration of the Langevin Equation: Monte Carlo Simulation , 169-l 82.

European Commission. (2006). Integrated Pollution Prevention and Control, Reference Document on the Best Available Techniques for Waste Incineration. Brussels, Belgium: European Commission.

Feng, C. L., & Yu. A. D. (1998). Effect of liquid addition on the packing of mono-sized coarse spheres. Powder technology, 99(1), 22–28.

Fornes, T.D., & Paul, D.R. (2003). Modeling Properties of Nylon 6/Clay Nanocomposites Using Composite Theories. Polymer, 44(17), 4993-5013.

Förster, H., Thajudeen, T., Funk, C., & Peukert, W. (2016). Separation of Nanoparticles: Filtration and Scavenging from Waste Incineration Plants. Waste Management, 52(6), 346-352. doi:10.1016/j.wasman.2016.03.050.

Frenklach, M., & Wang, H. (1994). Detailed mechanism and modeling of soot particle formation. In Soot formation in combustion, 165–192.

Glassman, I. (1989). Soot formation in combustion processes. Symposium (international) on Combustion, 22(4), 295–311.

Guiraud, P. (2004). Modélisation des systèmes diphasiques dispersés. Cours Master Recherche INPT-INSA Toulouse.

Gupta, A., Vincent, J., Biswas, N.P, & Monson, P.R. (1993). Effect of humidity and particle hygroscopicity on the mass loading capacity of high efficiency particulate air (hepa) filters. Aerosol Science and Technology, 19(1), 94-107.

Gupta, D., and Peters, M.H. (1984). A Brownian Dynamics Simulation of Aerosol Deposition onto Spherical Collectors. Journal of Colloid and Interface Science, 104(2), 375-389.

Haynes, R.S, & Wagner, H.Gg (1982). The surface growth phenomenon in soot formation.

Helsper, C., Mölter, W., Löffler, F., Wadenpohl, C., Kaufmann, S., & Wenninger, G. (1993). Investigations of a new aerosol generator for the production of carbon aggregate particles, Atmospheric Environment. Part A. General Topics, 27(8), 1271–1275.

Hesketh, H.E. (1979). Fabric filtration. Air and Noise Pollution Control, 41–60.

Hinds, W. C. (1982). Properties, behaviour and measurement of airbone particles. John Wiley, 141-49.

Hinds, W.C. (1999). Aerosol Technology: Properties, Behavior and Measurement of Airborne Particles.

Hinozaki, T., Matsumoto, M., Nozaki, K., Nakamura, K., Nanbu, K., & Maruta, T., (1998). Characterization of incineration ashes. J. Soc. Inorg. Mate., 5,149–58.

Holder, A., Eric, L., Vejerano, P., Zhou,X., & Marr, L.C. (2013). Nanomaterial Disposal by Incineration. Environ. Sci.: Processes Impacts, 15 (9),1652-1664.

Horvath, H., & Gangl, M. (2003). A Low-Voltage Spark Generator for Production of Carbon Particles. Journal of Aerosol Science, 34 (11),1581-1588.

Hung, C.H., & Leungw W.W.F. (2011). Filtration of nano-aerosol using nanofiber filter under low peclet number and transitional flow regime. Separation and Purification Technology, 79(1), 34-42.

Ivell, D.M. (2012). The use of bag filters in a dap plant. procedia engineering; 46, 83-88.

James, P., & Lodge, J., (1988). Methods of air sampling and analysis. CRC Press.

Japuntich, D. A., Stenhouse, J. I. T., & Liu, B. Y. H. (1994). Experimental results of solid monodisperse particle clogging of fibrous filters. Journal of aerosol science, 25(2), 385–393.

Jornitz, M.J, Jornitz, M.W., & Meltzer, T.H., (2003). Filtration and Purification in the Biopharmaceutical Industry, Second Edition.

Joubert, A., Laborde, J. C., Bouilloux, L., Callé-Chazelet, S., & Thomas, D. (2010). Influence of humidity on clogging of flat and pleated HEPA filters. Aerosol Science and Technology, 44(12), 1065‑76.

Joubert, A. (2009). Performances des filtres plissés à Très Haute Efficacité en fonction de l'humidité relative de l'air. Thèse de doctorat de l'INPL.

Kanaoka, C, Emi,H., Hiragi, S., & Myojo, T. (1986). Morphology of particulate agglomerates on a cylindrical fiber and collection efficiency of a dust loaded fiber. Aerosols formation and reactivity (Proceedings 2nd International Aerosol Conference, Berlin). 674–677.

Kasper, G., Preining, O., & Matteson, M. J. (1978). Penetration of a multistage diffusion battery at various temperatures. Journal of Aerosol Science, 9 (4), 331–338.

Kennedy, I. M. (1997). Models of soot formation and oxidation.

Kim, C., Bao, L., Okuyama, K., Shimada, M., & Niinuma, H. (2006). Filtration efficiency of a fibrous filter for nanoparticles. Journal of Nanoparticle Research, 8 (2),215‑21.

Kim, J.H., Liang, Y., Sakong, K.M., Choi, J.H, & Bak, Y.C. (2008). Temperature Effect on the Pressure Drop across the Cake of Coal Gasification Ash Formed on a Ceramic Filter. Powder Technology, 181(1), 67‑73.

Langevin, P. (1997). On the Theory of Brownian Motion" Am. J. Phys, 65, 1079.

Lantermann, U., é Hänel, D., (2007). Particle Monte Carlo and Lattice-Boltzmann Methods for Simulations of Gas–particle Flows. Computers & Fluids 36(2), 407‑22.

Lapuerta, M., Armas, O., & Gómez, A. (2003). Diesel Particle Size Distribution Estimation from Digital Image Analysis. Aerosol Science and Technology, 37(4), 369‑81.

Le Coq, L. (2006). Elimination des particules. Ed. Techniques Ingénieur.

Le Bihan, O., Durécu, S., Venditti, D., Meunier, T., Joubert, A., Le Coq, L (2014). Caractérisation et réduction des émissions particulaires issues des déchets contenant des matériaux manufacturés. Rapport Ademe Cortea NANOFlueGas, 22 juillet 2014.

Lee, J. (2014). Black carbon and elemental carbon concentrations of spark-generated carbon particles. ETH Zurich, Switzerland.

Lee, K. W., & Liu, B. Y. H. (1980). On the Minimum Efficiency and the Most Penetrating Particle Size for Fibrous Filters. Journal of the Air Pollution Control Association, 30(4), 377‑81.

Lee, K. W., & Liu, B. Y. H. (1982). Theoretical Study of Aerosol Filtration by Fibrous Filters. Aerosol Science and Technology, 1 (2), 147‑61.

Lee, K.S, Sohn, J.R., & Park, Y.O. (2015). Filtration Performance Characteristics of Ceramic Candle Filter Based on Inlet Structure of High-Temperature and High-Pressure Dust Collectors. Journal of Industrial and Engineering Chemistry, 21 (4), 101‑10.

Lee, K.W, Mukund. R. (2001). Filtration Collection. Aerosol Measurement - Principles, Techniques, and Application, 2nd John Wiley and Sons.

Le Gléau, F., (2012). Étude d'un dispositif de traitement de fumées issues de l'incinération de déchets industriels spéciaux. Thèse de L'École des Mines de Douai et l'université Lille Leparoux, M., & Stephan S. (2003). Development of a filtration unit with a by-pass sampling system for nanoparticle collection. Filtech Europa, 21–23.

Leung, W.W.F, & Hung, C.H., (2008). Investigation on Pressure Drop Evolution of Fibrous Filter Operating in Aerodynamic Slip Regime under Continuous Loading of Sub-Micron Aerosols. Separation and Purification Technology, 63(3), 691‑700.

Lewin, M., Pearce, E. M., Levon, K., Mey-Marom, A., Zammarano, M., Wilkie, C., A., & Jang, B.N. (2006). Nanocomposites at Elevated Temperatures: Migration and Structural Changes. Polymers for Advanced Technologies, 17(4), 226‑34.

Limpert, E., Stahel, W.A & Abbt. M., (2001). Log-normal distributions across the sciences: Keys and clues on the charms of statistics, and how mechanical models resembling gambling machines offer a link to a handy way to characterize log-normal distributions, which can provide deeper insight into variability and probabilitynormal or log-normal: That is the question. BioScience, 51 (5), 341–352.

Liu, B.Y.H., & Rubow. K.L. (1990). Efficiency, pressure drop and figure of merit of high efficiency fibrous and membrane filter, Proc. 5th World Filtration Congress;Nice, France édition.

Lu, S., Y. Ji, Buekens, A., Ma, Z., Jin, Y., Li, X. , & Yan, J. (2013). Activated Carbon Treatment of Municipal Solid Waste Incineration Flue Gas. Waste Management & Research 31(2), 169‑77.

Maricq, M.M., & Xu,N. (2004). The Effective Density and Fractal Dimension of Soot Particles from Premixed Flames and Motor Vehicle Exhaust. Journal of Aerosol Science, 35(10), 1251‑74.

Marney, D.C.O., Russell, L.J., Wu, D.Y., Nguyen, T., Cramm, D., Rigopoulos, N., Wright, N., & Greaves, M. (2008). The Suitability of Halloysite Nanotubes as a Fire Retardant for Nylon 6. Polymer Degradation and Stability, 93(10), 1971‑78.

Matteson, A., & Orr. (1986). Filtration: Principles and Practices. CRC Press.

Melling, A., Noppenberger, S., & Still, M., (1997). Interpolation Correlations for Fluid Properties of Humid Air in the Temperature Range 100°C to 200°C. J. Phys. Chem.,26 (4)112-118.

Miecret, G., & Gustavson. J. (1989). Mathematic Expression of HEPA and ULPA Filters Efficiency, Experimental Verification, Practical Alliance to New Efficiency Test Methods.

Miguel, A.F. (2003). Effect of Air Humidity on the Evolution of Permeability and Performance of a Fibrous Filter during Loading with Hygroscopic and Non-Hygroscopic Particles. Journal of Aerosol Science, 34(6), 783‑99.

Millikan, R. A., (1923). Relative motion between the particle and flow,. Phys. Rev., 22, 1-40.

Mukhopadhyay, A. (2010). Pulse-jet filtration: An effective way to control industrial pollution Part II: Process characterization and evaluation of filter media. Textile Progress 42,1‑97.

Mukhopadhyay, A., Pandit, V., & Dhawan, K. (2016). Effect of High Temperature on the Performance of Filter Fabric, Journal of Industrial Textiles, 45(6), 1587‑1602.

Niessen, W. R. (2010). Combustion and Incineration Processes: Applications in Environmental Engineering, Fourth Edition. CRC Press.

Novick, V. J., Monson, P. R., & Ellison, P. E. (1992). The effect of solid particle mass loading on the pressure drop of HEPA filters. Journal of aerosol science, 23 (6), 657–665.

Oh, Yong-Wha, Ki-Joon Jeon, An-Ick Jung, et Yong-Won Jung. A Simulation Study on the Collection of Submicron Particles in a Unipolar Charged Fiber. Aerosol Science and Technology 36, no 5 pp.573-82, (2002).

Ounoughene, G., Le Bihan, O., Chivas-Joly,C., Motzkus, C., Longuet, C., Debray, B., Joubert, A., Le Coq, L., & Lopez-Cuesta, J.M. (2015). Behavior and Fate of Halloysite Nanotubes (HNTs) When Incinerating PA6/HNTs Nanocomposite. Environmental Science & Technology, 49(9), 5450‑57.

Panneerselvam, S., & Choi, S. (2014). Nanoinformatics: Emerging Databases and Available Tools. International Journal of Molecular Sciences 15(5), 7158‑82.

Park, B.H. (2012). Filtration Characteristics of Fine Particulate Matters in a PTFE/Glass Composite Bag Filter. Aerosol and Air Quality Research, doi:10.4209/aaqr.2012.03.0071.

Payatakes, A. C., & Gradoń, L., (1980). Dendritic deposition of aerosols by convective Brownian diffusion for small, intermediate and high particle Knudsen numbers. AIChE Journal, 26 (3), 443–454.

Payatakes, A.C., & Tien, C., (1976). Particle deposition in fibrous media with dendrite-like pattern: a preliminary model. Journal of Aerosol Science, 7(2), 85IN195–94100.

Petean, P.G.C., & Aguiar, M.L, (2015). Determining the Adhesion Force between Particles and Rough Surfaces. Powder Technology, 274 (4), 67‑76.

Peukert, W., & Loffler, F. (1991). Influence of temperature on particle separation in granular bed filters. Powder Technology, 68, 263-70.

Rader, D.J. (1990). Momentum slip correction factor for small particles in nine common gases. J. Aerosol Sci, 21(2), 161‑68.

Ramarao, B.V., TIEN, C., & Mohan, S. Calculation of single fiber efficiencies for interception and impaction with superposed brownian motion. Pergamon J. Aerosol Sci., (1994).

Renoux, A, & Boulaud, D. (1998). Les aérosols : physique et métrologie. Lavoisier Technique et documentation.

Report of Design and Operating Criteria. (1992). National Guidelines fro Hazardous Waste Incineation Facilities.

Richter, H., & Howard, J.B., (2000). Formation of polycyclic aromatic hydrocarbons and their growth to soot a review of chemical reaction pathways. Progress in Energy and Combustion science, 26(4), 565–608.

Ristimäki, J., Virtanen, A., Marjamäki, M., Rostedt, A., & Keskinen, J., (2002). On-line measurement of size distribution and effective density of submicron aerosol particles. Journal of Aerosol Science 33(11), 1541–1557.

Roco, M.C., Mirkin, C.A., & Hersam, M.C. (2011). Nanotechnology Research Directions for Societal Needs in 2020: Summary of International Study. Journal of Nanoparticle Researc, 13(3), 897‑919.

Roy, W. R., Richard, G., Thiery, Rudolph M. Schuller, & Subway, J.J (1981). Coal fly ash: a review of the literature and proposed classification system with emphasis on environmental impacts.

Rudnick, S. N., & First, M.W. (1978). Third Symposium on Fabric Filteers fbr Particulate Collection, EPA-60017-78-007, 251‑88.

Sagot, B. (2013). Thermophoresis for Spherical Particles. Journal of Aerosol Science, 65 (11), 10‑20.

Saleem, M.,, Khan, R.U., Tahir, M.T., & Krammer, G,. (2011). Experimental Study of Cake Formation on Heat Treated and Membrane Coated Needle Felts in a Pilot Scale Pulse Jet Bag Filter Using Optical In-Situ Cake Height Measurement. Powder Technology, 214(3), 388‑99.

Saleem, M., & Krammer, G. (2007). Effect of Filtration Velocity and Dust Concentration on Cake Formation and Filter Operation in a Pilot Scale Jet Pulsed Bag Filter. Journal of Hazardous Materials, 144(3), 677‑81.

Saleem, M., Grnot Krammer, G., & Tahir, M.S., (2012). The Effect of Operating Conditions on Resistance Parameters of Filter Media and Limestone Dust Cake for Uniformly Loaded Needle Felts in a Pilot Scale Test Facility at Ambient Conditions. Powder Technology 228(9), 100‑107.

Shapiro, M., & Zarutskaya, T. (2000). Capture of nanoparticles by magnetic filters. J. Aerosol Sci.

Scheibel, H. G., & Porstendörfer, J. (1984).Penetration measurements for tube and screen-type diffusion batteries in the ultrafine particle size range, J. Aerosol Sci. 15(6), 673-582.

Senthil K. R. (2013). Textiles for Industrial Applications. CRC Press.

Seville, J. P. K. (1997). Gas Cleaning in Demanding Applications, Blackie academic and profesional, (Chapman & Hall).

Silva, C. R. N., Negrini, V. S., Aguiar, M. L., & Coury, J. R., (1999). Influence of gas velocity on cake formation and detachment. Powder Technology, 101(2), 165–172.

Simon, X. (2005). Etude du décolmatage pneumatique des dépoussiéreurs à manches. Thèse de doctorat de l'INPL.

Siret, B. (1994). Depoussierage Devesiculage. Ed. Techniques Ingénieur.

Song, C.B., Park, H.S., & Lee, K.W. (2006). Experimental Study of Filter Clogging with Monodisperse PSL Particles. Powder Technology 163(3), 152‑59.

Spurny, K.R. (1998). Advances in Aerosol Gas Filtration.

Stechkina, I.B.& Fuchs, N. A. (1966). Ann Occup. Hyg., 9, 59.

Stöcklmayer, C,, & Höflinger, W., (1989). The effect of dust-compression on the residual pressure drop of dust filters – a simulation approach ; PARTEC 98. In 4th European Symposium Separation of particles from gases. Nürnberg / Germany.

Sztuk, E., Przekop, R., & Gradoń, L (2012). Brownian dynamics for calculation of the single fiber deposition efficiency of submicron particles. Chemical and Process Engineering 33(2).

Theo S., Kögel, A., Klein, G.M., GmbH & Co. KG, Langenberg, V. (1998). The evolution of the jet pulse bag filter technology, Industrial dedusting with bag filters.

Thomas, D. (2001). Clogging o fibrous filters by solid aerosol particles Experimental and modelling study. Chemical Engineering Science, 56(35) 49‑61.

You-Im, C., & Jue-Joan, W. (1999). Particle Deposition Behavior Simulated by the Stochastic Method. Journal of Petroleum Science and Engineering. 22(1), 189-203.

Xuan, Y., & Yao, Z., (2004). Lattice Boltzmann Model for Nanofluids. Heat and Mass Transfer 4(4), 199-205.

Wagner, H. Gg. (1978). Soot Formation in Combustion. Max-Planck-Institut für Strömungs forschung.

Wang, Hwa-Chi, et Gerhard Kasper. 1991. Filtration efficiency of nanometer-size aerosol particles. Journal of Aerosol Science, 22(1),31–41.

Wang, M., Gao, B., & Tang, D., (2016). Review of Key Factors Controlling Engineered Nanoparticle Transport in Porous Media. Journal of Hazardous Materials, 318(1), 233‑46.

Wang, Y., Raj, A., & Chung, S.H. (2013). A PAH Growth Mechanism and Synergistic Effect on PAH Formation in Counterflow Diffusion Flames. Combustion and Flame, 160(9), 1667‑76.

Zhou, R., Shen, H., & Zhao, M. (2012). Simulation Studies on Protector of Pulse-Jet Cleaning Filter Bag. Energy Procedia, 16(2), 426‑31.

Züttel, A., Borgschulte, A., & Schlapbach, L., (2008). Hydrogen as a Future Energy Carrier. Weinheim: Wiley-VCH.

UNIVERSITE BRETAGNE LOIRE

IMT Atlantique
Bretagne-Pays de la Loire
École Mines-Télécom

Thèse de Doctorat

Rachid BOUDHAN

Performances d'un filtre à manche pour la capture de particules en conditions représentatives de l'incinération de nano-déchets.

Performance of pulse-jet bag filter regarding particle removal for nano-waste incineration conditions.

Résumé

Les performances de filtration d'un filtre à manche vis-à-vis de particules submicroniques et nanométriques ont été évaluées à l'échelle du laboratoire durant plusieurs cycles de colmatage/décolmatage. La distribution granulométrique des particules (aérosol de combustion) était représentative de celle rencontrée en incinération de nano-déchets en sortie de chambre de combustion à l'échelle du laboratoire. Le filtre à manche opérait en conditions réalistes, représentatives de celles rencontrées dans les lignes de traitement des fumées d'incinération de déchets en termes de température, humidité, vitesse de filtration, présence de réactifs et conditions de décolmatage. Le flux d'air et le filtre à manche étaient chauffés à 150°C, la teneur en eau était de 10-12% (soit 3% d'humidité relative HR), et la vitesse de filtration était fixée à 1,9 $cm.s^{-1}$. Un mélange de particules de taille submicronique de charbon actif et de bicarbonate de sodium, utilisées dans les lignes de traitement des fumées d'incinération pour l'abattement des dioxines/furanes et des gaz acides, était généré simultanément avec l'aérosol de combustion.

L'étude s'est centrée sur les performances de filtration au début de la durée de vie du filtre à manche, avant stabilisation de la perte de charge résiduelle du filtre résultant des précédents cycles de filtration. La perte de charge maximale du filtre était fixée à 150 Pa pour tous les cycles de filtration avant décolmatage par rétro-soufflage à air comprimé. Les performances du filtre à manche ont été évaluées en termes d'évolution de sa perte de charge et de son efficacité de collecte (totale et fractionnelle) au cours des cycles de colmatage/décolmatage.

De plus, des études expérimentales et théoriques ont été menées afin d'étudier l'influence de divers paramètres sur les performances de filtration du filtre en configuration manche ou plane, tels que l'humidité de l'air (3% HR versus 0% HR à 150°C), la température (150°C versus 24°C), la vitesse de filtration (1,9 $cm.s^{-1}$ versus 1,4 $cm.s^{-1}$) et l'influence de l'injection de réactifs.

Les principaux résultats de cette étude sont : (i) importante efficacité de capture des particules du filtre à manche en conditions représentatives des lignes de traitement des fumées d'incinération : efficacité minimale de collecte de 98,5% mesurée pour des particules de taille 74 ± 15 nm (diamètre de mobilité électrique), (ii) influence du gâteau résiduel de particules au début de chaque cycle de filtration sur les performances de traitement, (iii) influence significative de l'humidité de l'air sur la structure du gâteau de particules probablement due à l'augmentation des forces d'adhésion entre les particules en présence d'humidité (150°C – 3% HR soit environ 100 g d'eau par kg d'air sec) ; augmentation plus rapide de la perte de charge du filtre à manche en présence d'humidité (150°C – 3% HR) qu'en conditions d'air sec (150°C – 0% HR).

Mots clés

Incinération de déchets, performances de filtration, filtre à manche, cycles de colmatage/décolmatage, particules submicroniques et nanométriques

Abstract

Filtration performance of a pulse-jet bag filter was evaluated at the laboratory-scale regarding submicronic particles with a nanosized fraction during clogging/unclogging cycles. The particle size distribution was representative to those encountered at the outlet of a nano-waste incineration device at laboratory-scale. The bag filter was operated in conditions as similar as possible to those found in flue gas treatment of waste incineration plants, in terms of temperature, humidity, filtration velocity, injection of sorbent reagents and unclogging conditions. The air flow and the bag filter were heated to 150°C, the water content was maintained in the air flow in the range of 10-12% (3% of relative humidity RH), and filtration velocity throughout the bag filter was fixed at 1.9 $cm.s^{-1}$. A mixture of submicronic suspended particles of activated carbon and sodium bicarbonate, both used in flue gas treatment systems mainly for the removal of dioxins/furans and acid gases, was generated simultaneously with the aerosol representative of combustion emissions.

The study focused on the filtration performance at the beginning of the bag filter's lifetime filter for the 11 first clogging-unclogging cycles before stabilizing the residual pressure drop reached after pulse-jet unclogging. The maximum pressure drop was set at 150 Pa for all filtration cycles. Once the maximum pressure drop was reached, the filter was unclogged using the pulse-jet system. The performance of the bag filter was evaluated in terms of the evolution of pressure drop, fractional and total particle collection efficiencies, during the clogging/unclogging cycles.

Moreover, an experimental and theoretical study was carried out on the influence of different parameters on the filtration performance of bag filter and flat filter, such as influence of humidity (3% RH versus 0% RH at 150°C), temperature (150°C versus 24°C), filtration velocity (1.9 $cm.s^{-1}$ versus 1.4 $cm.s^{-1}$) and the influence of the injection of sorbent reagents.

The main results of this study are: (i) high collection efficiency of the bag filter in representative conditions of flue gas treatment of waste incineration: minimun particle collection efficiency of 98.5% for particle diameter of 74 ± 15 nm (electrical mobility diameter), (ii) influence of residual particle cake at the beginning of the filtration cycles on the bag filter performance, (iii) significant influence of humidity on the porosity of the particle cake due to the capillary condensation of water between the particles in presence of humidity (150°C - 3% RH i.e. almost 100 g of water per kg of dry air). Faster increase of bag filter pressure drop in presence of humidiy (150°C - 3% RH) as compared to the dry conditions (150°C - 0% RH).

Key Words

Waste incineration, filtration performance, bag filter, clogging/unclogging cycles, submicronic and nanosized particles

L'Université Bretagne Loire